الجـمـهـوريـــة الجـــزائـــريـــة الديمـقـراطـيـــة الـشـــعـبـيـــة
PEOPLE'S DEMOCRATIC REPUBLIC OF ALGERIA
وزارة التـــــعـــــليـــــم العـــــالي والبـــــحث العـــــلـــــمـــــي
MINISTRY OF HIGHER EDUCATION AND SCIENTIFIC RESEARCH
جـــــامعة أبي بـكـــــــر بـــلـــقـــايـد – تـــــلمســـــــــان –
TLEMCEN UNIVERSTIY
FACULTY OF TECHNOLOGY

Thesis

Presented to obtain a Masters Degree
in : Mechanical Engineering

Option :Energy

By : Panisi Tinashe

Subject

Design of a new agricultural greenhouse with a water recovery system from evapo-transpiration.

Defended on 29 / 06 / 2021 , infront of the jury :

Mr. GHERNAOUT ME	Professeur	UAB. Tlemcen	PRESIDENT
Mr. GUELLIL Houcine	MCB	UAB. Tlemcen	EXAMINATOR
M. SELADJI Chakib	Professor	UAB. Tlemcen	SUPERVISER

2020-2021

Dedication

I dedicate this work to my parents, Mr and Mrs Panisi , my Sister- Irene Panisi and to the loving and caring Takabvakure family.

Acknowledgment

I would like to thank God for his grace and sustenance, who gave me the power and the means to accomplish this work throughout my study. I owe a big thanks to my parents, Mr. and Mrs. Panisi for their support and encouragement.

Secondly I would like to thank my supervisor Professor Seladji Chakib .I gratefully appreciate his valuable guidance and constructive suggestions as well as his patience with me throughout the research period.

Thirdly I would like to acknowledge with appreciation my vise supervisor Miss Taeib Bouderbal Sabrina. Her numerous and valuable comments, suggestions and constructive critism made it all possible to finish this work.

My heartfelt thanks also goes to the members of the jury: Mr. GHERNAOUT ME and Mr. GUELLIL Houcine. I express our gratitude and gratitude to the administration and all the teaching staff of the University of Abu Bakr Belkaid for their efforts to guarantee us the continuity and culmination of this Master program.

Lastly, thanks to my loving and caring Friends, Takemore Zvisanza, Hamid Chirara and Louisa Mutimhodyo, for being there when things got tough and their words of encouragement and hope.

Abstract

The greenhouse is considered water use efficient compared to open-field production systems; nonetheless, conventional semi-arid greenhouses use large amounts of water, for both evaporative cooling and irrigation. The goal of this project is to examine the feasibility of installing a water recovery system for reducing semi-arid greenhouse water consumption. The present investigation represents an integrated computational study of heat transfer, mass transfer and humidity inside greenhouse. The aim was to model and validate the micrometeological variables for subsequent comparison between different greenhouses. This work was adapted for the Saharan region in Adrar under regional parameters (longitude: 0.28, latitude 27.86, timezone GMT+2).

The micrometeorological variables, humidity, mass transfer and temperature were observed and monitored for a transient regime on 6 June 2021.The observance and monitoring of the physical quality of these variables help us to know the amount of water evaporated from the water droplets from transpiration of the plants. Our Simulation is based on 2 types of geometries, 2 inclined on the roof and 2 without an inclination. Numerical Investigation was conducted to simulate an experimental result in greenhouse of sizes 5m x 3m x 8m (W x H x L). The results demonstrated the computational capabilities to adequately represent the physical phenomenon under consideration and that the integration of a water recovery system to a semi-arid Greenhouse is technically feasible.

KEYWORDS: Greenhouse, Numerical simulation, micrometeorology, Condensation, controlled environment.

Résumé

La serre est considéré comme économe en eau par rapport aux systèmes de production en plein champ ; néanmoins, les serres semi-arides conventionnelles utilisent de grandes quantités d'eau, à la fois pour le refroidissement par évaporation et pour l'irrigation. L'objectif de ce projet est d'examiner la faisabilité d'installer un système de récupération d'eau pour réduire la consommation d'eau des serres semi-arides. La présente enquête représente une étude informatique intégrée du transfert de chaleur, du transfert de masse et de l'humidité à l'intérieur de la serre. L'objectif était de modéliser et de valider les variables micrométéologiques pour une comparaison ultérieure entre différentes serres. Ce travail a été adapté pour la région saharienne de l'Adrar sous paramètres régionaux (longitude : 0,28, latitude 28,86, fuseau horaire GMT+2). Les variables micrométéorologiques, humidité, transfert de masse et température ont été observées et suivies pour un régime transitoire le 6 juin 2021. Le respect et le suivi de la qualité physique de ces variables permettent de connaître la quantité d'eau évaporée des gouttelettes d'eau issues de la transpiration des plantes. Notre Simulation est basée sur 2 types de géométries, 2 inclinées sur le toit et 2 sans inclinaison. Une étude numérique a été menée pour simuler des résultats expérimentaux dans une serre de tailles 5m x 3m x 8m (W x H x L). Les résultats ont démontré les capacités de calcul pour représenter adéquatement le phénomène physique à l'étude et que l'intégration d'un système de récupération d'eau à une serre semi-aride est techniquement faisable.

MOTS CLÉS : Serre, Simulation numérique, micrométéorologie, Condensation, environnement contrôlé.

الملخص

تعتبر الدفيئة مقتصدة في استخدام المياه مقارنة بأنظمة الإنتاج في الحقول المفتوحة؛ ومع ذلك، فإن الدفيئة الزراعية شبه القاحلة التقليدية تستخدم كميات كبيرة من المياه للتبريد بالتبخير والري.

الهدف من هذا المشروع هو دراسة امكانية تركيب نظام لاستعادة المياه للتقليل من استهلاك مياه الدفيئة شبه القاحلة.

يمثل البحث الحالي دراسة حسابية متكاملة لانتقال الحرارة وانتقال الكتلة والرطوبة داخل الدفيئات الزراعية من اجل نمذجة متغيرات الأرصاد الجوية الدقيقة والتحقق من صحتها للمقارنة اللاحقة بين الدفيئات الزراعية المختلفة.

تم تكييف هذا العمل للمنطقة الصحراوية في أدرار وفقًا للمعايير الإقليمية (خط الطول: 0.28 ، خط العرض 27.86 ، المنطقة الزمنية GMT + 2)
لوحظت متغيرات الأرصاد الجوية الدقيقة , الرطوبة , انتقال الكتلة ودرجة الحرارة وتم رصدها من أجل نظام عابر في 6يونيو 2021 ، وتساعدنا مراقبة الجودة الفيزيائية لهذه المتغيرات ومراقبتها على معرفة كمية الماء المتبخرة من قطرات الماء من نتح النباتات. تعتمد محاكاتنا على نوعين من الأشكال الهندسية، نوعان ذو سطح مائل ونوعان بدون ميل. تم إجراء التحقيق العددي لمحاكاة نتائج تجريبية في صوبة زجاجية بأحجام 5 م × 3 م × 8 م (عرض × ارتفاع × طول).

أظهرت النتائج القدرات الحسابية لتمثيل الظاهرة الفيزيائية قيد الدراسة بشكل كافٍ وأن تكامل نظام استعادة المياه إلى دفيئة شبه قاحلة أمر ممكن تقنيًا .

الكلمات المفتاحية: الدفيئة، المحاكاة العددية، الأرصاد الجوية الدقيقة، التكثيف، البيئة الخاضعة

SUMMARY

CHAPTER 1: Greenhouse Generalities

CHAPTER 2: Bibliographic Analysis on the microclimate of the greenhouse and feasibility of a water recovery system.

CHAPTER 3: Mathematical modelling and Numerical approach

Figures List

List of Tables

Symbols and units

BF	Bypass factor (dimensionless)
c_{air}	Specific heat of air at constant pressure (kJ·kg DA^{-1}·K^{-1})
c_{fw}	Specific heat of water at constant pressure (kJ·kg^{-1}·K^{-1})
dh_{air}	Change of enthalpy between state 1 and state 2 (kJ·kg DA^{-1})
dt_{fw}	Change of coolant water temperature (˚C)
h_{fg}	Enthalpy of condensation at temperature of feed water to the condenser(kJ·kg^{-1})
h_1	Enthalpy of air intake at state 1(kJ·kg DA^{-1})
h_2	Enthalpy of discharge air at state 2, reaching 100% relative humidity (kJ·kg DA^{-1})
$h_{2,BF}$	Enthalpy of discharge air at state 2 with a given BF (kJ·kg DA^{-1})
m_a	Mass flow rate of air (kg DA·s^{-1})
m_{fw}	Mass flow rate of water (kg·s^{-1})
m_w	Water condensation rate (kg·s^{-1})
$m_{a,b}$	Portion of the bypassing air (kg DA·s^{-1})
$m_{a,d}$	Portion of air passed through the coil (kg DA·s^{-1})

q	Total heat transfer rate (kW)
q_L	Latent heat transfer rate (kW)
q_s	Sensible heat transfer rate (kW)
Q_{air}	Volumetric flow rate of air to condenser ($m^3 \cdot s^{-1}$)
Q_{fw}	Volumetric flow rate of water inside the cooling coil ($m^3 \cdot s^{-1}$)
RH_{in}	Incoming air relative humidity to condenser (%)
RH_{out}	Outgoing air relative humidity from condenser (%)
SHR	Sensible heat ratio (dimensionless)
t_d	Apparatus dew point temperature of cooling coil (˚C)
t_{dp}	Dew point temperature (˚C)
t_{air1}	Air temperature at State 1 of condenser (˚C)
t_{air2}	Air temperature at State 2 of condenser, reaching 100% relative humidity (˚C)
$t_{air2,BF}$	Air temperature at State 2 of condenser with given BF (˚C)
t_{fw1}	Incoming water temperature to the condenser (˚C)
t_{fw2}	Outgoing water temperature from the condenser (˚C)
V_{air}	Face air velocity of condenser ($m \cdot s^{-1}$)
w_1	Humidity ratio of air intake at State 1 ($kg \cdot kg\ DA^{-1}$)
w_2	Humidity ratio of discharge air at State 2 ($kg \cdot kg\ DA^{-1}$)
a_1	empirical parameter
b_{ij}	second-order anisotropy tensor
C	empirical constant in turbulence model
$\frac{D}{Dt}$	$\partial/\partial t + u_j(\partial/\partial x_j) =$ total differential
D	diffusion of dependent variable Φ
F_i	external body force (X_i -component); also interfluid friction forces
g	gravitational acceleration
$k \quad = \frac{1}{2}u_i'u_i',$	kinematic turbulence kinetic energy
l	Prandtl's mixing length
L, L_k	length scale (characteristic of large eddies) of turbulence
p	instantaneous pressure
Q	set (ξ_i, t_i) of co-ordinates
Re	Reynolds number

Greek symbols

ρ_{air}	Dry air density (kg DA·m^{-3})
ρ_{fw}	Density of feed water (kg·m^{-3})

GENERAL INTRODUCTION

GENERAL INTRODUCTION

Greenhouse crop production has been recognized as a potential solution for reducing the demand on resources such as water. In a world where 70% of fresh water is used for irrigation, finding alternatives to traditional farming and irrigation practices will be essential for earth's growing population .In arid and semi-arid regions around the world, water used for irrigation is as high as 91% in the Middle East and 85% in Asia and Africa (Ragab and Prudhomme, 2002).

In these regions the majority of farms use surface (or flood) irrigation practices, creating huge inefficiencies of water use. Large amounts of water need to be consumed when irrigating plants and when using evaporative cooling. There is a real need for creating agricultural practices to decrease water consumption for food production. Although reducing overall water use for agriculture is important, with increasing world populations, it may become even more critical to increase food productivity with existing water resources, especially in water-starved countries.

One typical strategy to increase water use efficiency in commercial greenhouses is to recycle water used for irrigation. Employing this strategy can save 30–40% of the water used for irrigation. A semiarid greenhouse equipped with a pad and fan cooling system reportedly used 3.2–8.4 × 10^{-3} $m^3 \cdot m^{-2} \cdot d^{-1}$ water (floor area basis) for cooling during a dry early summer day, as affected by ventilation rate, while the amount of water used by the canopy transpiration inside the greenhouse was approximately 2.3–2.9 × $m^3 \cdot m^{-2} \cdot d^{-1}$ (Sabeh, 2007). The water use in evaporative cooling and plant transpiration varies depending on canopy leaf area index and environmental conditions such as solar radiation and vapor pressure deficit (VPD) inside and outside the greenhouse.

A typical pad and fan evaporative cooling system, with an evaporative surface (pad) in one side and mechanical exhaust fans on the opposite side of the greenhouse, creates a unique one-way water vapor pathway through the greenhouse. Wet pads reduce the air temperature to approximately the wet bulb temperature (the theoretically lowest temperature that air can attain by means of evaporative cooling). As air travels through the greenhouse, dry bulb temperature increases and more moisture is added to the air by canopy evapotranspiration, thus increasing its dew point to a level greater than the wet bulb temperature outside the greenhouse. Theoretically, by placing a condensation surface in the humid air stream of the greenhouse, water vapor can be recovered from the air before its exit to the outside, and the condensate can be collected and recycled and used in irrigation. Furthermore, greenhouses could produce large amounts of fresh water, as demonstrated theoretically by Davies and Paton (2005) and Wahlgren (2002). Both studies used seawater as a cold water source. When such a cold water source is not available, the chilled water naturally generated as efflux from the pad of an evaporative cooling system could possibly be used as an alternative. A similar attempt has been reported using an experimental greenhouse without plant canopy but with a humidification apparatus (Perret et al., 2005) in which no measurable condensation rates were

obtained (reportedly due to the low condensation efficiency caused by the high face air velocity) **[1].**

For the greenhouse understudy the principal objectives are:

- To add water recovery capability to the existing greenhouse designs widely used by commercial operations in arid and semiarid regions.
- To study the transient regime to see the variation in solar flux during the day.
- Aims at the numerical modelling of 3D radiation and convection transfers within a closed cropped greenhouse, with a focus on the coupling between microclimate and crop transpiration.
- To study the Influence of the structure of the greenhouse in different aspects.

The description of the work carried out is in Thesis is structured in 4 chapters:

Chapter 1 - The generalities of Greenhouses, their microclimate conditions and microclimate control.

Chapter 2- Bibliographic study on the modelling of micrometeorology in a closed greenhouse using Computational Fluid Dynamics and Analysis of the greenhouse water recovery system for crop production in semi-arid climate.

Chapter 3- Mathematical and Numerical Modelling.

Chapter 4- Results Analysis and Interpretation.

This Thesis will end with a general conclusion.

Chapter 1:

Greenhouse Generalities

1.1. Introduction

The greenhouse comes **from** the verb "to tighten", so we can logically deduce that this is a small space, where we will try to fit as many plants as possible. This is probably only a very partial aspect of the role of the modern greenhouse. The greenhouse is originally designed as

a simple shelter, or an enclosure intended for the cultivation or protection of plants by exploiting solar radiation. It has become an industrial room for the production of plant, where we try to adapt the immediate environment of the plant so as to improve its productivity and quality, freeing it from the external climate, the local soil and even the seasons.

The climatic factors which influence the climate inside the greenhouse are the temperature and humidity, solar radiation and the outside wind. In reality, each of these factors generates a combination of effects which may or may not be favorable to the operation of the greenhouse according to the prevailing local conditions. Temperature plays a major role in the growth and development of vegetation; the concentrations of CO_2 and water vapor play a determining role in the transpiration and photosynthesis of plants as well as in the development of fungal diseases. Solar radiation is also involved in photosynthesis. Some roofing materials such as glass, transparent to short-wavelength radiation and opaque to infrared radiation creates a greenhouse effect which itself causes a rise in temperature in the greenhouse. The wind generates pressure differences on the greenhouse which can damage it in extreme cases. It also causes losses by convection and makes a decisive contribution to natural ventilation. Well-controlled control of the climate's energy balance therefore makes it possible to manage these parameters and improve the physiological functioning of plants **[2].**

1.2. Greenhouse materials and structures

A greenhouse is designed in such a way that it can be verified that it does not exceed the load limits at any time. This is determined according to the type of greenhouse and the materials used. For an intelligent greenhouse containing high value equipment and crops, they should not be designed for a life-cycle less than 10 years.

1.2. 1. Structure materials

Using the proper type of material to construct a structure is important for the resilience and efficiency of the finished product. Harsh weather conditions (snow, rain, hail, wind or hot weather) are the most common cause of failure of greenhouse structures. The structure should be able to take all the necessary types of loads; dead, live, wind and snow. The foundation, columns and trusses are designed accordingly. The main loads, which have to be taken into account in the greenhouse design, are (Elsner et al., 2000):

1. Dead load or permanent load.
2. Imposed loads (crop loads).
3. Installations.
4. Snow load.
5. Wind load.
6. Seismic load.

This classification is based on the estimation of the lifetime of the greenhouse from the economic and technical point of view. To avoid structural damages, stress limits should be

considered, which are associated with a structure collapse endangering human life .The ultimate limit states, which may require consideration, are the following: loss of balance of the structure and loss of load bearing capacity due to breakage, shakiness, fatigue, excessive tensions and deformations.

Regardless of the type of material used, the stress limits will be analysed mechanically in a plane structure, which is a set of discrete elements connected to each other in a rigid way, which is designed to withstand the external forces applied and transmit them to the foundation, without which there would be an excessive breakage or deformation of the material **[3].**

1.2. 1. A. **Galvanized Steel:** Has mechanical properties of high resistance.
Advantages:

- It can resist both the damage of humid and extremely dry climates.
- It ensures structural integrity due to natural disasters such as high-speed winds.
- The roof is easier to be built in a rounded shape or in a pointed arch (chapel shaped like).
- It can be used with polyethylene coatings or glass.

Disadvantages:

- High cost.

1.2. 1. B. Wood: The pine and maple are the most commonly used, combined with steel tubes and foundations of cement or concrete to ensure their structural integrity in case of natural shocks of great intensity

- Advantages:
- A wood frame provides natural insulation for the greenhouse.
- The wood absorbs the rays of the sun during the day and holds in the heat at night.

Disadvantages:

- It may be needed to treat the wood to prevent wood rot, and the chemicals out-gassing from the pre-treated wood can be toxic to the plants that are grown inside the greenhouse.

1.2. 1. C. Low carbon steel (AISI 1010): Contains less carbon than other steels and is much easier to cold-form due to their soft and ductile nature.
Advantages:

- Cheaper than the galvanised steel.
- Less impact on the environment

Disadvantages:

- It is neither externally brittle nor ductile due to its low carbon content. It has lower tensile strength and is malleable.

1.2. 1. D. High-strength low alloy Steel (HSLA 340): The steels in the HSLA range are suitable for structural parts. Since they generally have lower carbon than the SS steels, their ductility is superior.
Advantages:

- It is recommended to be used in some pipes and in the foundations.
- It is recommended to be used in some basic junctions of the structure as well as in the screws and nails.

Disadvantages:

- Do not use a material such as this in areas where there is planted land or agricultural production as it cannot be left outside for a long time.

1.2. 1. E. Aluminium: Round or square tubing is used, depending on the covering material to be used on it.
Advantage:

- It is a strong material and will not rust, and is lightweight. Drilling holes in it is fairly easy.

Disadvantage:

- Fiberglass panels or polycarbonate sheets could be fastened to the structure.

In terms of structural materials, approximately 50% of the greenhouses have metallic structures, 30% is made of wood and the rest is of mixed structures, understood as the combined use of laminated wood, metallic profiles, etc. **[4]**

1.2. 2. Cladding materials

The characteristics of the cladding material determine the quality of the light transmitted into the greenhouse, and radiation transmittance can be improved qualitatively and quantitatively. The cladding material must have characteristic such as: strength, consistency, durability, manufacturing quality control, safety, transmission of solar radiation and energy conservation. Greenhouse designs vary widely and choosing the correct type of greenhouse is an important decision faced by growers. The glazing will drastically affect the amount and type of sunlight that reaches the crop.

The glazing will also determine the heat loss of the structure. When selecting a cladding or cover for a greenhouse, it is important to consider the next question (Giacomelli 2002):

- How much energy (light) does it let into the greenhouse, and how much energy (heat) will go out?
- What are the purchase, installation, and maintenance costs?
- How well can the grower manage the environment which is imposed by the glazing to produce a quality, salable product for profit?

These questions can be answered with the experience of the grower, the crop produced, the glazing, the local outside environment, and the greenhouse environmental control systems. There are also other variables that affect the cover used for the crop, such as transmittance, dust and dirt, the gases and also salt **[5].**

In order to solve the current necessities there are 3 types of coverings typically used for greenhouses: glass, plastic films and rigid plastic panels.

1.2. 2.A. Glass

Glass is the traditional covering. It is available in many designs to blend with almost any style or architecture. Glass greenhouses may have slanted sides, straight sides and eaves, or curved eaves.

The glass that is used as a cover in the greenhouses is always the printed glass or glass "cathedra''. Its thickness varies from 2 to 6 mm, and the plates measure approx., 60 cm. Its thickness is measured in gauges and sold in coils in variable widths (from 80 cm up to 12m and thicknesses from 200 to 1200 gauges, i.e., from 0.05 to 0.3 mm).

Advantage:

- Good-quality glass is an attractive, very transparent, and formal (in appearance) covering material.
- It is very strong (tensile strength).

Disadvantage:

- It is subject to shattering and can become brittle with age.
- It is also very expensive.
- Its weight requires sturdier framing support than is required with other covering materials.

1.2. 2.B. Plastic films

The use of plastic is increasing in the building of greenhouses due to its cost per square foot. It can be heated as satisfactorily as glass greenhouses, crops that grow under plastic are of equal quality to those grown under glass, it is considered a temporary structure and usually carries a low assessment rate for tax purposes, or may not be taxed at all. Plastic structures can be made of polyethylene (PE), polyvinyl chloride (PVC), copolymers of these materials, and other readily available clear films. Plastic film is the most applied cladding material in countries with tropical, subtropical and arid climates (Zabeltitz 1990).

1.2. 2.C. Polyethylene (PE)

Permits passage of much of the reradiated heat energy given off by the soil and plants inside the structure. When it is used an Ultraviolet-inhibited polyethylene, it lasts longer than regular polyethylene. It has an inhibitor that prevents the rapid breakdown caused by ultraviolet light. UV-inhibited polyethylene is available in 2- and 6-mil thickness up to 40 feet wide and 100

feet long. Therefore, a polyethylene type loses heat more quickly than glass both during sunny periods and after sunset. This is an advantage during the day and a disadvantage at night. These films are reported to reduce 20% of the heat loss from the greenhouse and have become common in today's industry, especially in Europe.

A newly developed polyethylene film in Israel has been designed to allow very low levels of UV light to be transmitted. There is good evidence that UV blocking films have an adverse effect on flying insects such as Bemisia tabacci, aphids and thrips (Merle 2001).

Advantage:

- It is low in cost and lightweight.
- It also stands well in fall, winter, and spring weather, and lets through plenty of light for good plant growth.

Disadvantage:

- Constantly exposed to the sun deteriorates during the summer and must be replaced each year.
- Ultraviolet light energy causes polyethylene to break down..

1.2. 3. Floor materials

A foundation is one of the most important parts of the greenhouse. No matter where the foundation lies, it must be level and square. The materials of greenhouse floors range from bare ground to concrete and some examples are:

1.2. 3.A. Standard Concrete – Regular concrete will endure about 2500 pounds per square inch. This mix is appropriate for heavy loads such as soil-mixing areas and locations in the greenhouse where heavy equipment is used.

1.2. 3.B.Porous Concrete – Allows drainage preventing puddling and still provides a barrier for weed control. Properly cured porous concrete will have a capacity to endure 600 pounds per square inch of surface. A four-inch floor of this mixture will adequately endure light equipment and personnel.

1.2. 3.C. Gravel or Dirt Floors – They are inexpensive but often not worth the initial savings. Floors will be mud with frequent irrigations and will generally appear unacceptable.

In fact, these muddy and unstable floors are a problem in terms of the cost and pollution to the extent that they have prompted the search for substitutes in the shape of eco-materials.

1.2. 4. Eco-materials

Some of the materials used for building a greenhouse could not be environment-friendly due to their long period of degradation inducing air pollution. Eco-materials appear to handle this situation, these are the materials which combine less environmental burden in production with high recyclability, and realize more effective utilization of material. Materials should be friendly not only to the nature but also to mankind.

Eco-materials can be referred to the materials used for the life-cycle product design developed in order to protect the environment. There are seven elements of eco-efficiency such as:

- Reducing the material requirements for goods and services.
- Reducing the energy intensity of goods and services.
- Reducing toxic dispersion.
- Enhancing material recyclability.
- Maximizing sustainable use of renewable resources.
- Extending product durability.
- Increasing the service intensity of goods and services.

The eco-materials can be classified into four main categories:

  - Non-linear source materials.
  - Materials for ecology and environmental protection.
  - Materials for society and human health.
  - Materials for energy based on two main criteria as their sources and functions.

Some examples for eco-materials are shown in table1.1. As it can be seen, some combinations of eco-materials may serve for the greenhouse structure and floor in future developments.

Table 1.1: List of Eco-materials Applications

Categories	Example
-Recycled Renewable	-Eco-cement, coal ash concrete, marine block. Wood based materials, biodegradable plastic

	made of a Vegetable base.
Material for efficiency	-Wear-resistant metals and alloys, pre-paint steels, corrosion resistant steel and alloy.
Material for easy disposal or recycle	Biodegradable plastics, functionally graded material, colorbetos which replaces asbestos.
Hazardous free materials	Chromium-free steel, heavy metals free polyesters
Materials for reducing human health impacts	Vibration damping steel sheet, sound proof panels.
Materials for energy efficiency	Ultra-light steel, high magnetic induction steel sheets, highly endothermic steel.
Materials for green energy	Selective transparent glass, highly durable sealing sheets for solar batteries.

Greenhouses are required to allow high light transmittance, low heat consumption, sufficient ventilation efficiency, adequate structural strength and good overall mechanical behavior, low construction and operating costs.

Greenhouses are designed taking into account safety, serviceability, general structural integrity and suitability. The location, size and frame design of the greenhouse determines the type of material and structure form to be used during the construction of the greenhouse. The components of greenhouse structures are: poles, ridges, belts, and downspouts. The greenhouses' mainstay could be made of glass, whose mission is to secure the cover to protect the crop. Besides protection, they support any loads, such as wind, rain, snow, or irrigation facilities staking, to prevent problems like infiltration, minimal shade during the day, and reduce the problem of nightly temperature drops (usually weather). The ventilation, the shape and the material of the greenhouse are factors to be taken into account. It is important to mention that the resilience of the greenhouse, is not only based on the materials it is built of, but also on its design. Among consideration are the structures used, the stresses to which the parties submit (there must be tension and no compression), the braces of these structures should be longitudinal and tangential to counteract the horizontal force of the wind, and have good anchor roofing materials, etc. In respect to generating loads due to the irrigation, refrigeration and other types of equipment, these should not be below 15 kg/m^2. When staking crops overloads of 14–16 kg/m^2 should be considered.

1.3. Types of greenhouses

Another important factor to have a good structure, in addition to materials, is to determine the structural conformation or external profile **[5].**

1.3.1. Modular parral:

It is used in areas of low rainfall. The structure of these greenhouses is composed of two parts: a vertical and horizontal structure.

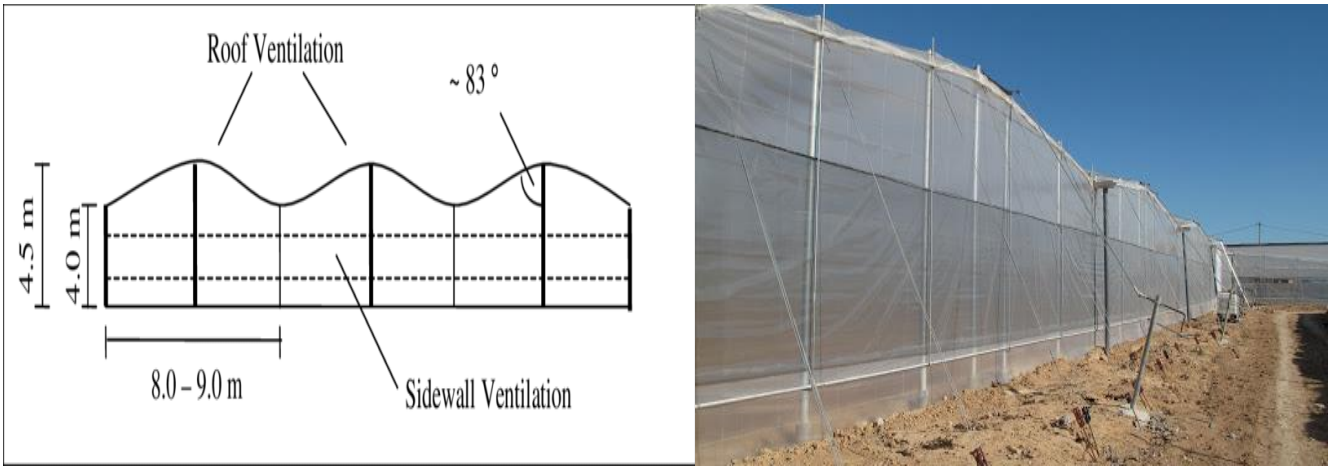

Figure 1.1 *Modular parral*

1.3.2. Multi-tunnel greenhouses

Its structure is similar to the Parral type but it varies the shape of the cover. It increases the maximum height of the greenhouse in the ridge, which ranges between 3 and 4.2 m, forming what it is known as scraped. In the lowest part, known as threatened, the mesh cover is joint to the floor by iron winds and forks that allow to place the gutters for rainwater drainage. The height of the threatened range goes from 2 to 2.8m of the bands between 2 and 2.5 m.

Figure 1.2 *Multi-tunnel greenhouses*

1.3.3. Asymmetric

Differs from the scraped and threatened types in that it increases of the surface in the exposed south face, with the aim of increasing its capacity for taking up solar radiation. For this reason, the greenhouse is oriented East-West, parallel to the sun's apparent path. The tilt of

the cover should allow the solar radiation to impact perpendicularly on the cover at the solar noon during the winter solstice, the time where the sun reaches its lowest point. This angle must be close to 60◦, but this causes great inconvenience due to the instability of the structure caused by strong winds. Therefore the angle has to be set between the 7 and 9◦ in the south face and between the 15 and 23◦ in the north face.

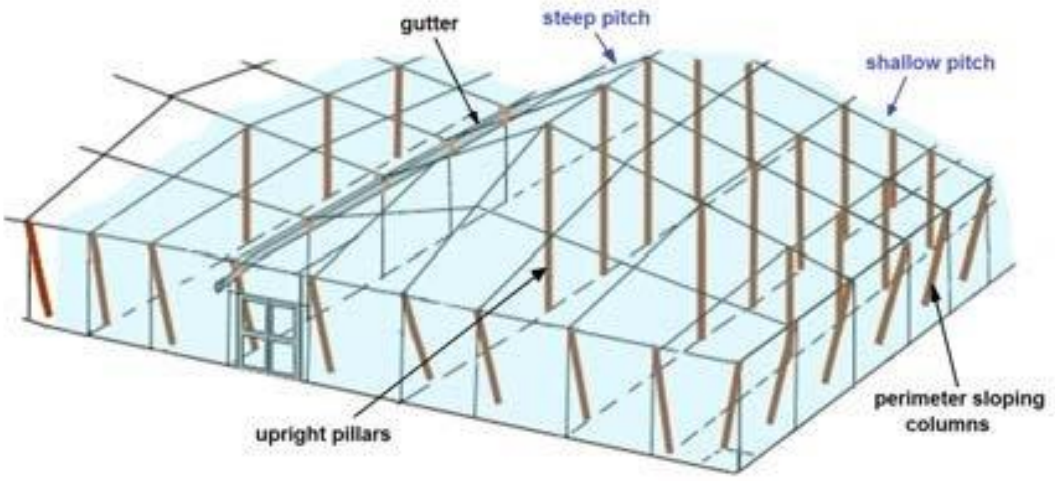

Figure 1.3 Asymmetric

1.3.4. Standard peak or chapel

The greenhouses of simple chapel have the roof forming one or two inclined planes, according to a water or gable. If the inclination of the planes of the roof is greater than 25◦, it offers no drawbacks in the evacuation of the rain water. Ventilation is by the front and side windows. When it comes to structures formed by uniting several ships, in the absence of windows, the ceiling skylights provide the ventilation.

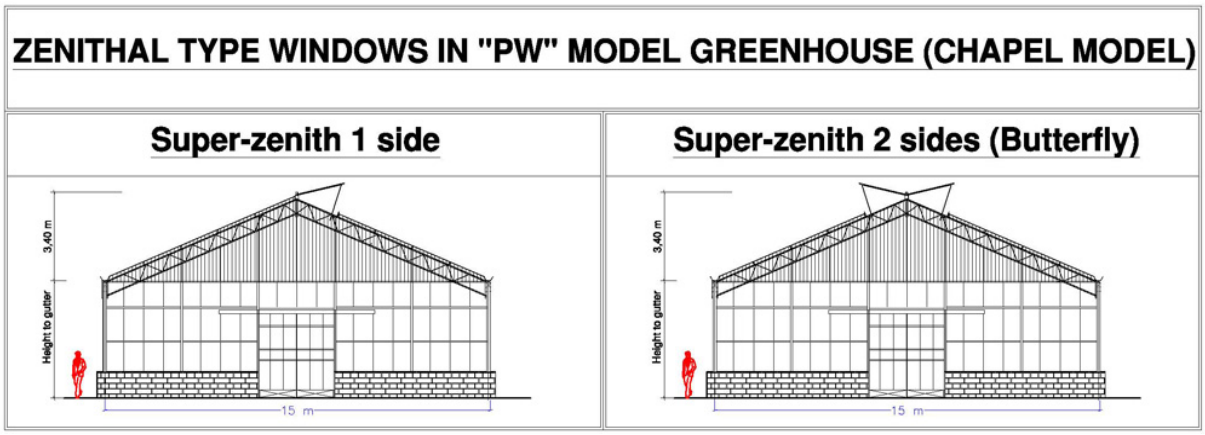

(a) **(b)**

Figure 1.4 *Standard peak or chapel.*

1.3.5. Double chapel

Figure 1.5 *Double chapel*

Consist of two naves juxtaposed. Ventilation is better than in other types of greenhouse, due to the zenithal ridge of the two steps that form the juxtaposition of the two ships; these ventilation openings usually remain open constantly and generally have mosquito mesh. In addition they also have a vertical vent in the front and side walls. This type of greenhouse is not widely used due to its construction, which is more difficult and expensive than the simple chapel or gabled type of greenhouse.

1.3.6. Arch roof

Has a greater capacity for the control of climatic factors, great resistance to strong winds and speed of installation due to the use of prefabricated structures. These structures have some variants for example butterfly, Chinese hat, with zenithal ventilation type, etc.

Figure 1.6 *Arch roof*

Regardless of the selection of the structure type, the dimensions should be considered, for example the average height of a greenhouse characterizes its volume; a large greenhouse volume results in a slow response of the indoor environment to changes of the external

weather conditions. Therefore, higher greenhouses exhibit smaller fluctuations in their indoor microclimate (Elsner et al., 2000b). Higher greenhouses have increased energy consumption and are more demanding in terms of structural stability due to larger wind loads. The height of a greenhouse is optimized with respect to these two competing factors: light transmittance of greenhouses and ventilation.

Considering the variable of light transmittance and ventilation as a reference to optimize the greenhouse, one must also select the best cover, based on the climatic needs of the area and type of crop.

1.4. Greenhouse Climate Control and Energy use

1.4.1. Driving forces for greenhouse climate control and sustainable energy use in greenhouses

All greenhouse cultivation systems, regardless of geographic location, comprise fundamental climate control components; depending on their design and complexity, they provide more or less climate control, and condition to a varying degree plant growth and productivity.

Air temperature – as well as solar radiation and air relative humidity – is one of the most important variables of the greenhouse climate that can be controlled. It conditions not only crop development and production but also energy requirements, which can account for up to 40 percent of the total production costs. The majority of plants grown in greenhouses are warm-season species, adapted to average temperatures in the range 17–27 °C, with approximate lower and upper limits of 10 and 35 °C. If the average minimum outside temperature is < 10 °C, the greenhouse is likely to require heating, particularly at night. When the average maximum outside temperature is < 27 °C, ventilation will prevent excessive internal temperatures during the day; however, if the average maximum temperature is > 27–28 °C, artificial cooling may be necessary. The maximum greenhouse temperature should not exceed 30–35 °C for prolonged periods.

The second important variable is *humidity*, traditionally expressed in terms of relative humidity. Relative humidity within the range of 60–90 percent has little effect on plants. Values below 60 percent may occur during ventilation in arid climates, or when plants are young with small leaves, and this can cause water stress. Serious problems can occur if relative humidity exceeds 95 percent for long periods, particularly at night as this favours the rapid development of fungus diseases such as *Botrytis cinerea*. The increased interest in maintaining adequate transpiration to avoid problems associated with calcium deficiency (Fig 1.7) has resulted in humidity being expressed in terms of the vapour pressure deficit (VPD) or the moisture deficit, both of which are directly related to transpiration. Maintaining the VPD above a minimum value helps to ensure adequate transpiration and also reduces disease problems. During the day, humidity can usually be reduced using ventilation. However, at night, unless the greenhouse is heated, the internal and external temperatures may be similar; if the external humidity is high, reducing the greenhouse humidity is not easy.

Figure 1.7 Pepper *fruit with BER symptoms associated with calcium deficiency*

Following the energy crisis of the early 1980s, when limited energy supplies led to the first significant rise in energy prices, greenhouse energy use became a major research issue. With the recent increased interest in global warming and climate change, the use of fossil fuels is again on the political agenda and many governments have set maximum CO_2 emission levels for various industries, including the greenhouse sector. There are two main ways to increase greenhouse energy efficiency:

- reduce the energy input into the greenhouse system; and
- Increase production per unit of energy.

The challenge is to meet both needs: improved energy efficiency combined with an absolute reduction in the overall energy consumption and related CO_2 emissions of the greenhouse industry. Technological innovations must focus on energy consumption for the return to productivity, quality and societal satisfaction.

1.4.2. CLIMATE CONTROL

Ventilation cooling and shading

Removal of heat load is the major concern for greenhouse climate management in arid and semi-arid climate conditions. This can be achieved by:

- reducing incoming solar radiation;
- removing extra heat through air exchange; and
- increasing the fraction of energy partitioned into latent heat

Shade screens and whitewash are the principle measures taken to reduce incoming solar radiation; greenhouse ventilation is an effective way to remove extra heat through air exchange between the inside and outside (when the outside air temperature is lower); and evaporative cooling is the common technique for reducing sensible heat load by increasing the latent heat fraction of dissipated energy. Other technological cooling solutions are available (heat pump, heat exchangers), but are not widely used because they require a high level of investment.

1.4.2.1.Ventilation

Ventilation is typically the first step taken toward cooling the greenhouse. Ventilation is the process of air exchange that removes heated and humidified air from the greenhouse and replaces it with fresh outside air. The two primary methods of ventilation are mechanical and natural.

Figure 1.8 Different types of ventilation openings

Mechanical Ventilation

Mechanical ventilation (MV) employs the use of fans to provide air exchange.

Figure 1.9 Fans for greenhouse forced ventilation

Typically fans are located along the wall at one long end of the greenhouse. Vent inlets may be located along the opposite wall, along the side walls, or even in the roof (Arbel et al., 2003). One of the primary advantages to using MV is the ability to control ventilation rates. Another advantage is in knowing the direction and speed of airflow in the greenhouse. The main disadvantages to MV are the use of energy and maintenance, and the creation of non-uniform conditions within the greenhouse (ASABE, 2006).

Natural Ventilation

Air exchange by natural ventilation (NV) relies on pressure differences between the outside and inside created by wind (forced convection) and temperature gradients (natural convection) .The major advantage to NV systems is that there is essentially zero operational cost. However, because ventilation depends on outside conditions, air exchange rates and direction can be unpredictable. The configuration of vents is a very important consideration for designing natural ventilation systems. Studies have shown that windward vents increase the rate of air exchange but also decrease the uniformity of conditions within the greenhouse (6).

Ventilation Effects on Greenhouse Climate

The effects of solar radiation on greenhouse air temperature are reduced by increasing the ventilation rate (7). Also, increasing the ventilation rate of both naturally and mechanically ventilated greenhouses has been shown to increase the uniformity of temperature and humidity (8).

However, increasing the ventilation rate has a diminishing return when it comes to lowering the greenhouse air temperature, and little advantage has been shown to using ventilation rates greater than 0.035 m^3 m^{-2} s^{-1} and 0.05 m3 $m^{-2}s^{-1}$ (Willits, 2003a). Furthermore, without evaporative cooling in semi-arid climates, high ventilation rates used to reduce greenhouse temperature may have the unwanted effect of removing too much moisture from the air. A study using computational fluid dynamics (CFD) supported this finding for arid climates (T_{Out} = 45°C, RH_{Out} = 10%), demonstrating that lower ventilation rates maintain higher relative .humidities (9).

1.4.2.2.Shading

Natural or forced ventilation is generally not sufficient for extracting the excess energy during sunny summer days (Baille, 1999), and other cooling methods must be used in combination with ventilation. The entry of direct solar radiation through the covers into the greenhouse enclosure is the primary source of heat gain. The entry of unwanted radiation (or light)can be controlled by shading or reflection. Shading can be achieved in several ways: paints, external shade cloths, nets (of various colours), partially reflective shade screens (Plate 6), water film over the roof and liquid foams between the greenhouse walls.

Figure 1.10 *Thermal screen used for energy saving and greenhouse shading*

Shading is the last resort for cooling greenhouses, because it affects productivity;however, shading can in some cases result in improved quality. A method widely adopted by growers because of its low cost is white painting, or whitening, of the cover material. The use of screens has been progressively accepted by growers and the last decade has seen an increase in the area of field crops cultivated under screenhouses (Cohen et al., 2005).

1.4.2.3.Evaporative cooling

One of the most efficient solutions for alleviating climatic conditions is to use evaporative cooling systems, based on the conversion of sensible heat into latent heat through evaporation of water supplied directly into the greenhouse atmosphere (mist or fog system, sprinklers) or via evaporative pads (wet pads). Evaporative cooling allows simultaneous lowering of temperature and vapour pressure deficit, and its efficiency is higher in dry environments. The advantage of mist and fog systems over wet pad systems is the uniformity of conditions throughout the greenhouse, eliminating the need for forced ventilation and airtight enclosure. Before installing a system, the air- and waterflow rates required must be calculated.

1.4.2.4.Fog system

Water is sprayed as small droplets (in the fog range, 2–60 nm in diameter) with high pressure into the air above the plants in order to increase the water surface in contact with the air (Plate 7)

Figure 1.11 *Fog system used for greenhouse cooling*

Freefall velocity of these droplets is slow and the air streams inside the greenhouse easily carry the drops. This can result in high efficiency of water evaporation combined with keeping the foliage dry. Fogging is also used to create high relative humidity, along with cooling inside the greenhouse. A wide range for fog system cooling efficiency ($n_{f,cool}$) is reported in the literature. According to Arbel et al. (2003)[10], increased efficiency in the cooling process in relation to water consumption can be expected if fogging is combined with a reduced ventilation rate. Furthermore, a close relationship has been observed between $n_{f,cool}$ and system operation cycling (Abdel-Ghany and Kozai, 2006)[11]. Similar values for $n_{f,cool}$ have been reported by Li et al. (2006), who concluded that fog cooling efficiency increases with spray rate and decreases with ventilation rate.

1.4.2.5.Fan and pad cooling

The fan-and-pad cooling system (fig 1.12) is most commonly used in horticulture. Air from outside is blown through pads with as large a surface as possible and which are kept permanently wet by sprinkling. The water from the pads evaporates and cools the air; outside air humidity must therefore be low.

Figure 1.12 *Pad (left) and fan (right) greenhouse cooling system*

There are basically two systems of fan-and-pad cooling: the negative-pressure system and the positive-pressure system.

- The negative-pressure system consists of a pad on one side of the greenhouse and a fan on the other. The fans suck the air through the pad and through the greenhouse. The pressure inside the greenhouse is lower than the pressure outside; hot air and dust can therefore get into the greenhouse. There is a temperature gradient from pad to fan.
- The positive-pressure system consists of fans and pads on one side of the greenhouse and vents on the other. The fans blow the air through the pads into the greenhouse. The pressure inside the greenhouse is higher than outside; dust cannot get into the greenhouse.

In order to achieve optimal cooling, the greenhouse should be shaded. The waterflow rate, water distribution system, pump capacity, recirculation rate and output rate of the fan-and-pad cooling system must be carefully calculated and designed to provide a sufficient wetting of the pad and to avoid deposition of material.

1.4.2.6.Heating

Greenhouse heating is essential even in countries with a temperate climate, like the Mediterranean region, in order to maximize crop production in terms of quantity and quality and thus to increase overall efficiency. Heating costs are not only directly connected to profitability, but in the long term they may determine the survival of the greenhouse industry. In addition to the costs of high energy consumption, heating is associated with environmental problems through the emission of noxious gases.

Heating needs There are various ways to calculate greenhouse heating needs $(\mathrm{H_g})(\mathrm{W})$. The simplest is proposed by ASAE (2000):

$$H_g = UA(T_i - T_o)$$

where:

$\mathrm{U} =$ heat loss coefficient $(\mathrm{Wm^{-2}\ K^{-1}})$ (see Table 1)

$\mathrm{A} =$ exposed greenhouse surface area $(\mathrm{m^2})$

$\mathrm{T_i} =$ inside air temperature (K)

$\mathrm{T_o} =$ outside air temperature (K)

Table 1.2 Total heat loss coefficient U at wind speed of n m/s

Covering materials	U value W/m²/K)
Single glass	6.0–8.8
Double glass, 9 mm air space	4.2–5.2
Double acrylic 16 mm	4.2–5.0
Single plastic	6.0–8.0
Double plastic	4.2–6.0
Single glass plus energy screen of	
- single film, non-woven	4.1–4.8
- aluminized single film	3.4–3.9

ASAE, 2000

Note that the estimation of greenhouse needs using the equation above did not take into account heat loss due to leakage. However it is a simple formula which can be used in order to estimate heating needs according to the greenhouse covering area and the desired temperature difference between inside and outside air.

1.4.2.7.Heating systems

The heating system must provide heat to the greenhouse at the same rate at which it is lost. There are several popular types of heating systems for greenhouses. The most common and least expensive is the unit heater system.

a) Unit heaters

Warm air is blown from unit heaters with self-contained fireboxes. Heaters are located throughout the greenhouse, each heating a floor area of 180–500 m^2.

b) Central heating

Steam or hot water is produced, plus a radiating mechanism in the greenhouse to dissipate the heat (**fig 1.13**). The typical cost of a central boiler system for 1 ha, including heat distribution and installation, is €30–80/m2 of greenhouse floor space, depending on the number of heat zones and the exact heat requirement

Figure 1.13 *Central boiler (left) and heating pipes for dissipating the produced heat (right)*

Unlike unit heater systems, a portion of the heat from central boiler systems is delivered to the root and crown zone of the crop, resulting in improved growth and to a higher level of disease control. Placement of heating pipes is very important as it is directly related to

heat loss; for example, the placement of pipes in the walls resulted in high losses through the sides.

1.4.2.8.CO_2 enrichment

The lack of climate control in many greenhouses results in an inadequate microclimate that negatively affects yield components and input-use efficiency. CO_2 enrichment is essential to increase quality of produce; indeed, continuous or periodical increase of CO_2 inside the greenhouse may lead to an increase of over 20 percent in fruit production for both dry and fresh matter Better control of the greenhouse aerial environment can improve marketable yield and quality, and extend the growing season (Baille, 1999). Inside an unenriched greenhouse, the CO_2 concentration drops below the atmospheric level whenever the CO_2 consumption rate by photosynthesis is greater than the supply rate through the greenhouse vents .Possible solutions are:

- increase the ventilation rate through forced air;
- improve design and management of the ventilation system; or
- provide CO_2 enrichment.

The latter is widely adopted in the greenhouse industry in northern Europe to enhance crop photosynthesis under the low radiation conditions that prevail during winter. Enrichment reportedly increases crop yield and quality under a CO_2 concentration of 700–900 μmol mol-1 (Nederhoff, 1994).

An important constraint is the short time period available for the efficient use of CO_2 enrichment, due to the need to ventilate for temperature control (Enoch, 1984). The fact that greenhouses have to be ventilated during a large part of the day makes it uneconomical to maintain a high CO_2 concentration during the day. However, some authors advise supplying CO_2 even when ventilation is operating (Nederhoff, 1994) in order to maintain the same CO_2 concentration both in the greenhouse and outside, enriching to levels of about 700–800 μmol mol-1 when the greenhouse is kept closed (usually in the early morning and the late afternoon).

1.4.2.9.Dehumidification

Condensation refers to the formation of drops of water from water vapour. Condensation occurs when warm, moist air in a greenhouse comes into contact with a cold surface such as glass, fibreglass, plastic or structural members. The air in contact with the cold surface is cooled to the surface temperature. If the surface temperature is below the dew point temperature of the air, the vapour in the air will condense onto the surface. Condensation is heaviest in greenhouses from sunset to several hours after sunrise. During daylight hours, there is sufficient heating from solar radiation to minimize or prevent condensation, except on very cold, cloudy days. Greenhouses are most likely to experience heavy condensation at sunrise or shortly before. Condensation is a symptom of high humidity and can cause significant problems (e.g. germination of fungal pathogen spores, including Botrytis and powdery mildew.) Condensation can be a major problem – at certain times of the year, impossible to avoid entirely.

1.4.2.10. How to dehumidify the greenhouse

a) Combined used of heating and ventilation

A common dehumidification practice is simply to open the windows, allowing moist greenhouse air to be replaced by relatively dry outside air. This method does not consume any energy when excess heat is available in the greenhouse and ventilation is needed to reduce the greenhouse temperature. However, when the ventilation required to reduce the temperature is less than that needed to remove moisture from the air, dehumidification consumes energy. Warm greenhouse air is replaced by cold dry outside air, lowering the temperature in the greenhouse.

b) Absorption using hygroscopic material

There has been little research on the application of hygroscopic dehumidification in greenhouses, because installation is complex and the use of chemicals is not favourable. During the process, moist greenhouse air comes into contact with the hygroscopic material, releasing the latent heat of vaporization as water vapour is absorbed. The hygroscopic material has to be regenerated at a higher temperature level. A maximum of 90 percent of the energy supplied to the material for regeneration can be returned to the greenhouse air with a sophisticated system involving several heat exchange processes including condensation of the vapour produced in the regeneration process.

c) Condensation on cold surfaces

Wet humid air is forced to a cold surface located inside the greenhouse and different from the covering material. Condensation occurs on the cold surface, the water is collected and can be reused, and the absolute humidity of the wet greenhouse air is reduced. One metre of finned pipe used at a temperature of 5 °C can remove 54 g of vapour per hour from air at a temperature of 20 °C and with 80 percent relative humidity.

d) Forced ventilation usually with combined use of a heat exchanger

Mechanical ventilation is applied to exchange dry outside air with moist greenhouse air, exchanging heat between the two airflows. Based on the results of Campen et al. (2003), a ventilator capacity of 0.01 m3 s^{-1} is sufficient for all crops. The energy needed to operate the ventilators is not considered; an experimental study (Speetjens, 2001) showed the energy consumption by the ventilators to be less than 1 percent of the energy saved.

e) Anti-drop covering materials

The use of anti-drop covering materials is an alternative technology for greenhouse dehumidification. “Anti-dripping” films contain special additives which eliminate droplets and form instead a continuous thin layer of water running down the sides. The search for anti-drip cover materials has been mainly focused on the optical properties of the cover materials.

When should dehumidification take place?

- Dusk: Reduce humidity to 70–80% as night falls to prevent condensation.
- Dawn: Reduce humidity to prevent condensation, and jumpstart transpiration as the sun rises.

1.5. Rational use of energy and renewable energy sources

Rational energy use is fundamental since energy accounts for a substantial proportion of total production costs. Increase in production per unit of energy (energy efficiency) can be achieved through reduction of energy use and/or improvement of production. The major challenge in greenhouse operation is to find ways to contribute to improved energy efficiency combined with an absolute reduction of the overall energy consumption.

In general, the Mediterranean and north European regions have similar objectives with respect to optimizing production efficiency:

- autumn/winter – maximize the radiation quantity and minimize the energy loss;
- spring/summer – reduce high temperatures.

For rational use of energy (or fossil fuels) and reduction of greenhouse energy consumption, greater investment is required in order to achieve:

- efficient use of energy (i.e. amount of product per input of energy);
- reduction of energy requirement; and
- replacement of fossil fuels by more sustainable sources.

1.5.1. Energy-efficient climate control

Rational use of energy largely depends on energy-efficient greenhouse environmental control, which requires knowledge of the physiological processes (photosynthesis and transpiration, crop growth and development) in relation to the various environmental factors (temperature, light, humidity and carbon dioxide). However, to achieve the maximum benefits of energy-efficient environmental control, it is essential that the greenhouse itself and the control equipment (heating and ventilation system, CO2 supply, lighting) are properly designed and frequently checked (at least at the start and once during the growth season). For example, optimized designs of pipe heating systems may prevent uneven temperature distribution and subsequent loss of energy and crop production.

1.5.1.1.Temperature control

a. Wind-dependent heating

One way to substantially reduce energy use is to lower heating temperatures: a 1 °C reduction gives an energy saving of around 10 percent. However, lowering temperature slows down growth and development of most crops and may significantly reduce quality. Thus a lower heating temperature will save energy,but is generally not economically feasible as it results in reduced crop production which is not usually compensated for by the lower energy costs. A more economic application of reduced heating temperatures is wind-dependent temperature control. Heat losses increase linearly as wind speed increases, therefore, energy can be saved by reducing the heating setpoints when it is windy and compensating for this using increased temperatures at low wind speeds. This method results in energy savings of 5–10 percent.

b. Temperature integration

Another option for energy-efficient temperature control is the so-called temperature integration (TI) method. This method is based on the fact that the effect of temperature on crop growth and production depends on the 24-hour average temperature rather than distinct day/night temperatures (de Koning, 1988). However, there are limits to this approach and plants have to be grown within the sub- and supra-optimal temperatures (e.g. tomato: > 15 °C and < 30 °C, and chrysanthemum: > 14 °C and < 24 °C) to prevent reduced quality and/or production levels due to poor fruit or flower development.

In general, application of TI leads to higher temperatures during daytime and lower temperatures at night. However, the approach of using higher ventilation set points can also be combined with the use of lower day heating set points and higher temperatures under thermal screens at night. The aim is to fully exploit solar gain and, when additional heat is required, to add it preferably at night when heat losses are limited due to the closed thermal screen. There are potential energy savings of up to 20 percent; Rijsdijk and Vogelezang (2000) demonstrated an 18 percent energy saving in pot plants, rose and sweet pepper with a band width of 8 °C. However, when setting band widths for temperature integration, a balance must be found between maximizing energy savings and minimizing detrimental effects on yield or quality. The balance varies enormously depending on the crop,so specific crop knowledge is required.

1.5.1.2.Humidity control

On a year round basis, a major fraction of the energy transfer from the greenhouse to the environment is by natural ventilation. Under relatively low radiation and moderate ambient temperatures, natural or forced ventilation is generally used to prevent high humidity. Consequently a substantial fraction (5–20%) of the total energy consumption is related to

humidity control. Although high humidity is generally associated with increased risk of fungal diseases and reduced quality (e.g. Botrytis, blossom end rot), it may also be positive for crop production and quality (Montero, 2006). Reducing the level of humidity of the air is costly as a result of the energy required and should be assessed against the added value of the crop. An increase in the humidity setpoint of 5 percent decreases the energy consumption by approximately 6 percent. To reduce "humidity control related" energy consumption, there are several options:

- higher humidity setpoints
- reduction of the transpiration level of the crop
- active dehumidification with heat recovery

1.5.1.3.Thermal screens

Energy-efficient thermal screen control involves achieving a balance between the production and quality effects related to humidity and light, and energy saving. Energy-efficient (humidity) screen control can be achieved by opening the screen prior to the ventilators to maintain a given humidity setpoint. By closing the screen at night, an additional energy saving (4%) can be obtained without any production losses if the opening of the screen is delayed until radiation levels are outside 50–150 Wm-2; the heat exchange of the greenhouse is thereby reduced for a longer period during the early morning hours (Figure 1.14).

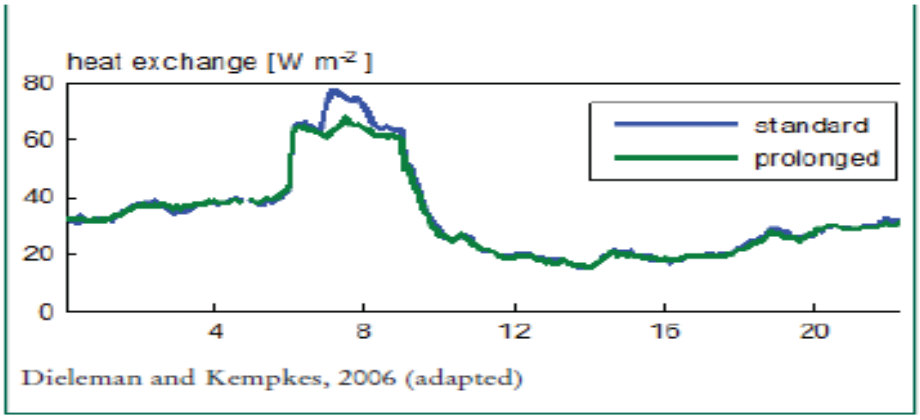

Figure 1.14 *Heat exchange (Wm-²) of greenhouse with thermal screen opening at sunrise (standard) or a delayed opening at outside radiation level of 50Wm-²* **.**

1.5.1.4.Reduction of transpiration

Reduction of transpiration may have positive effects on energy efficiency since lower transpiring crops bring less water into the air and therefore require less energy for humidity control under low irradiation conditions (Figure 1.15). Higher CO2 levels, by decreasing stomatal conductance and thus transpiration, may also improve energy efficiency by 5–10 percent without affecting photosynthesis or growth. Controlled reduction of the leaf area for crops with a high leaf area index, such as pepper, may reduce energy use without any impact on production. Halving the leaf area by removing old leaves in tomatoes resulted in a 30 percent reduction in transpiration with no detrimental effect on crop yields (Adams et al., 2002).

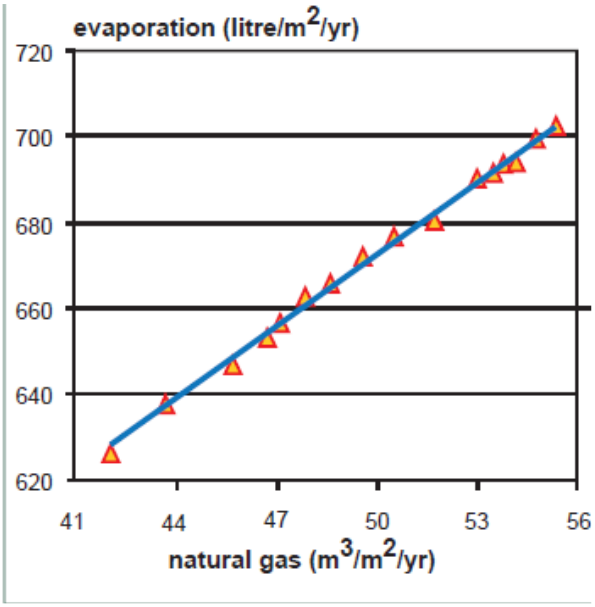

Figure 1.15 *Relation between yearly evaporation and energy use for a traditionally grown tomato crop under northwestern European conditions*

1.5.1.5.Crop-based environmental control

Operational control should not aim at individual environmental factors (temperature, humidity, CO2) but at energy-efficient crop production and quality control, taking into account the impact of control actions on both crop production and energy consumption. While this (model-based) approach has been under research since the early 1980s, its practical application in on-line control of greenhouses remains limited because it requires the enduser to adopt an entirely new approach and abandon current practices.

1.6. Replacement of fossil fuel by other sustainable sources

As CO2 emission is directly related to the use of fossil fuels for heating and cooling greenhouses, alternatives (e.g. solar and geothermal energy, biomass and waste heat) can significantly help achieve the reduced CO_2 emission targets. Using waste heat and CO_2 supply from combined heat and power generators (CHP) and feeding the electricity to the national grid can save a significant fraction of fossil fuel. While energy is not directly saved at greenhouse level, CHP reduces CO_2 emission at national level by reducing the CO_2 emission of the central power plants.

However, the economically feasible application of CHP largely depends on the local situation. Sometimes it is not allowed or is not technically feasible to feed electricity into the national grid, or the price of electricity is (too) low. Standalone use of CHP (for electricity used at greenhouse farm level) is only an option in large-scale greenhouses and requires solutions for the imbalance between the not-synchronized heat and power use at farm level, for example, using heat storage systems.

Biomass and anaerobic digestion are good alternatives for fossil fuel but the availability and massive quantities needed and uncertainty about the energy content are major drawbacks for large-scale application. For example, a 1-MW biomass source may require up to 2 500 tonnes of dry mass per year. This not only requires significant investments but also logistic solutions and the availability of this biomass in the surrounding area. Furthermore, the continuity of the

biomass supply may be a problem as the storage of required amounts of gas is almost impossible. With regard to CO2 from this gas, special attention should be paid to pollution aspects after burning components like SO2/SO3 and NOx may seriously damage the crop. However, for small-scale application and stand-alone greenhouses without connection to energy infrastructure, it may be a valid option.

Depending on the geology of the area, geothermal energy (water temperatures > 60 °C) is a promising alternative. Large (volcanic) areas in the world (e.g. Turkey) have geothermal potential which can be economically feasible for greenhouse heating but so far the number of geothermal heated greenhouses is limited, primarily because of the high financial risks related to drilling the hot water well. In the Netherlands a geothermal source (water 65 °C, depth 1 700 m) for greenhouse heating required an investment of about € 5.5 million (price level 2007). The total costs, however, can differ greatly as in other areas of the world geothermal energy is available at lesser depths. For the economic application of deep geothermal energy, in general a large greenhouse area (> 20 ha) has to be connected to the source.

Chapter 2:

Bibliographic Analysis on the microclimate of the greenhouse and feasibility of a water recovery system.

2.1. Introduction

By utilizing advanced CFD modeling embedded with transport models and user defined functions, it can be possible to simulate and evaluate complex phenomena that govern the environmental variables and interactions in greenhouses. Once validated, these models may be used as a tool to for design optimizations, installations, and operations for a given greenhouse design, climate, ventilation configuration, and control strategy. CFD techniques numerically solve the Navier-Stokes equation, mass and energy conservation equation and other activated equations, using a finite volume numerical scheme.

Mistriotis et al. (1997) used CFD to study greenhouse ventilation to provide greenhouse ventilation systems with maximum efficiency and optimum vent configuration while using different turbulence models. Kacira et al. (1998) used CFD modeling to determine air exchange rates for sawtooth greenhouses and compared the results to the existing standards of design at the time. CFD has also been used to simulate radiative exchanges between greenhouse surfaces, including the effect of radiation on a crop, as performed by Boulard and Wang (2002) who created a radiation-dependent user defined function to simulate evapotranspiration through water and energy balances. Nebbali et al. (2012) used a similar approach to analyze radiative and convective conditions within a canopy active with evapotranspiration. To simulate the effect of the crop on the airflow patterns, many researchers have assumed the crop to be a porous media with sufficient validation (Molina-Aiz et al., 2004; Bartzanas et al., 2004). In regards to humidity, Sapounas et al. (2007) used an integrated species transport model to calculate water mass fraction throughout a simulated greenhouse domain.[12]

In this chapter we are going to review CFD researches undertaken and then adopt the methodology for our current work.

.

2.2. Modelling of Heat Distribution and Air Turbulent Flow inside a Greenhouse at Different Air Flow Rates

2.2.1. Introduction

The greenhouse microclimate provides the plants with good environmental conditions for growing, one of which is the inside air temperature. This temperature is the result of complex and interactive heat and mass exchanges between the inside air and the several elements of the greenhouse (construction, vegetation, etc.) and the outside boundaries (outside air, sky, solar radiation). Computational fluid dynamics is a simulation tool which has emerged from the development stage and is now a robust design tool. It is widely used to study the behaviour of all kinds of transport processes which involve fluid flow, heat and mass transfer.

The CFD method allows the explicit calculation of all physical variables of a flow (pressure, velocity, temperature, etc.) by numerically solving the corresponding transport equations,. In a flow field, the continuity equation and the three momentum equations describe the velocity components and the pressure as functions of time and space. When energy is transported, an extra equation describes the temperature field. Solving analytically the set of continuity, momentum and energy equations is only possible for limited cases such as the laminar flow. The use of numerical techniques is indispensable for problems with more complex nature involving turbulence. It was concluded that the temperature distribution in greenhouse is one

of the factors that influence the uniformity of crop growth and was remarked that not much work has been published on the temperature and humidity distribution within a naturally ventilated greenhouse. A study on airflow resistance of greenhouses ventilators with and without insect screens had been conducted in temperate region.They focused on the measurement of discharge coefficient of ventilation openings with and without flaps. An integrated study on the effect of wind speed, wind angle and vent openings angle (type of design vents) on air exchange rate and temperature rise for a 7.2 × 7.2 m, single-span greenhouse had been carried out by Kozai et al., They reported that air exchange in single-span houses did not appear to vary remarkably, but with a continued wind velocity increase, air changes increased linearly except where the wind angle was parallel to the greenhouse length. About 60 air changes per hour were generally considered necessary to avoid heating above the outside air temperature or extreme temperature rise inside the greenhouse. Another study conducted by Albright, [2] mentioned that in bright sunshine, air temperature inside the greenhouse is a function of vent area as percentage of floor area. Indoor air temperature does not begin to approach outdoor air temperature until vent area (both roof and side wall) is more than 10% of floor area. A greenhouse which is not able to maintain the inside temperature within 5 to 6 °C of outside air temperature is considered to be performing poorly in terms of ventilation. The adoption of roof ventilated greenhouse or the combination of both roof and side wall opening ventilation is widely used and more appropriate for humid tropic greenhouses. This allows better air exchange rate between inside and outside the greenhouse condition as a result that the microclimate inside the greenhouse is expected to be close to the ambient temperature. The best way to achieve this goal is to keep the ratio of ventilation opening to floor area to be as large as possible Von Zabeltitz, [13].

2.2.2. Model Equations

FLUENT® is used to solve the differential equations governing the transport of mass, three momentum components, and energy in 3D configurations under steady conditions the different governing partial differential equations are typically expressed in a general form as

$$\frac{\partial}{\partial x}\rho U\Phi + \frac{\partial}{\partial y}\rho V\Phi + \frac{\partial}{\partial z}\rho W\Phi = \frac{\partial}{\partial x}\left(\Gamma_{\Phi,eff}\frac{\partial \Phi}{\partial x}\right) + \frac{\partial}{\partial y}\left(\Gamma_{\Phi,eff}\frac{\partial \Phi}{\partial y}\right) + \frac{\partial}{\partial z}\left(\Gamma_{\Phi,eff}\frac{\partial \Phi}{\partial z}\right) + S_{\Phi}$$

Where: ρ = Air density, kg/m^3

Φ = Dependent variable

S_Φ = Source term of Φ

$\Gamma_{\Phi,\text{eff}}$ = Effective diffusion coefficient.

U, V, W =Velocity vectors.

The effective diffusion coefficients and source terms for the various differential equations are listed in the following table1. Turbulence model of Launder et al., was incorporated in the present work. Details of the modeling technique and assumptions can be found in references Launder et al, to Nielsen.

2.2.3. Computational Technique

Over 260 000 tetrahedral computational cells were used to map the greenhouse interior, the minimum computational volume was 8.11e-10 m^3 and the maximum volume 1.19e-03 m^3. The minimum cell face area 1.199e-0^6 (m2) and the maximum face area 2.89e-02(m2). Computational grid conducted in greenhouses of sizes 1.6 m x 2.4 m x 1.2 m (W x L x H). Figure 2.1 illustrates the layout of the greenhouse. To study the effect of roof opening on spatial distribution of air-temperature two cases were considered. Case A, where both inlet and outlet roof opening are close together as shown in figure 2.2. Case B, where the distance between the inlet and outlet roof opening is half the span as shown in figure 2.3. Main parameters and data used in the present study are summarized in table 2.2.

Table 2.1: Terms of Partial Differential Equations (PDE)

	Φ	$\Gamma_{\Phi,eff}$	S_Φ
Continuity	1	0	0
X-momentum	U	μ_{eff}	$-\partial P/\partial x + \rho g_x$
Y-momentum	V	μ_{eff}	$-\partial P/\partial y + \rho g_y(1+\beta\Delta t)$
Z-momentum	W	μ_{eff}	$-\partial P/\partial z + \rho g_z$
H-equation	H	μ_{eff}/σ_H	SH
k-equation	K	μ_{eff}/σ_k	G - $\rho\,\varepsilon$
ε-equation	ε	$\mu_{eff}/\sigma\varepsilon$	C1 ε G/k – C2 ρ ε2/k

$\mu_{eff} = \mu_{lam} + \mu_t$ $\qquad$ $\mu_t = \rho\, C\mu\, k2 / \varepsilon$

$G = \mu_t [2\{(\partial U/\partial x)^2 + (\partial V/\partial y)^2 + (\partial W/\partial z)^2\} + (\partial U/\partial y + \partial V/\partial x)^2 + (\partial V/\partial z + \partial W/\partial y)^2 + (\partial U/\partial z + \partial W/\partial x)^2]$

$C_1 = 1.44$, $C_2 = 1.92$, $C_\mu = 0.09$

$\sigma_H = 0.9$, $\sigma_\tau = 0.9$, $\sigma_k = 0.9$, $\sigma_\varepsilon = 1.225$

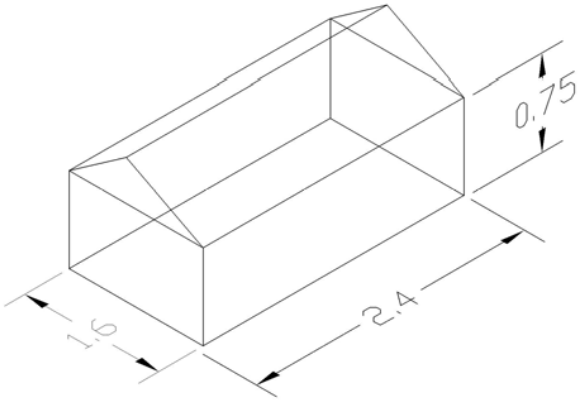

Figure 2.1 Layout of the greenhouse

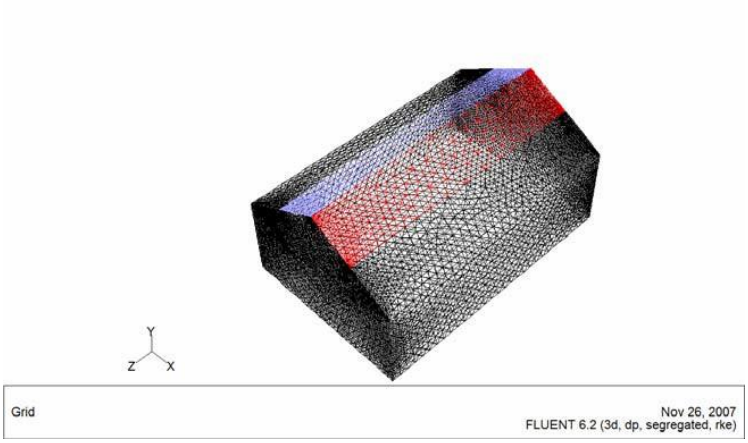

Figure 2.2 Computational grid of Case A

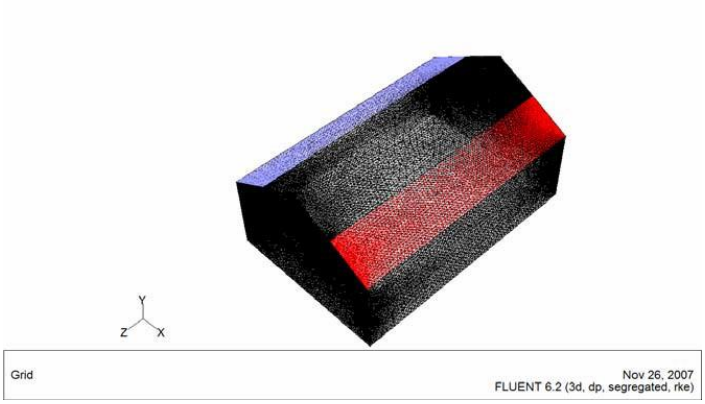

Figure2. 3 Computational grid of Case B

Table 2.2 Constant main input values for the 3- dimensional CFD model

Factor	**Value**
Roof cover temperature	40°C
Side wall temperature	40°C
Inside ground temperature	43°C
Temperature of inlet (outside) air	27°C
Density of inlet air	1.225 kg/m³
Viscosity of inlet air	1.97E-05 kg/m·s
Specific heat of inlet air	1007.2 J/kg·°C
Turbulence intensity	5%

2.2.4. Results and Discussion

The comparison in figure 2.4 and 2.5 for the predicted air distribution at different opening locations show that the velocity reach about 50% of the maximum velocity magnitude at about 0.6 m above the ground in the vertical plane at the middle of greenhouse .Region of secondary vortices appear near the ground area for both east and west side walls. At west wall below the opening inlet area the velocity decreases more rapidly than the east side due to the jet of air strike the east wall before leaving the greenhouse.

In the other hand the static pressure distribution with the opening area locations for both cases are shown in figure 2.5.In case A the maximum pressure coefficient appears towards all the east wall while in case B the maximum pressure coefficient occupy east corner near the ground.

The air velocity distribution contours for case B as well as the pressure coefficient distribution became more symmetric than that in case A and the secondary vortices nearly vanished in the east wall and directed to the west corner above the ground. It is also noticed that an area of low velocity distribution is created under the roof between the inlet and exit opening in case B.

Air temperature distribution is illustrated in figure 6. In case A the minimum temperature is located at the opening and towards east wall, in the west wall the temperature increases from the roof till its maximum value at the ground due to the secondary vortices. In west side wall temperature decrease with increasing in velocity magnitude the temperature distribution in case B became more symmetric about the mid plane, the minimum temperature occupy most of greenhouse except near the corner above the ground and under the roof opening.

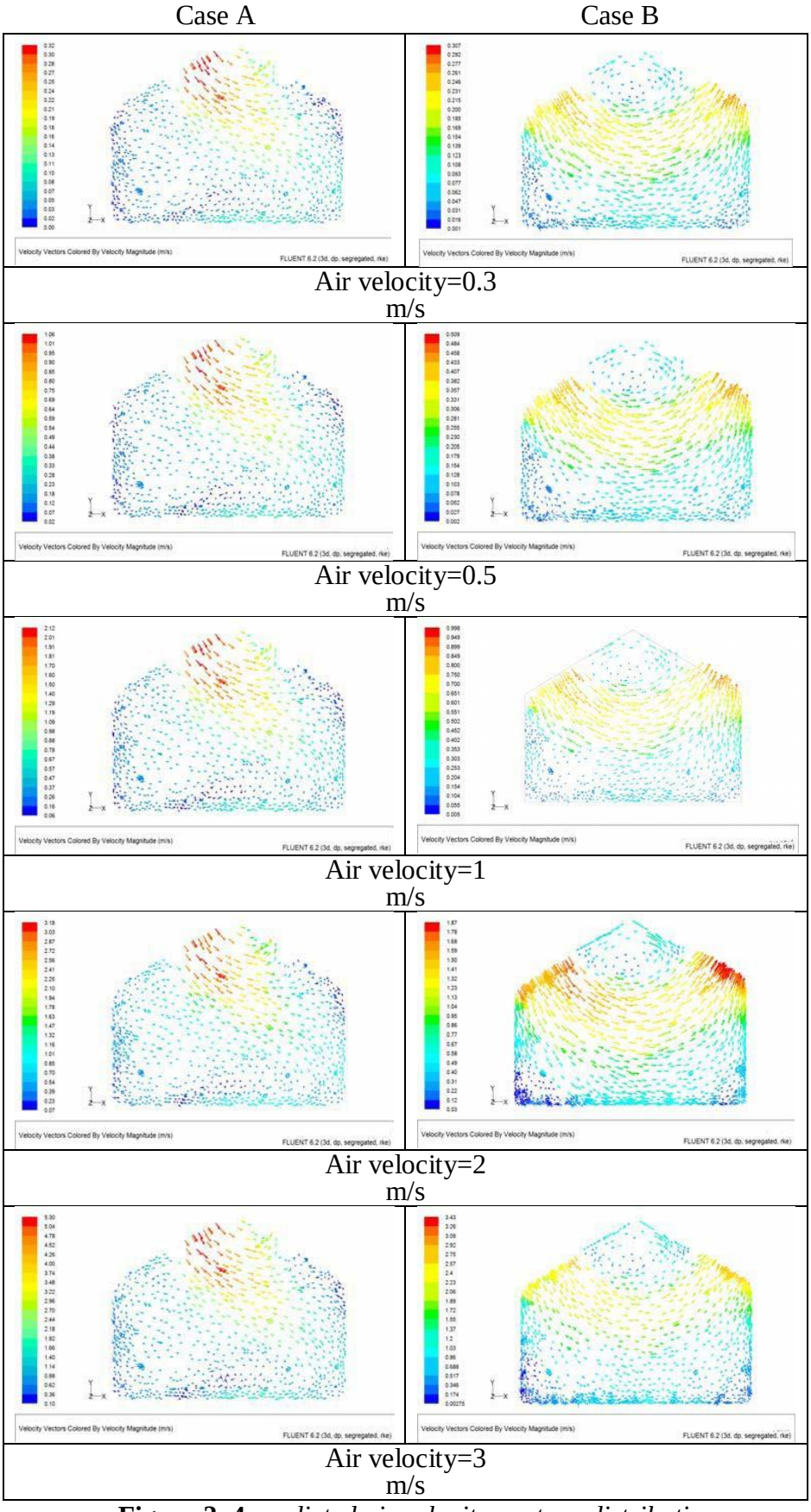

Figure 2. 4 *predicted air velocity contour distribution for different flow velocities at vertical plane at z=1.2m*

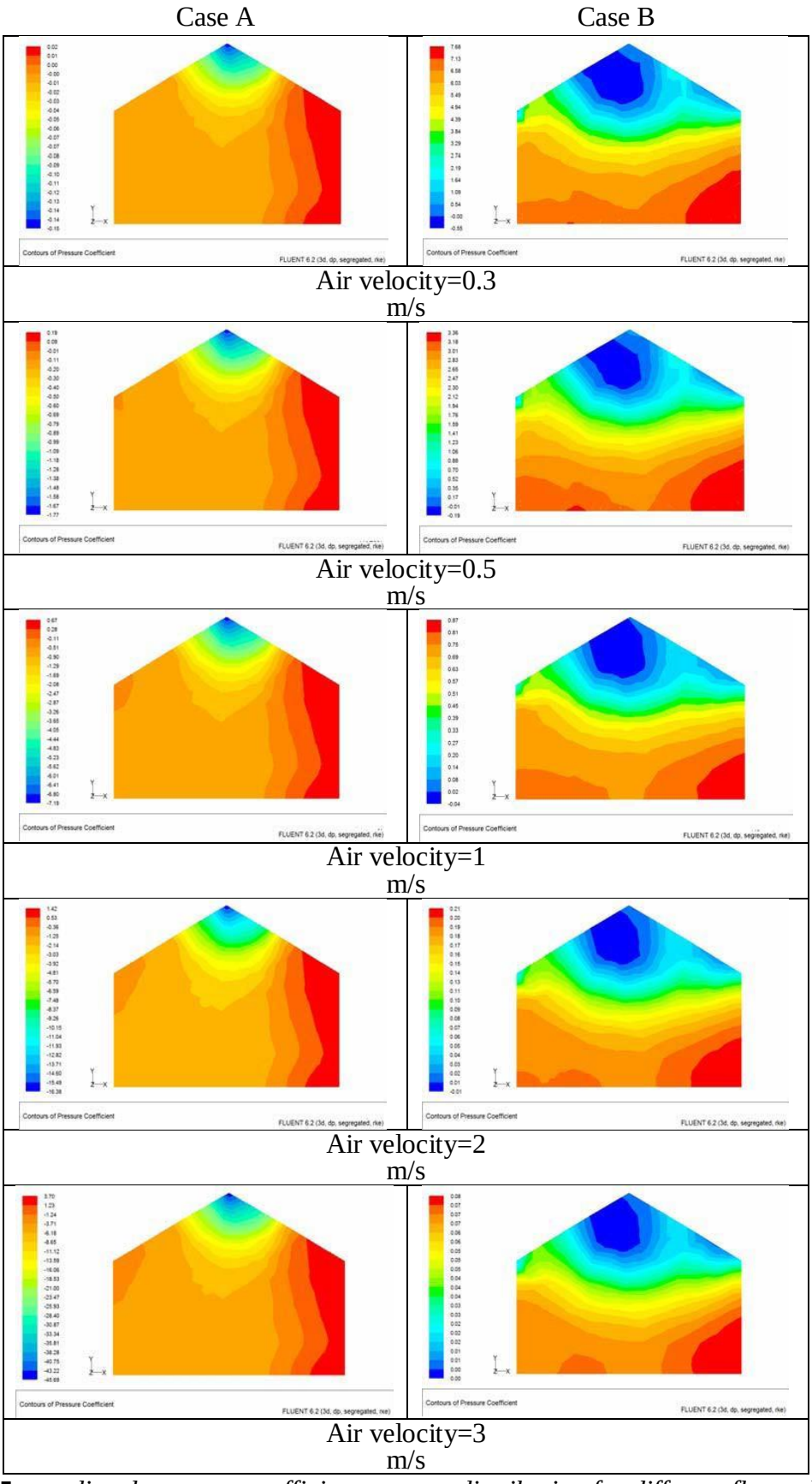

Figure 2.5 *predicted pressure coefficient contour distribution for different flow velocities at vertical plane at z=1.2m*

Case A **Case B**

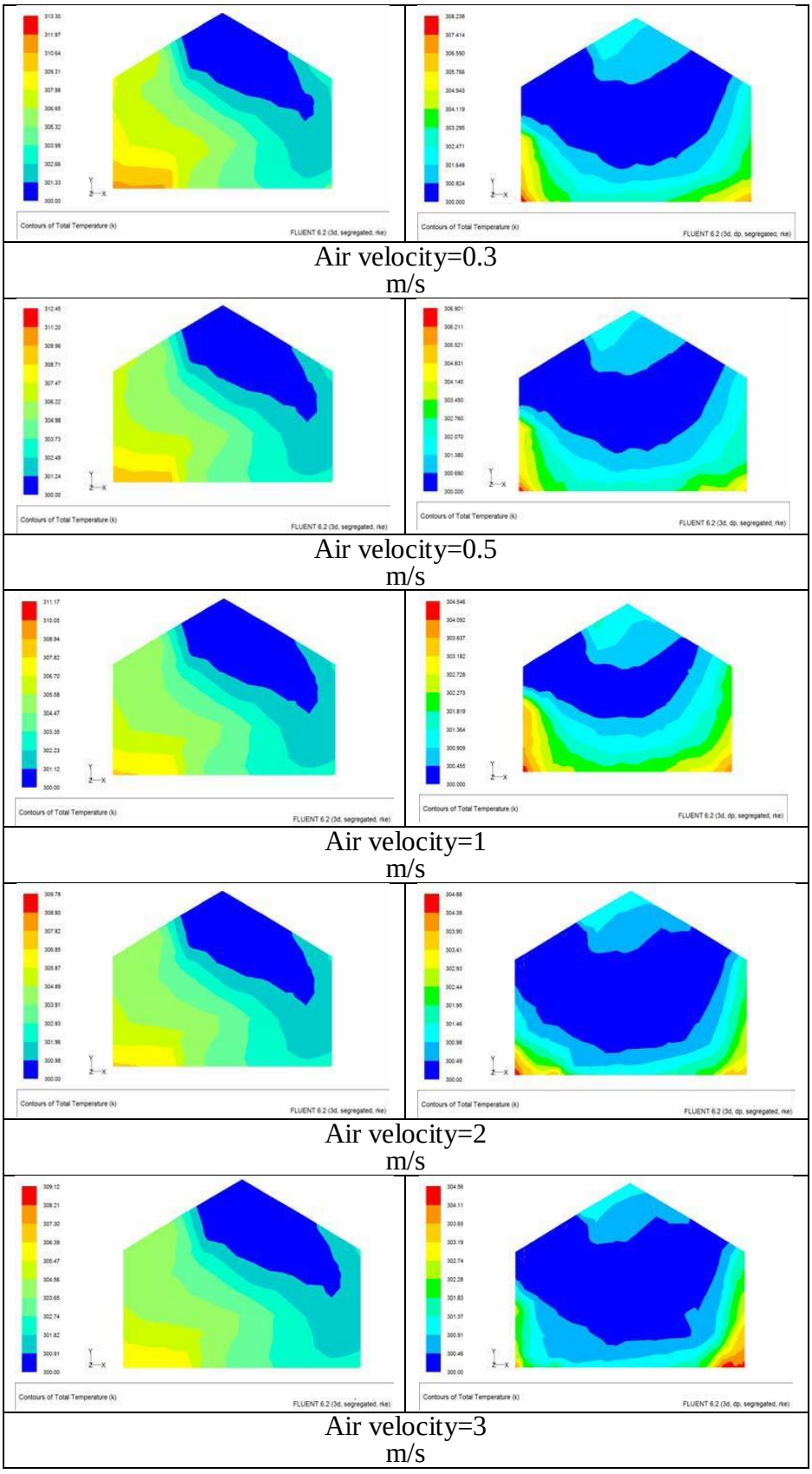

Figure2.6 *predicted air temperature contour distribution for different flow velocities at vertical plane at z=1.2m*

2.2.5. Concluding Remarks

In this paper, the effects of roof vent location and the change in air velocity inlet on natural ventilation and airflow characteristics of greenhouses which are becoming popular in Egypt were studied by numerical simulations using the CFD approach. From the previous results, it can be concluded that the location of airside openings have a strong influence on the velocity and temperature distribution and consequently on the emerging greenhouse air distribution. The location and intensity of secondary vortices affected the temperature distribution in both cases. One must take into account that the numerical results discussed in the present paper were obtained in empty greenhouses. Thus, they offer an image of the ventilation process in a greenhouse without the effects the plants and the internal structural elements that may also change the internal airflow patterns.

2.3. Greenhouse Water Recovery System for Crop Production in Semi-Arid Climate

2.3.1. Experiment Description

The ultimate goal of this project is to study the feasibility of installing water recovery system in the direction of saving water and energy in greenhouse crop production. This study attempts to contribute to development of a new greenhouse technology which helps saving water and to demonstrate the future water saving crop production in semi-Arid Lands. Specifically, this experiment to report the theoretical evaluation of the condenser capacity in a typical commercial greenhouse setting under semi-arid climate

2.3.2. Materials and Methods

Modeling and Simulation of Condensation

Over the cooling coil surface inside the condenser unit, water is condensed when moist air is cooled to a temperature below its dew point. In our simple model, the incoming moist air (State 1) passes through the cooling coil, uniformly processed and exits from the condenser (State 2). The condensed water could be extracted at various temperatures ranging from the initial dew point of the moist air of State 1 to the final saturation temperature; however it is assumed that condensed water is cooled to the temperature equal to the temperature of the exit air before it comes out of the system. Coolant or chilled water (State 1) enters the cooling coil and exits with a temperature rise (State 2) as a result of the energy gain in the condensation process (Fig.2. 7).

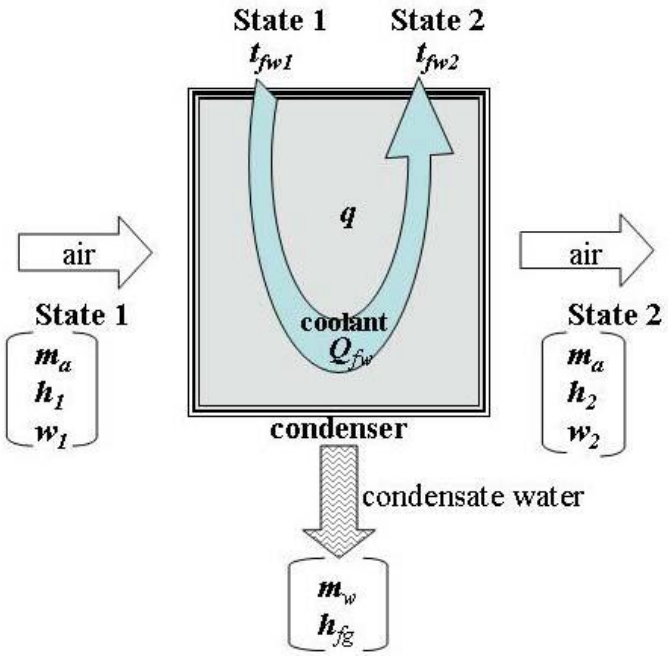

Note: the symbols are defined in nomenclature section

Figure. 2.7. Simple diagram of condenser and related variables in its energy and mass balance.

During the condensation process from State 1 to State 2 of the air and the water, there is a steady state energy balance and mass balance between the air and water flows when the heat is transferred from the warm air to the cool water at the condenser. Initial energy content of the moist air of State 1 is expressed using its enthalpy (h_1) and the dry mass of the air (m_a). After the condensation process, a portion of initial energy is transferred in forms of sensible (q_s) and latent heat ($m_w \cdot h_{fg}$). Therefore,

$$m_a \cdot h_1 = ma \cdot h_2 + q \qquad (1)$$

where h_1 and h_2 are the enthalpy of air of State 1 and State 2, and the total heat transfer (q) is the sum of sensible heat transfer (q_s) and latent heat transfer $(m_w \cdot h_{fg})$.
The total heat transfer (q) in the air was equal to that in the coolant water in the condenser; thus:

$$m_a \cdot dh_{air} = m_{fw}\, C_{fw}\, dt_{fw} \qquad (2)$$

which is rewritten as shown below, using specific heat (C_{air}, C_{fw}) and density ($\rho_{air,}, \rho_w$) of the air and water and their mass flow rates (Q_{air}, Q_{fw}) :

$$\rho_{air}\, Q_{air} \cdot dh_{air} = C_{fw}\, \rho_{fw}, Q_{fw} \cdot dt_{t\,w} \qquad (3)$$

For maximum condensation conditions, t_{fw2} will be equal to air dew point temperature (t_{dp}). Therefore the temperature drop in the coolant water (dt_w) was expressed as:

$$dt_{t_w} = t_{Iw\,2} - t_{Iw\,1} = t_{dp} - t_{fw\,1} \qquad (4)$$

From rearranging Eq (3), h_2 is now expressed as:

$$h_2 = h_1 - \left[\left(C_{fw}\rho_{fw}Q_{fw} \cdot dt_{fw}\right)/(\rho_{\text{air}} \cdot Q_{\text{air}})\right] \qquad (5)$$

If we assumed that the State 2 air reaches 100% relative humidity (saturated humidity ratio), the dry bulb air temperature in State 2 could be obtained psychometrically by solving the following equation:

$$h_2 = (1.006 \cdot t_{\text{air2}}) + w_2 \cdot (2501 + 1.805 \cdot t_{\text{air2}}) \qquad (6)$$

Where $t_{\text{air 2}}$ is the dry bulb temperature of State 2 that reaches 100% relative humidity (State d in **Fig. 2.8**) and w_2 is the humidity ratio (saturated humidity ratio) at the dry bulb temperature. The $t_{\text{air 2}}$ at 100% relative humidity is called the apparatus dew point temperature of cooling coil (t_d) (**Fig 2.9**).

In the real process (**Fig. 2.8 and 2.9**), not all air passing through the condenser is cooled to the surface temperature. Some portions of the air will be brought to saturation at the apparatus dew point temperature of cooling coil (t_d), whereas the remaining air bypassed the condenser. The final state (State 2) is considered as the adiabatic mixture of the bypassed air (from State 1 and the saturated air at State d in Fig.2.8 and 2.9). For this reason, Bypass Factor (BF) is also commonly used to express the cooling coils efficiency.

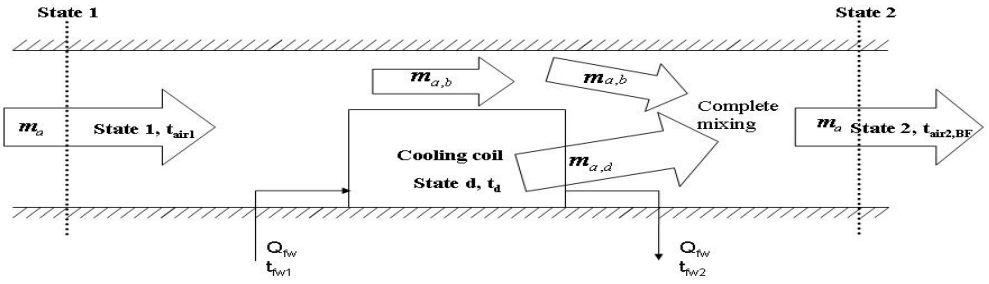

Figure 2.8 *Schematic representation of bypass factor approach for condensation process (afterKuehn et al. (1998)).*

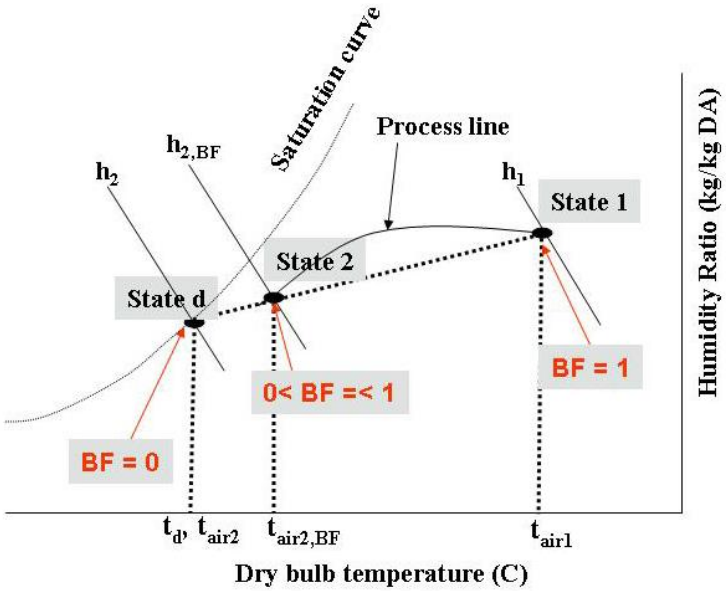

Figure 2.9 *Schematic psychometric chart of bypass factor approach for condensation process (after Kuehn et al. (1998)).*

Bypass Factor (BF, dimensionless) was defined as the proportion of the bypassing air $(m_{a,b})$ to the total of air (m_a)

$$BF = m_{a,b}/m_a \quad (7)$$

Applying the adiabatic process equation

$$t_{\text{air }2,BF} = (m_{a,d}/m_a) \cdot t_d + (m_{a,b}/m_a) \cdot t_{\text{air }1} \quad (8)$$

Therefore

$$t_{air2,BF} = (m_{a,d}/m_a) \cdot t_d + (m_{a,b}/m_a) \cdot t_{\text{air1}} \quad (9)$$

From Eq (7) and Eq (9), thus

$$t_{\text{air }2,BF} = t_d + BF \cdot (t_{\text{air }1} - t_d) \quad (10)$$

where $t_{\text{air }2,BF}$ is dry bulb temperature of State 2 air with a given BF (Fig. 2.9) and t_d is an apparatus dew point temperature of cooling coil and is always referred under $\text{BF} = 0$ condition (maximum condensation) (Kuehn et al.,1998).

If every portion of the air passing through the cooling coil contributes energy gain to the water (coolant), the temperature increases from t_{w1} to $\text{t}_{\text{dp.}}$ But, we know that not all portion of the air contributes to the heat exchange, and therefore t_{iw2} is lower than $\text{t}_{\text{dp.}}$ The enthalpy of State2 with a given BF $(\text{h}_{\text{2,BF}})$ is now expressed as follows, considering BF of the condenser (Fig.3).

$$h_{2,BF} = BF \cdot (h_1 - h_2) + h_2 \quad (11)$$

The water-air heat exchange equation in Eq (3) is modified to represent the enthalpy of the air of State 2 with a given BF.

$$\rho_{\text{air}}\, Q_{\text{air}} \left(h_1 - h_{2,BF}\right) = C_{fw} \cdot \rho_{fw} \cdot Q_{\text{fw}} \left(t_{\text{fw}\,2} - t_{\text{fw}1}\right) \qquad (12)$$

Therefore,

$$t_{\text{fw}\,2} = \left[\rho_{\text{air}} \cdot Q_{\text{air}} \left(h_1 - h_{2,BF}\right)/C_{fw} \cdot \rho_{fw} \cdot Q_{\text{fw}}\right] + t_{\text{fw}\,1} \qquad (13)$$

The sensible heat transfer $(\mathrm{q_s})$ of condenser unit (including bypass factor) is

$$q_s = C_{\text{air}} \cdot \rho_{\text{air}} \cdot Q_{\text{air}} \cdot \left(t_{\text{air}\,1} - t_{\text{air}\,2,BF}\right) \qquad (14)$$

The total heat transfer (q) of condenser unit (including bypass factor) was computed by using sensible heat ratio (SHR) and sensible heat transfer$(\mathrm{q_s})$.

$$q = q_s/SHR \qquad (15)$$

where SHR is calculated from $\mathrm{SHR} = \mathrm{C_{air}} \cdot [(\mathrm{t_d} - \mathrm{t_{air1}})/(\mathrm{h_d} - \mathrm{h_1})]$, where $\mathrm{t_d}$ and $\mathrm{h_d}$ can be computed
from Eq (6) and Eq (5), respectively (where $t_{\text{air2}} = t_d$ and $h_2 = h_d$). Since SHR was independent from efficiency, sensible heat ratio (SHR) was computed under the maximum condensation condition.

The latent heat transfer (qu) was delivered by subtracting total heat transfer (q), which can be computed from Eq (15), with sensible heat transfer (q_s) from Eq (14).

$$q_L = q - q_s \qquad (16)$$

For estimating condensation rate $(\mathrm{m_w}, \mathrm{kg \cdot s^{-1}})$, we introduced the following equation

$$m_w = q_L/h_{fg} \qquad (17)$$

where $\mathrm{h_{fg}}$ is the enthalpy of condensation of feed water temperature to the condenser $(\mathrm{t_{fw1}})$.

2.3.3. Experimental setup:

A small testing system, consisting of a condenser unit, an air guide and sensors, was built and located inside a double-layer polyethylene film-covered arched-roof greenhouse (28 m L × 9.7 m W × 6.3 mH) (Tucson, AZ, USA) where mature tomato plants were grown hydroponically using a high-wire system. The overall dimension of the testing system was 1.42 m(L) × 0.55 m(W) × 0.55 m(H) and the entire system was placed on a platform 0.9 m above the ground. A re-circulating water chiller (VWR 1155, Poly Science Corporation, IL, USA) was used to control the temperature of the coolant water circulating through the condenser at a $0.0002\ \mathrm{m^3 \cdot s^{-1}}$ flow rate. The testing system had an air guide composed of transparent Plexiglas@) wall of 0.76 m before and 0.66 m after the condenser, attached to a variable speed fan (0.55 m × 0.55 m). The air guide had an access ports for the temperature and relative humidity sensors (CS500L, Campbell Scientific Inc., UT, USA) 0.13 m before and after the condenser. Smooth metal sheet was used as the duct at the end to

minimize frictional losses and created the testing unit long enough to ensure that air would not flow back to the flow enter. The air velocity (V_{air}) were measured using a hot-wire anemometer (A004, Kanomax Inc., NJ, USA) which was mounted in the access port 0.2 m away from the temperature and humidity probe and 0.36 m before the condenser surface. The structure of condenser was a cross flowtyped condenser with copper coiled and coated with aluminum fins. The dimension of condenser in the testing unit was 0.3 m$(\mathrm{L}) \times 0.3$ m$(\mathrm{W}) \times 0.08$ m(D). Two type-T $0.5-$ mm thermocouples were used for measuring the temperature of incoming water (t_{fw1}) and outgoing water (t_{f2}) of the condenser. All the sensors were connected to a data logger (CR10X, Campbell Scientific Inc., UT, USA) to scan the sensor readings every 1 second and record the average every minute. Three holes were drilled through the bottom metal frame of the condenser in order to drain the condensate water into a tray placed on an electrical balance below the condenser unit. The output from the balance was recorded using a PC with a RS-232 interface program.

2.3.4. Case studies: Potential of water recovery system from the air of semi-arid greenhouses

Sump water and dew point temperatures during summer in a typical commercial greenhouse in semi-arid climate: In collaboration with a Eurofresh Farms (Willcox, Arizona, USA), which operates 100 ha of greenhouse hydroponic crop production in Arizona, we monitored the sump water temperature and dew point temperature of the exhaust air from the greenhouse, necessary for the case study simulation. The company's Willcox operation (32 ° 27' 59.75" N, 109° 56' 20.34"W) had a total of six large Venlo-type glass greenhouse complexes. Each complex or "site" had 16 one-hectare greenhouse compartments to grow hydroponic tomatoes and cucumbers. Our sensors were located in one complex (third site from the east). The greenhouse compartment was 200 m$(\mathrm{L}) \times 48$ m$(\mathrm{W}) \times 5$ m (gutter height) filled with mature tomato plants grown using a high-wire system, oriented north-south. Evaporative cooling pad (200 m L $\times 1.5$ m W $\times 0.1$ mD) were located at either east or west side and the exhaust fans were located the other side. Tomato plant rows were north-south direction. There were 2 m(L) $x8$ m$(\mathrm{W}) \times 2$ m(D) sump tanks each serving for two compartments. The sump tanks were placed underground outside of the exhaust fans, and therefore, the distance between pad and sump was more than 46 m, connected underground.

Type-T thermocouples connected with CR10X data logger were used to collect the sump water temperature. Air temperature and relative humidity sensor (HOBO() H08-032-08 Pro, Onset computer Corp., MA, USA) were used to obtain exhaust air dew point temperature. All data at Eurofresh Farms were read every 30 seconds and averaged every 15 minutes from May to September 2006. All data during pre-monsoon and monsoon season were separately evaluated. Data obtained from the first date of measurement (May 16,2006) until the official monsoon start date (the first date of three consecutive days when the average daily dew point is $12.2°\mathrm{C}$ or greater) (July 4, 2006) were considered as a pre-monsoon season, and afterward until September 30, 2006 was considered as a monsoon season.

2.3.5. Simulation scenario

As our first step of feasibility study of installing condenser in a commercial greenhouse compartment, we selected the following design and assumptions to simulate condensation rates using the models (Eqs $1-17$) and the data collected from the Eurofresh Farms: 1) Greenhouse compartment size and design are the same as that in Eurofresh farms, 2) Condenser units are installed inside the greenhouse, before the air exhausted from the fans, 3). Total face area of condensers is equal to the evaporative cooling pad (200 m $\times 1.5$ m) which is installed the opposite side of the greenhouse, consisting of two hundreds of 1 m$(\mathrm{L}) \times$

1.5 m(W) × 0.08 m (D) condenser units, and 4) return water from the condenser was used elsewhere and does not affect the sump water temperature. The face air velocity (Vair) used in the simulation was 1 $m \cdot s^{-1}$, equal to the expected average air velocity at the windward side of evaporative cooling pad.

We tested two variables (BF and water flow rate to the condenser unit) in the simulation. The BF that we simulated was0.3,0.5, and 0.7, in addition to $0.92, \mathrm{BF}$ of our experimental condenser unit. The water flow rate was $0.003\ m^3 \cdot s^{-1}$ which is the equivalent flow rates for the condenser unit with face area 17 times greater than that of the condenser used in the experiment, and $0.006\ m^3 \cdot s^{-1}$, the twice of the equivalent flow rate. , The Berkley Madonna software simulated the amount of condensate water during average day of pre-monsoon and monsoon season for given configuration and dimension of condenser and face air data. The software allowed many parameters to be varied according to experimental conditions. Computation of psychometric equations such as saturated humidity ratio, specific volume, enthalpy and dew point temperature etc. were written in $C++$ and integrated into the Berkeley Madonna software as a plug-in function. Four major input data, dry bulb temperature(t_{air1}), relative humidity (RH_{in}), feed water temperature (t_{iw1}) and assuming bypass factor (BF) from a representative day of pre-monsoon and monsoon season were used in the condenser model to simulate condensation rate and also outgoing air properties.

2.3.6. Results

Comparison of theoretical condensation rates simulated using Eqs. (1)– (17) and experimental data of condensation rates from the small testing system was shown in Fig. 2.10(a). The result showed that the original model overestimated the condensation rate at all air velocities. The reason of overestimation is considered as inaccurate BF measured based on the air temperatures of State 1 and State 2 in the experiment. One of variables used for computing BF was data from air temperature and humidity sensor at outgoing air of condenser, which was placed only 0.13 m from the condenser. This sensor location may have provided incomplete mixing air measurement.

The BF was optimized so as to minimize the least square errors under each velocity condition. The bypass factor that gives the minimum error square was selected mathematically for each velocity. In this way, BF of 0.90, 0.92, 0.92, 0.94 and 0.94 for 0.4, 0.8, 1.2, 1.8, and 2.4 $m \cdot s^{-1}$ face air velocities, respectively were obtained. Simulated condensation rates using improved models with corrected BF value are shown in Fig. 2.10(b).

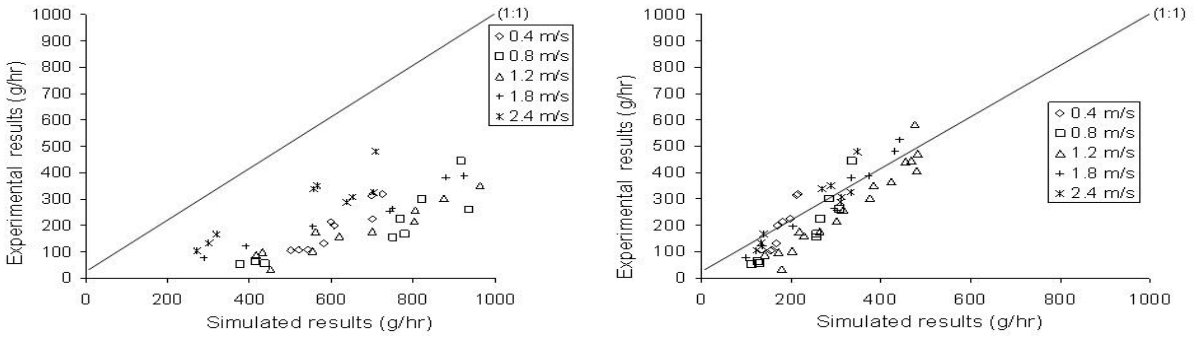

(a) **(b)**

Figure 2.10 *Condensation rates simulated with the original models (a) and the improved models with corrected bypass factor (b), compared with the greenhouse experiment data.*

In Figure 2.11, the result was shown that the actual and simulated outgoing water temperatures of condenser are close to each other. It was clearly shown that the model is reasonably accurate

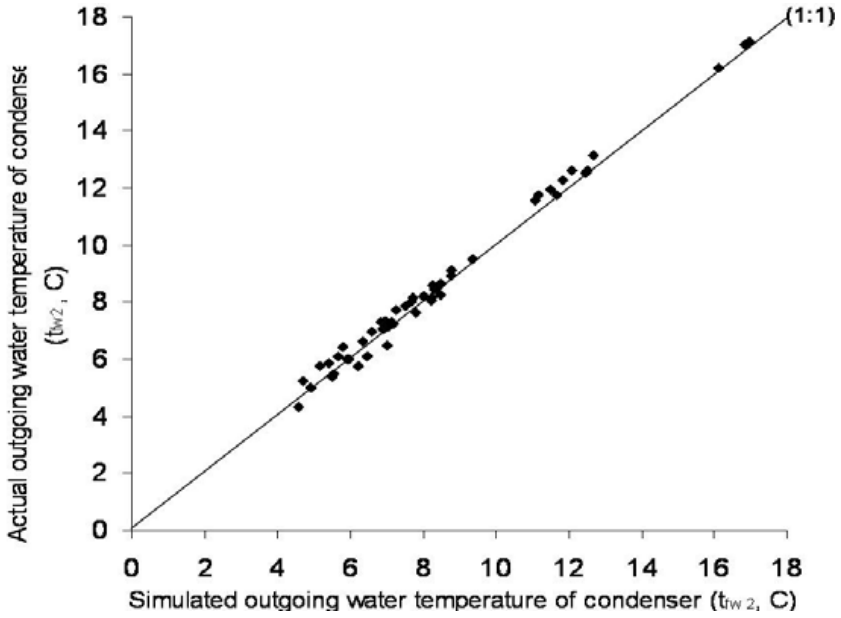

Figure 2.11 *Outgoing water temperature of condenser simulated with the improved model*

2.3.6.1.Sump water temperature and potential condensation rate

During the day, the raw data of sump water temperature remained lower than the dew point temperature of the greenhouse exhaust air by $3.3 - 12.3°C$ and $2.3 - 8.0°C$ in pre-monsoon (May to June 2006) and the monsoon season (July to September 2006), respectively (data not shown). The averaged diurnal fluctuations of both temperatures were shown in Fig. 6. In both pre-monsoon and monsoon seasons, the sump water temperature showed almost constant value through the day, but it was an average of 2.62 degree higher in monsoon than in premonsoon seasons. Also, the dew point temperature was higher during day time than night time, due to the evapotranspiration inside the greenhouse. During the monsoon season, the evaporative cooling pad performed less efficiently in more humid condition. Air with higher relative humidity (or more specifically, lower vapor pressure deficit) during monsoon season has a less capacity to absorb moisture causing the lower exchange rate of latent heat through the evaporation process. This results in smaller heat removal rate from the water on the pad. However, sump water temperature was still lower than dew point temperature, which shows some condensation capability even in the monsoon season (Fig.2.12).

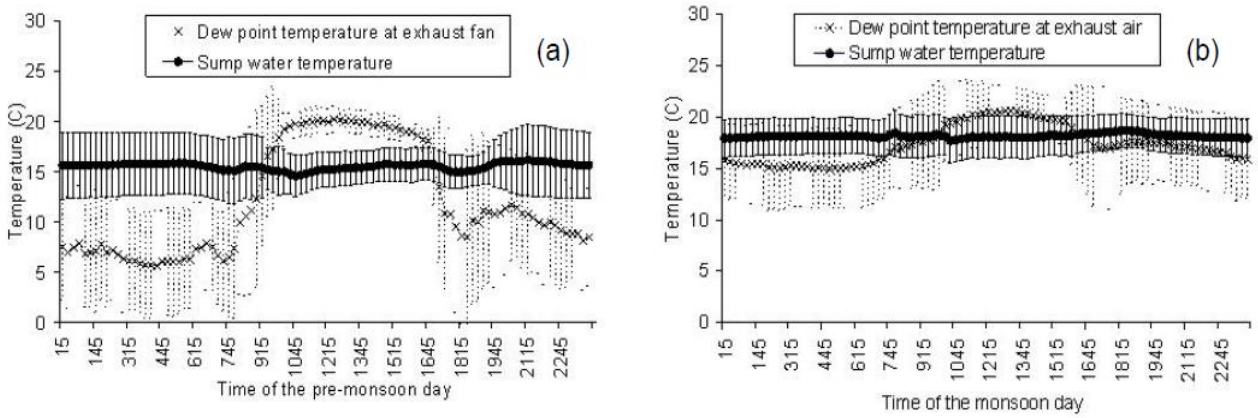

Figure 2.12 *Averaged diurnal changes in sump water temperature and dew point temperature of the exhaust air at a commercial greenhouse (Willcox, AZ, USA) during pre-monsoon (May 16 to July 4, 2007) (a) and monsoon (July 5 to September 30, 2007) (b) seasons*

In pre-monsoon and monsoon seasons, the overall simulated amount of condensate water increased when water flow rate in the cooling coil increased from 0.003 to 0.006 $m^3 \cdot s^{-1}$ in each condenser regardless of BF (**Fig. 2.13**). Less amount of water was condensed during the monsoon day because the ambient air outside was humid (average of 12.2°C and 17.5°C wet bulb temperature during the day in pre-monsoon and monsoon season, respectively) and re sulted in higher water temperature inside the evaporative cooling pad.

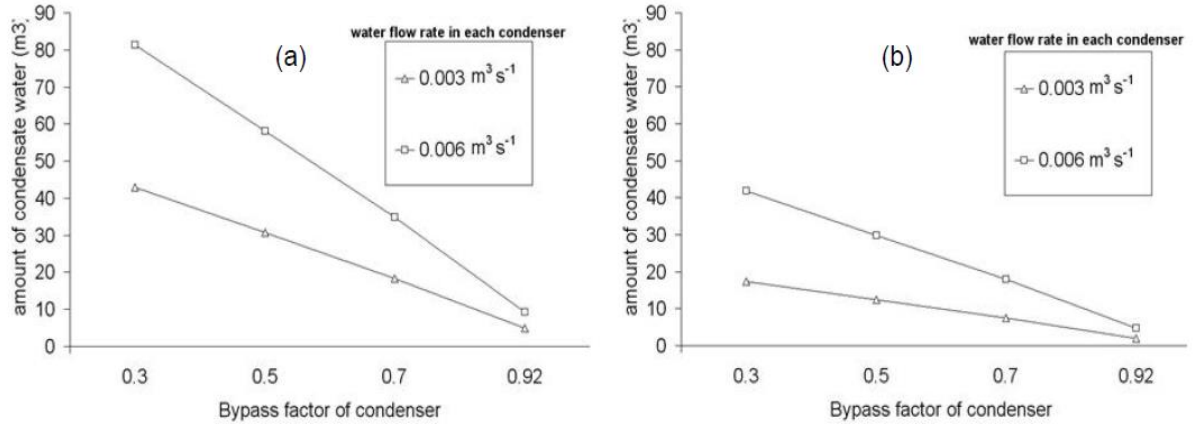

Figure 2.13 *Simulated amount of condensate water (m3 per greenhouse compartment) with assuming certain parameters in the model for a pre-monsoon day (a) and monsoon day (b)*

In greenhouse hydroponic tomato production, the total daily water use by plant canopy transpiration is estimated around $0.0036 - 0.0105\ m^3\ m^{-2}\ d^{-1}$ and $0.0033\ 0.0081\ m^3\ m^{-2}\ d^{-1}$ during the pre-monsoon day and monsoon day, respectively, for mature tomato plants growing at a density of 3.6 plants $\cdot\ m^{-2}$, according to the recorded value in our research greenhouse (Kubota and Kroggel, unpublished data). Based on these values, the minimum and maximum potential plant canopy water usage in one compartment $(9600\ m^2)$ per day is estimated as $34.6 - 101\ m^3 \cdot d$ and $31.7 - 77.8\ m^3 \cdot d^{-1}$ during the pre-monsoon day and monsoon day, respectively. At $BF = 0.92$ and $0.003\ m^3 \cdot s^{-1}$ water flow rate, the most inefficient condensation condition examined in the present study, the water

recovery percentage relative to plant water use was 4.9-14.2% and 2.6-6.3% during the pre-monsoon and monsoon day, respectively (Table1 and 2).

By decreasing BF to 0.5 at the same flow rate, a BF level commonly achieved in industrial condensing unit, the water recovery percentage reached $30.4 - 88.7\%$ and $16 - 39.2\%$ during the pre-monsoon and monsoon day, respectively (Table1 and 2). A very efficient condenser ($BF = 0.3$) could recover up to $42.6 - 100\%$ in pre-monsoon day and up to $22.4 - 54.9\%$ recovery in monsoon day, suggesting that under efficient condenser condition, all water evapotranspirated by the plant canopy and therefore lost in the air were possibly recovered.

In monsoon day, the overall water recovery percentage was less than those in pre-monsoon day. However, the other water saving techniques can be the alternative way to save amount of water during the monsoon season such as stromwater harvesting. Also it may be worth considering a heat pump system to bring the chilled water temperature down by a few degrees before introducing to the condenser unit.

Table 2.3 The simulated amounts of condensate water ($m^3 \cdot d^{-1}$) and the recovery percentage relative to minimum ($34.6\ m^3 \cdot d^{-1}$) and maximum ($101\ m^3 \cdot d^{-1}$) plant canopy water use in a 9600 m^2 semi-arid greenhouse compartment during pre-monsoon day.

Bypass factor	water flow rate ($m^3 \cdot s^{-1}$)	
	0.003	0.006
0.92	4.9 (14.2%, 4.9%)	9.3 (26.9%, 9.2%)
0.7	18.4 (53.2%, 18.3%)	34.8 (100%, 34.6%)
0.5	30.7 (88.7%, 30.4%)	58.1 (100%, 57.6%)
0.3	42.9 (100%, 42.6%)	81.3 (100%, 80.6%)

Table 2.4 The simulated amounts of condensate water ($m^3 \cdot d^{-1}$) and the recovery percentage relative to minimum ($31.7\ m^3 \cdot d^{-1}$) and maximum ($77.8\ m^3 \cdot d^{-1}$) plant canopy water use in a 9600 m^2 semi-arid greenhouse compartment during monsoon day.

Bypass factor	water flow rate ($m^3 \cdot s^{-1}$)	
	0.003	0.006
0.92	2.0(6.3%, 2.6%)	4.8(15.1%, 6.2%)
0.7	7.5(23.5%, 9.6%)	17.9(56.6%, 23.1%)
0.5	12.4(39.2%, 16%)	29.9(94.3%, 38.4%)
0.3	17.4(54.9%, 22.4%)	41.8(100%, 53.8%)

2.3.7. Conclusions

The model developed in this study generated reasonably accurate condensation rates after adjusting the condenser bypass factor. The case study showed that the water recovery system using the evaporative cooling sump water as the chilled water source could be integrated into crop greenhouse production under semi-arid conditions. Although, during the monsoon season, the simulation showed that the amounts of water recovery from the greenhouse exhaust air would be less than those in pre-monsoon season. Further design improvement of this water recovery system should be examined based on the cost and benefits of operating the system at various air flow rate and water flow rate. [13]

Chapter 3

Mathematical modelling and Numerical approach

3.1.Mathematical Modelling of Laminar Flows

3.1.I. Introduction

CFD is fundamentally based on the governing equations of fluid dynamics. They represent mathematical statements of the conservation laws of physics. It is important that anyone concerned with CFD possesses some understanding of the physical phenomena of fluid motion, as it is these phenomena that CFD analyzes and predicts. All of CFD is based on these equations;

3.1.2. THE CONTINUITY EQUATION

Mass Conservation

The conservation of mass principle for a control volume can be expressed as: The net mass transfer to or from a control volume during a time interval *dt* is equal to the net change (increase or decrease) of the total mass within the control volume during *dt*

$$\frac{\partial \rho}{\partial t} + \frac{\partial (\rho u)}{\partial x} + \frac{\partial (\rho v)}{\partial y} + \frac{\partial (\rho w)}{\partial z} = 0$$

partial differential form of the continuity equation

a differential coordinate-free form of the continuity equation:

$$\frac{\partial \rho}{\partial t} + \nabla \cdot (\rho \mathbf{v}) = 0$$

For an incompressible fluid (i.e. a liquid) the density ρ is constant and equation above becomes

$$\text{div u} = 0$$

3.1.3. THE MOMENTUM EQUATION

Newton's second law states that the rate of change of momentum of a fluid particle equals the sum of the forces on the particle.

$$\frac{\mathrm{d}\vec{\mathrm{V}}}{\mathrm{dt}} = \rho\vec{\mathrm{f}} - \vec{\nabla}P + \vec{\nabla}\tau$$

This equation expresses the balance between the rate of change in momentum per unit of volume and the external forces applied to the unit of volume: the forces of volume $\rho\vec{\mathrm{f}}$, the pressure force $\vec{\nabla}P$, viscosity force $\vec{\nabla}\tau$.

In the case of Newtonian fluids, equation above takes the simplified form of, Navier-Stokes equations:

$$\frac{d\vec{V}}{dt} = \rho\vec{f} - \mu\vec{V}^2\vec{V} + \frac{\mu}{3}\vec{\nabla}(\vec{\nabla}\cdot\vec{V})$$

Where: μ is the dynamic viscosity of air. It characterizes its viscous properties.

Based on the concept of substantial derivative , the conservative form of momentum equations be rewritten as:

$$\frac{\partial(\rho u)}{\partial t}+\frac{\partial(\rho uu)}{\partial x}+\frac{\partial(\rho vu)}{\partial y}+\frac{\partial(\rho wu)}{\partial z}=\frac{\partial\sigma_{xx}}{\partial x}+\frac{\partial\tau_{yx}}{\partial y}+\frac{\partial\tau_{zx}}{\partial z}+\sum F_x^{\text{body force}}$$

$$\frac{\partial(\rho v)}{\partial t}+\frac{\partial(\rho uv)}{\partial x}+\frac{\partial(\rho vv)}{\partial y}+\frac{\partial(\rho wv)}{\partial z}=\frac{\partial\tau_{xy}}{\partial x}+\frac{\partial\sigma_{yy}}{\partial y}+\frac{\partial\tau_{zy}}{\partial z}+\sum F_y^{body\ \text{force}}$$

$$\frac{\partial(\rho w)}{\partial t}+\frac{\partial(\rho uw)}{\partial x}+\frac{\partial(\rho vw)}{\partial y}+\frac{\partial(\rho ww)}{\partial z}=\frac{\partial\tau_{xz}}{\partial x}+\frac{\partial\tau_{yz}}{\partial y}+\frac{\partial\sigma_{zz}}{\partial z}+\sum F_z^{\text{body force}}$$

3.1.4. THE ENERGY EQUATION

Energy Conservation

The energy equation is derived from the first law of thermodynamics, which states that the rate of change of energy of a fluid particle is equal to the rate of heat addition to the fluid particle plus the rate of work done on the particle.(14)

To establish the energy equation, we apply the first principle of thermodynamics on an element of volume and we obtain at the end, the energy balance of considered system:

$$\frac{\mathrm{d}}{\mathrm{dt}}\left(\rho c_{\mathrm{p}}\mathrm{T}\right)=\underbrace{\vec{\nabla}(\lambda\vec{\nabla}\mathrm{T})}_{(a)}+\underbrace{\mathrm{T}\beta\frac{\mathrm{dP}}{\mathrm{dt}}}_{(b)}+\underbrace{\mu\phi}_{(c)}+\underset{(d)}{q}$$

The four terms of the right hand side balance the total energy variation of the system ρcpT. This is the variation due to

- (a), conduction
- (b), the energy variation due to compressibility
- (c) viscous dissipation energy
- (d) internal production of heat

Based on the concept of substantial derivative the conservative form of the energy equation can be rewritten as

$$\frac{\partial(\rho E)}{\partial t}+\frac{\partial(\rho uE)}{\partial x}+\frac{\partial(\rho vE)}{\partial y}+\frac{\partial(\rho wE)}{\partial z}=\frac{\partial}{\partial x}\left[\lambda\frac{\partial T}{\partial x}\right]+\frac{\partial}{\partial y}\left[\lambda\frac{\partial T}{\partial y}\right]+\frac{\partial}{\partial z}\left[\lambda\frac{\partial T}{\partial z}\right]$$
$$-\frac{\partial(up)}{\partial x}-\frac{\partial(vp)}{\partial y}-\frac{\partial(wp)}{\partial z}+\Phi$$

3.1.5. Water Vapour Equation

Describing the transport of water vapour through a binary mixture of water vapour and air, the mass flux of water vapour j_{wv}=j_{wv}(x,t) (in kg s^{-1} m^{-2}) in one dimension can be described as (Bird et al. 2002)

$$j_{\mathrm{wv}} = j \cdot \frac{\rho_{\mathrm{wv}}}{\rho} - \rho D_a \cdot \frac{\partial}{\partial x}\left(\frac{\rho_{\mathrm{wv}}}{\rho}\right)$$

with

$\rho_{\mathrm{wv}} = \rho_{\mathrm{wv}}(x,t)$ being the local mass concentration of water vapour (in kgm^{-3})

, $\rho = \rho(x,t)$ the local mass concentration of the water vapour-air mixture,

$j = j(x,t)$ the sum of water vapour and air mass flux

$D_{\mathrm{a}} = D_{\mathrm{a}}(x,t)$ the diffusion coefficient of water vapour into air (in $\mathrm{m}^2\ \mathrm{s}^{-1}$).

Assuming the total pressure and temperature to be constant during the interdiffusion of the two gases and treating the two gases as ideal gases, the mass flux of water vapour can be evaluated as

$$j_{\mathrm{wv}} = \frac{-D_{\mathrm{a}}}{1 + \frac{\mathrm{m_{Air}} - \mathrm{m_{H_2O}}}{\mathrm{m_{H_2O}}} \cdot \frac{\rho_{\mathrm{wv}}}{\rho}} \cdot \left(\frac{\partial \rho_{\mathrm{wv}}}{\partial x} - \frac{\rho_{\mathrm{wv}}}{\rho} \cdot \frac{\partial \rho}{\partial x}\right)$$

$\mathrm{m_{H_2O}}$ is the molecular weight of water and $\mathrm{m_{Air}}$ the mean molecular weight of dry air. As the water vapour concentration at room temperature is much smaller than the concentration of the water vapour-air mixture, this equation can be simplified to

$$j_{\mathrm{wv}} \simeq -D_{\mathrm{a}} \cdot \frac{\partial \rho_{\mathrm{wv}}}{\partial x}$$

With an error of less than 1.2% for T=25∘C. Using the equation of continuity, an ordinary diffusion equation can thus be derived for the diffusion of water vapour through air.(15)

3.2. The Mathematical modelling of Turbulent Flows

3.2.1The partial differential equations for turbulent physical systems

Turbulence is the most complicated kind of fluid motion, making even its precise definition difficult. A fluid motion is described as turbulent if it is rotational, intermittent, highly disordered, diffusive and dissipative. It is generally accepted s that turbulence can be described by the Navier-Stokes momentum-transport equations (the second-order Chapman-Enskog approximation to the Bolzmann equation for molecular motion), which express the conservation of momentum for a continuum fluid with viscous stress directly proportional to rate of strain. This description is the simplest that can be imagined. According to this principle, the 'Eulerian' equations governing the dynamics and heat/mass transfer of a turbulent fluid can be written as follows, in Cartesian tensor notation, and using the repeated-suffix summation convention:

- Mass conservation:

$$\frac{\partial \rho}{\partial t} + \frac{\partial}{\partial x_j}\left(\rho u_j\right) = 0 \qquad (1)$$

- Momentum conservation for the x_i -component of velocity, u_i, in 'divergence' form:

$$\frac{\partial \rho u_i}{\partial t} + \frac{\partial \rho u_i u_f}{\partial x_j} = -\frac{\partial p}{\partial x_i} + \frac{\partial \sigma_{ij}}{\partial x_j} + F_i \qquad (2)$$

- Scalar conservation (e.g. enthalpy, h, concentration, C, etc):

$$\frac{\partial \rho \phi}{\partial t} + \frac{\partial \rho \phi u_j}{\partial x_j} = \frac{\partial}{\partial x_j}\left(\Gamma_\phi \frac{\partial \phi}{\partial x_j}\right) + \frac{\partial p}{\partial t} + u_t \frac{\partial p}{\partial x_i} + S_\phi \qquad (3)$$

(where for $\phi \equiv C$, the second and third terms on the right hand side should be excluded).

Here F_i is the x_i -component of body force (for instance in a gravitational field $F_i = \rho g_i$ where g_i is a component of the gravitational acceleration),

ρ is the instantaneious density,

ϕ is a scalar quantity,

Γ_ϕ is the diffusion coefficient of ϕ,

S_ϕ is the volumetric source/sink term,

and $\sigma_{\ddot{q}}$ the stress tensor components (stress due to deformation and bulk dilatation).

Equation (2) applies generally, whatever the constitutive law for σ_{ij}, even if the mean velocities in turbulent flow are concerned, provided that then σ_{ij} includes apparent turbulence (Reynolds) stresses.

For Newtonian fluids, the instantaneous deformation stress is:

$$\sigma_{ij} = \mu\left(\frac{\partial u_i}{\partial x_j} + \frac{\partial u_i}{\partial x_i}\right) + \left(\mu^b - \frac{2}{3}\mu\right)\delta_{ij}\frac{\partial u_l}{\partial x_l} \qquad (4)$$

where δ_{ij} is the Kronecker delta, and μ^b is the bulk viscosity of the same order as μ. [6] In the most general case $\partial \sigma_{ij} / \partial x_j$ is very complicated. [7,8] In Newtonian fluids $\sigma_{ij} = \sigma_{ji}$, so σ_{ij} is a diagonally-symmetric tensor. Finally, an equation of state (single-component fluid) relates pressure to density and temperature:

$$p \equiv p(\rho, T) \quad (5)$$

where p, T, are the instantaneous values of density and absolute temperature, respectively. Fortunately, viscosity does not usually affect the larger scale eddies which are primarily responsible for turbulent mixing, with the exception of the 'viscous sublayer' very close to a solid surface. Furthermore, the effects of density fluctuations on turbulence are small if, as in the majority of practical situations, the density fluctuations are small compared to the mean

density, the exception being the effect of temporal fluctuations and spatial gradients of density in a gravitational field. Therefore, one can usually neglect the direct effect of viscosity and compressibility on turbulence. It is also important to note that it is the fluctuating velocity field that drives the fluctuating scalar field, the effect of the latter on the former usually being negligible.

Equations (1)-(5) constitute the mathematical representation of fluid flows, under the assumptions [9] that the turbulent fluid is a continuum, Newtonian (equation (4)) in nature,'and that the flow can be described by the Navier- Stokes (NS) equations.

For turbulent flows, equations (1)-(5) represent the instantaneous values of the flow properties. The equations for turbulence fluctuations are obtained by Reynolds decomposition which describes the turbulent motion as a random variation about a mean value:

$$\phi = \bar{\phi} + \phi' \qquad (6)$$

where the mean value $\bar{\phi}$ is defined [10] as:

$$\bar{\phi} \equiv \langle \phi, w_1 \rangle = \int_D \phi(x_i - \xi_i, t - t_1) w(\xi_i, t_1) dQ \qquad (7a)$$

with the weighting function w normalized as:

$$\int_D w(\xi_i, t_1) dQ = 1 \qquad (7b)$$

where Q denotes the set (ξ_i, t_1) over the domain D. The averaging procedure can be either temporal (i.e. time-averaging) or Favre (i.e. mass weighted) averaging. . The latter appears promising for flows with variable density, leading to all double correlations with density fluctuations vanishing, by definition. Favre-averaged quantities, however, are not easily comparable with experimentally measured quantities, which are normally time-averaged. The weighting function for the temporal averaging can be expressed as:

$$\begin{aligned} w \quad &= \frac{\delta(\xi_i)}{\Delta t}, |t_1| < \Delta t \\ &= 0, \ |t_1| > \Delta t \end{aligned} \qquad (8)$$

with the averaged quantity having the form:

$$\bar{\phi} = \frac{1}{\Delta t} \int_{t_1}^{t_1 + \Delta t} \phi \mathrm{d}t \text{ and } \bar{\phi}' = 0 \qquad (8a), (8b)$$

Using equations (6) and (8), equations (1)-(5) can be manipulated to derive the following equations:
Mass conservation:

$$\frac{\partial \bar{\rho}}{\partial t} + \frac{\overline{\partial \rho u_j}}{\partial x_j} = 0 \qquad (9a)$$

Or

$$\frac{\partial \bar{\rho}}{\partial t} + \frac{\partial \bar{\rho}\bar{u}_j}{\partial x_j} \simeq 0, \overline{\rho' u_j'} \ll \rho\bar{\rho}\overline{u_j} \text{ (for weak density fluctuations)} \qquad (9b)$$

Momentum conservation:

$$\begin{aligned} &\frac{\partial \bar{\rho}\bar{u}_i}{\partial t} + \frac{\partial \bar{\rho}\bar{u}_i\bar{u}_j}{\partial x_j} + \partial\bar{\rho}\overline{u_i' u_j'}/\,\partial x_j \\ &= -\frac{\partial \bar{p}}{\partial x_i} + \frac{\partial}{\partial x_j}\left[\mu S_{ij} + \left(\mu^b - \frac{2}{3}\mu\right) S_{ll}\delta_{ij}\right] \\ &- \left[\frac{\partial \overline{\rho' u_i'}}{\partial t} + \frac{\partial \overline{\rho' u_i' u_j}}{\partial x_j} + \frac{\partial \overline{\rho' u_j' \overline{u_i}}}{\partial x_j} + \frac{\partial \overline{\rho' u_i' u_j'}}{\partial x_j}\right] + f_i \end{aligned} \qquad (10)$$

Where:

$$S_{ij} = \left(\frac{\partial \bar{u}_i}{\partial x_j} + \frac{\partial \bar{u}_j}{\partial x_i}\right); S_{ll} = \frac{\partial \bar{u}_l}{\partial x_l}; \frac{\partial \bar{u}_l'}{\partial x_j} = 0$$

Scalar conservation:

$$\begin{aligned} &\frac{\partial \bar{\rho}\bar{\phi}}{\partial t} + \frac{\partial \bar{u}_j\bar{\rho}\bar{\phi}}{\partial x_j} + \frac{\partial \bar{\rho}\overline{u_j'\phi'}}{\partial x_j} \\ &= \frac{\partial}{\partial x_j}\left(\Gamma_\phi \frac{\partial \bar{\phi}}{\partial x_j}\right) + \frac{\overline{D_l}}{Dt} - \left[\left(\frac{\partial \overline{\rho'\phi'}}{\partial t} + \frac{\partial \overline{u_j}\overline{\rho'\phi'}}{\partial x_j}\right)\right. \\ &\left. + \frac{\partial}{\partial x_j}\left(\overline{\rho' u_j'}\bar{\phi} + \overline{\rho' u_j'\phi'}\right)\right] + \bar{S}_\phi \end{aligned} \qquad (11)$$

Thermal equation of state (single-component gas):

$$p \equiv R\overline{\rho T} = R(\bar{\rho}\bar{T} + \overline{\rho' T'}) \qquad (12)$$

Equations $(9) - (12)$ are the first step towards modelling, as the averaging process itself masks some detailed characteristics of turbulence (16).

3.2.2. GENERIC FORM OF THE GOVERNING EQUATIONS FOR CFD

Here, we will present the three-dimensional form of the governing equations for the conservation of mass, momentum, energy, and the turbulent quantities. If we introduce a general variable ϕ and expressing all the fluid flow equations in the conservative incompressible form, the equation can be written as

$$\frac{\partial \varphi}{\partial t} + \frac{\partial (u\varphi)}{\partial x} + \frac{\partial (v\varphi)}{\partial y} + \frac{\partial (w\varphi)}{\partial z} = \frac{\partial}{\partial x}\left[\Gamma \frac{\partial \varphi}{\partial x}\right] + \frac{\partial}{\partial y}\left[\Gamma \frac{\partial \varphi}{\partial y}\right] + \frac{\partial}{\partial z}\left[\Gamma \frac{\partial \varphi}{\partial z}\right] + S_\varphi \quad (13)$$

whilst in the conservative compressible form, the equation is given by

$$\frac{\partial (\rho\phi)}{\partial t} + \frac{\partial (\rho u\phi)}{\partial x} + \frac{\partial (\rho v\phi)}{\partial y} + \frac{\partial (\rho w\phi)}{\partial z} = \frac{\partial}{\partial x}\left[\Gamma \frac{\partial \phi}{\partial x}\right] + \frac{\partial}{\partial y}\left[\Gamma \frac{\partial \phi}{\partial y}\right] + \frac{\partial}{\partial z}\left[\Gamma \frac{\partial \phi}{\partial z}\right] + S_\phi \quad (14)$$

Eqs 13 and 14 are the so-called the transport equations for the property ϕ. Each of them illustrates the various physical transport processes occurring in the fluid flow: the local

acceleration and advection terms on the left-hand side are, respectively, equivalent to the diffusion term (Γ=diffusion coefficient) and the source term (Sϕ) on the right-hand side. **Tables 3.1** and **3.2** present the governing equations for the incompressible and compressible flows in the Cartesian framework

Table 3.1 Governing Equations for Incompressible Flow in Cartesian Coordinates

Mass conservation	
(*m*)	$\frac{\partial \rho}{\partial t}+\frac{\partial(\rho u)}{\partial x}+\frac{\partial(\rho v)}{\partial y}+\frac{\partial(\rho w)}{\partial z}=0$
Momentum equations	
(M_x)	$\frac{\partial(\rho u)}{\partial t}+\frac{\partial(\rho uu)}{\partial x}+\frac{\partial(\rho vu)}{\partial y}+\frac{\partial(\rho wu)}{\partial z}=\frac{\partial}{\partial x}\left[(\mu+\mu_T)\frac{\partial u}{\partial x}\right]+\frac{\partial}{\partial y}\left[(\mu+\mu_T)\frac{\partial u}{\partial y}\right]+\frac{\partial}{\partial z}\left[(\mu+\mu_T)\frac{\partial u}{\partial z}\right]+\left(S_u=-\frac{\partial p}{\partial x}+S'_u\right)$
(M_y)	$\frac{\partial(\rho v)}{\partial t}+\frac{\partial(\rho uv)}{\partial x}+\frac{\partial(\rho vv)}{\partial y}+\frac{\partial(\rho wv)}{\partial z}=\frac{\partial}{\partial x}\left[(\mu+\mu_T)\frac{\partial v}{\partial x}\right]+\frac{\partial}{\partial y}\left[(\mu+\mu_T)\frac{\partial v}{\partial y}\right]+\frac{\partial}{\partial z}\left[(\mu+\mu_T)\frac{\partial v}{\partial z}\right]+\left(S_v=-\frac{\partial p}{\partial y}+S'_v\right)$
(M_z)	$\frac{\partial(\rho w)}{\partial t}+\frac{\partial(\rho uw)}{\partial x}+\frac{\partial(\rho vw)}{\partial y}+\frac{\partial(\rho ww)}{\partial z}=\frac{\partial}{\partial x}\left[(\mu+\mu_T)\frac{\partial w}{\partial x}\right]+\frac{\partial}{\partial y}\left[(\mu+\mu_T)\frac{\partial w}{\partial y}\right]+\frac{\partial}{\partial z}\left[(\mu+\mu_T)\frac{\partial w}{\partial z}\right]+\left(S_w=-\frac{\partial p}{\partial z}+S'_w\right)$
Energy equation	
(*E*)	$\frac{\partial(\rho h)}{\partial t}+\frac{\partial(\rho uh)}{\partial x}+\frac{\partial(\rho vh)}{\partial y}+\frac{\partial(\rho wh)}{\partial z}=\frac{\partial}{\partial x}\left[\lambda\frac{\partial T}{\partial x}\right]+\frac{\partial}{\partial y}\left[\lambda\frac{\partial T}{\partial y}\right]+\frac{\partial}{\partial z}\left[\lambda\frac{\partial T}{\partial z}\right]+\frac{\partial}{\partial x}\left[\frac{\mu_T}{\mathrm{Pr}_T}\frac{\partial h}{\partial x}\right]+\frac{\partial}{\partial y}\left[\frac{\mu_T}{\mathrm{Pr}_T}\frac{\partial h}{\partial y}\right]+\frac{\partial}{\partial z}\left[\frac{\mu_T}{\mathrm{Pr}_T}\frac{\partial h}{\partial z}\right]+\frac{\partial p}{\partial t}+\Phi+S_T$
Turbulence equations	
(*k*)	$\frac{\partial(\rho k)}{\partial t}+\frac{\partial(\rho uk)}{\partial x}+\frac{\partial(\rho vk)}{\partial y}+\frac{\partial(\rho wk)}{\partial z}=\frac{\partial}{\partial x}\left[\frac{\mu_T}{\sigma_k}\frac{\partial k}{\partial x}\right]+\frac{\partial}{\partial y}\left[\frac{\mu_T}{\sigma_k}\frac{\partial k}{\partial y}\right]+\frac{\partial}{\partial z}\left[\frac{\mu_T}{\sigma_k}\frac{\partial k}{\partial z}\right]+(S_k=\rho(P-D))$
(ε)	$\frac{\partial(\rho\varepsilon)}{\partial t}+\frac{\partial(\rho u\varepsilon)}{\partial x}+\frac{\partial(\rho v\varepsilon)}{\partial y}+\frac{\partial(\rho w\varepsilon)}{\partial z}=\frac{\partial}{\partial x}\left[\frac{\mu_T}{\sigma_\varepsilon}\frac{\partial \varepsilon}{\partial x}\right]+\frac{\partial}{\partial y}\left[\frac{\mu_T}{\sigma_\varepsilon}\frac{\partial \varepsilon}{\partial y}\right]+\frac{\partial}{\partial z}\left[\frac{\mu_T}{\sigma_\varepsilon}\frac{\partial \varepsilon}{\partial z}\right]+\left(S_\varepsilon=\rho\frac{\varepsilon}{k}(C_{\varepsilon 1}P-C_{\varepsilon 2}D)\right)$
where	$P=2\mu_T\left[\left(\frac{\partial u}{\partial x}\right)^2+\left(\frac{\partial v}{\partial y}\right)^2+\left(\frac{\partial w}{\partial z}\right)^2\right]+\mu_T\left[\left(\frac{\partial u}{\partial y}+\frac{\partial v}{\partial x}\right)^2+\left(\frac{\partial v}{\partial z}+\frac{\partial w}{\partial y}\right)^2+\left(\frac{\partial w}{\partial x}+\frac{\partial u}{\partial z}\right)^2\right]-\frac{2}{3}\mu_T\left(\frac{\partial u}{\partial x}+\frac{\partial v}{\partial y}+\frac{\partial w}{\partial z}\right)^2-\frac{2}{3}\rho\mu_T k\left(\frac{\partial u}{\partial x}+\frac{\partial v}{\partial y}+\frac{\partial w}{\partial z}\right)$ and $D=\varepsilon$

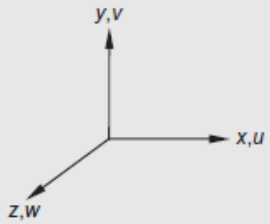

Table 3.2 General Form of Governing Equations for Incompressible Flow in Cartesian Coordinates

Φ	Γ_Φ	S_Φ
1	0	0
u	$\nu+\nu_T$	$-\frac{1}{\rho}\frac{\partial p}{\partial x}+S'_u$
v	$\nu+\nu_T$	$-\frac{1}{\rho}\frac{\partial p}{\partial y}+S'_v$
w	$\nu+\nu_T$	$-\frac{1}{\rho}\frac{\partial p}{\partial z}+S'_w$
T	$\frac{\nu}{Pr}+\frac{\nu_T}{Pr_T}$	S_T
k	$\frac{\nu_T}{\sigma_k}$	$P-D$
ε	$\frac{\nu_T}{\sigma_\varepsilon}$	$\frac{\varepsilon}{k}(C_{\varepsilon 1}P-C_{\varepsilon 2}D)$

3.2.3. Boussinesq Approximation

In flows accompanied by heat transfer, the fluid properties are normally functions of temperature. The variations may be small and yet be the cause of the fluid motion.If the density variation is not large, one may treat the density as constant in the unsteady and convection terms, and treat it as variable only in the gravitational term.This is called the Boussinesq approximation. One usually assumes that the density varies linearly with temperature. If one includes the effect of the body force on the mean density in the pressure term in Momentum equation the remaining term can be expressed as

$$(\rho-\rho_0)g_i=-\rho_0 g_i\beta(T-T_0), \qquad (15)$$

where β is the coefficient of volumetric expansion. This approximation introduces errors of the order of 1% if the temperature differences are below, e.g., 2° for water and 15° for air. The error may be more substantial when temperature differences are larger; the solution may even be qualitatively wrong [17].

3.2.4. k-ε Two-Equation Turbulence Model

There is a crucial difference when modelling the physical phenomena between laminar and turbulent flow. For the latter, the appearance of turbulence eddies occurs over a wide range of length scales. With the present day computing power, the computing requirements for a direct numerical solution (DNS) of the time-dependent Navier-Stokes equations of fully turbulent flows at high Reynolds numbers are still truly phenomenal.

Meanwhile, engineers require computational procedures that can supply adequate information about the turbulent processes but wish to avoid the need to predict all the effects associated with each and every eddy in the flow. This category of CFD users is almost always satisfied with information about the time averaged properties of the flow (e.g. mean velocities, mean pressures, and mean stresses). Since engineers are content to focus their attention on mean quantities, by adopting a suitable time-averaging operation on the momentum equations, we are able to discard all details concerning the state of the flow contained in the instantaneous fluctuations. This process, of obtaining mean quantities, can be applied on the compressible,

two-dimensional equations of continuity and the conservative forms of momentum and energy that produce the time averaged governing equations or more popularly known as the Reynolds averaged Navier-Stokes (RANS) equations given by

$$\frac{\partial \rho}{\partial t} + \frac{\partial (\rho \bar{u})}{\partial x} + \frac{\partial (\rho \bar{v})}{\partial y} = 0 \qquad (16)$$

$$\frac{\partial (\rho \bar{u})}{\partial t} + \frac{\partial (\rho \bar{u}\bar{u})}{\partial x} + \frac{\partial (\rho \bar{v}\bar{u})}{\partial y} = -\frac{\partial \bar{p}}{\partial x} + \frac{\partial}{\partial x}\left(\mu \frac{\partial \bar{u}}{\partial x}\right) + \frac{\partial}{\partial y}\left(\mu \frac{\partial \bar{u}}{\partial y}\right) + \frac{\partial}{\partial x}\left[\mu \frac{\partial \bar{u}}{\partial x}\right] + \frac{\partial}{\partial y}\left[\mu \frac{\partial \bar{v}}{\partial x}\right] - \left[\frac{\partial \left(\rho \overline{u'u'}\right)}{\partial x} + \frac{\partial \left(\rho \overline{u'v'}\right)}{\partial y}\right] \qquad (17)$$

$$\frac{\partial (\rho \bar{v})}{\partial t} + \frac{\partial (\rho \bar{u}\bar{v})}{\partial x} + \frac{\partial (\rho \bar{v}\bar{v})}{\partial y} = -\frac{\partial \bar{p}}{\partial y} + \frac{\partial}{\partial x}\left(\mu \frac{\partial \bar{v}}{\partial x}\right) + \frac{\partial}{\partial y}\left(\mu \frac{\partial \bar{v}}{\partial y}\right) + \frac{\partial}{\partial x}\left[\mu \frac{\partial \bar{u}}{\partial y}\right] + \frac{\partial}{\partial y}\left[\mu \frac{\partial \bar{v}}{\partial y}\right] - \left[\frac{\partial \left(\rho \overline{u'v'}\right)}{\partial x} + \frac{\partial \left(\rho \overline{v'v'}\right)}{\partial y}\right] \qquad (18)$$

$$\frac{\partial (\rho \bar{T})}{\partial t} + \frac{\partial (\rho \bar{u}\bar{T})}{\partial x} + \frac{\partial (\rho \bar{v}\bar{T})}{\partial y} = \frac{\partial}{\partial x}\left(\frac{k}{C_p}\frac{\partial T}{\partial x}\right) + \frac{\partial}{\partial y}\left(\frac{k}{C_p}\frac{\partial \bar{T}}{\partial y}\right) - \left[\frac{\partial \left(\rho \overline{u'T'}\right)}{\partial x} + \frac{\partial \left(\rho \overline{v'T'}\right)}{\partial y}\right] \qquad (19)$$

where $\bar{u}, \bar{v}, \bar{p}$, and $\bar{T}$ are mean values and u', v', p', and T' are turbulent fluctuations. The equations above are similar to those formulated for laminar flows, except for the presence of additional terms of the form $\overline{a'b'}$. As a result, we have three additional unknowns (in three dimensions, we will have nine additional unknowns), known as the Reynolds stresses, in the time-averaged momentum equations. Similarly, the time-averaged temperature equation shows extra terms $\overline{u'T'}$ and $\overline{v'T'}$ (in three dimensions, we have an extra term $\overline{w'T'}$). For incompressible, two-dimensional equations of continuity and the nonconservative forms of momentum and energy, the time-averaged governing equations can be expressed as

$$\frac{\partial \bar{u}}{\partial x}+\frac{\partial \bar{v}}{\partial y}=0 \tag{20}$$

$$\frac{\partial \bar{u}}{\partial t}+\frac{\partial(\overline{uu})}{\partial x}+\frac{\partial(\overline{vu})}{\partial y}=-\frac{1}{\rho}\frac{\partial \bar{p}}{\partial x}+\frac{\partial}{\partial x}\left(\nu\frac{\partial \bar{u}}{\partial x}\right)+\frac{\partial}{\partial y}\left(\nu\frac{\partial \bar{u}}{\partial y}\right)+\frac{\partial}{\partial x}\left[\nu\frac{\partial \bar{u}}{\partial x}\right]+\frac{\partial}{\partial y}\left[\nu\frac{\partial \bar{v}}{\partial x}\right]-\left[\frac{\partial(\overline{u'u'})}{\partial x}+\frac{\partial(\overline{u'v'})}{\partial y}\right] \tag{21}$$

$$\frac{\partial v}{\partial t}+\frac{\partial(\overline{uv})}{\partial x}+\frac{\partial(\overline{vv})}{\partial y}=-\frac{1}{\rho}\frac{\partial \bar{p}}{\partial y}+\frac{\partial}{\partial x}\left(\nu\frac{\partial \bar{v}}{\partial x}\right)+\frac{\partial}{\partial y}\left(\nu\frac{\partial \bar{v}}{\partial y}\right)+\frac{\partial}{\partial x}\left[\nu\frac{\partial \bar{u}}{\partial y}\right]+\frac{\partial}{\partial y}\left[\nu\frac{\partial \bar{v}}{\partial y}\right]-\left[\frac{\partial(\overline{u'v'})}{\partial x}+\frac{\partial(\overline{v'v'})}{\partial y}\right] \tag{22}$$

$$\frac{\partial \bar{T}}{\partial t}+\frac{\partial(\bar{u}\bar{T})}{\partial x}+\frac{\partial(\bar{v}\bar{T})}{\partial y}=\frac{\partial}{\partial x}\left(\frac{k}{\rho C_p}\frac{\partial \bar{T}}{\partial x}\right)+\frac{\partial}{\partial y}\left(\frac{k}{\rho C_p}\frac{\partial \bar{T}}{\partial y}\right)-\left[\frac{\partial(\overline{u'T'})}{\partial x}+\frac{\partial(\overline{v'T'})}{\partial y}\right] \tag{23}$$

where the term $k/\rho C_p$ in Eq. (23) is the thermal diffusivity α of the fluid.

The time-averaged equations can be solved if the Reynolds stresses and extra temperature transport terms can be related to the mean flow and heat quantities. It was proposed by Boussinesq (1868) that the Reynolds stresses could be linked to the mean rates of deformation. We obtain

$$-\rho\overline{u'u'}=2\mu_T\frac{\partial \bar{u}}{\partial x}-\frac{2}{3}\rho k;-\rho\overline{v'v'}=2\mu_T\frac{\partial \bar{v}}{\partial y}-\frac{2}{3}\rho k;\ -\rho\overline{u'v'}=\mu_T\left(\frac{\partial \bar{v}}{\partial x}+\frac{\partial \bar{u}}{\partial y}\right) \tag{24}$$

The right-hand side is analogous to Newton's law of viscosity, except for the appearance of the turbulent or eddy viscosity μ_T and turbulent kinetic energy k. In Eq. (24), the turbulent momentum transport is assumed to be proportional to the mean gradients of velocity. Similarly, the turbulent transport of temperature is taken to be proportional to the gradient of the mean value of the transported quantity. In other words,

$$-\rho\overline{u'T'}=\Gamma_T\frac{\partial \bar{T}}{\partial x};\ -\rho\overline{v'T'}=\Gamma_T\frac{\partial \bar{T}}{\partial y} \tag{25}$$

Where Γ_T is the turbulent diffusivity. Since the turbulent transport of momentum and heat is due to the same mechanisms-eddy mixing - the value of the turbulent viscosity can be taken to be close to that of turbulent viscosity μ_T. Based on the definition of the turbulent Prandtl number Pr_T, we obtain

$$\mathrm{Pr}_T=\frac{\mu_T}{\Gamma_T} \tag{26}$$

Experiments have established that this ratio is often nearly constant. Most CFD procedures assume this to be the case and use values of Pr_T around unity. Since the complexity of turbulence in most engineering flow problems precludes the use of any simple formulae, it is possible to develop similar transport equations to accommodate the turbulent quantity k and other turbulent quantities one of which is the rate of dissipation of turbulent energy ε. Here, we indicate the form of a typical two-equation turbulence model that is commonly used in handling many turbulent fluid engineering problems, the standard $k-\varepsilon$ model by Launder and Spalding (1974).

Some preliminary definitions are required first. The turbulent kinetic energy k and rate of dissipation of turbulent energy ε can be defined and expressed in Cartesian tensor notation as

$$k = \frac{1}{2}u_i'u_i' \text{ and } \varepsilon = \nu_T\overline{\left(\frac{\partial u_i'}{\partial x_j}\right)\left(\frac{\partial u_i'}{\partial x_j}\right)} \text{ where } i,j = 1,2,3$$

From the local values of k and ε, a local turbulent viscosity μ_T can be evaluated as

$$\mu_T = \rho C_\mu \frac{k^2}{\varepsilon} \qquad (27)$$

and the kinematic turbulent or eddy viscosity is denoted by $\nu_T = \mu_T/\rho$.

By substituting the Reynolds stress expressions in Eqs (17), (18), (21), and (22) and there extra temperature transport terms in Eqs (19) and (23), removing the overbar that is by default indicating the average quantities, we obtain the compressible form of governing equations as

$$\frac{\partial \rho}{\partial t} + \frac{\partial(\rho u)}{\partial x} + \frac{\partial(\rho v)}{\partial y} = 0 \qquad (28)$$

$$\frac{\partial(\rho u)}{\partial t} + \frac{\partial(\rho uu)}{\partial x} + \frac{\partial(\rho vu)}{\partial y} = -\frac{\partial p}{\partial x} + \frac{\partial}{\partial x}\left[(\mu+\mu_T)\frac{\partial u}{\partial x}\right] + \frac{\partial}{\partial y}\left[(\mu+\mu_T)\frac{\partial u}{\partial y}\right] + \frac{\partial}{\partial x}\left[(\mu+\mu_T)\frac{\partial u}{\partial x}\right] + \frac{\partial}{\partial y}\left[(\mu+\mu_T)\frac{\partial v}{\partial x}\right] \qquad (29)$$

$$\frac{\partial(\rho v)}{\partial t} + \frac{\partial(\rho uv)}{\partial x} + \frac{\partial(\rho vv)}{\partial y} = -\frac{\partial p}{\partial y} + \frac{\partial}{\partial x}\left[(\mu+\mu_T)\frac{\partial v}{\partial x}\right] + \frac{\partial}{\partial y}\left[(\mu+\mu_T)\frac{\partial v}{\partial y}\right] + \frac{\partial}{\partial x}\left[(\mu+\mu_T)\frac{\partial u}{\partial y}\right] + \frac{\partial}{\partial y}\left[(\mu+\mu_T)\frac{\partial v}{\partial y}\right] \qquad (30)$$

$$\frac{\partial(\rho T)}{\partial t} + \frac{\partial(\rho uT)}{\partial x} + \frac{\partial(\rho vT)}{\partial y} = \frac{\partial}{\partial x}\left[\left(\frac{\mu}{Pr} + \frac{\mu_T}{Pr_T}\right)\frac{\partial T}{\partial x}\right] + \frac{\partial}{\partial y}\left[\left(\frac{\mu}{Pr} + \frac{\mu_T}{Pr_T}\right)\frac{\partial T}{\partial y}\right] \qquad (31)$$

and the incompressible form of governing equations as

$$\frac{\partial u}{\partial x} + \frac{\partial v}{\partial y} = 0 \qquad (32)$$

$$\frac{\partial u}{\partial t} + \frac{\partial(uu)}{\partial x} + \frac{\partial(vu)}{\partial y} = -\frac{1}{\rho}\frac{\partial p}{\partial x} + \frac{\partial}{\partial x}\left[(\nu+\nu_T)\frac{\partial u}{\partial x}\right] + \frac{\partial}{\partial y}\left[(\nu+\nu_T)\frac{\partial u}{\partial y}\right] + \frac{\partial}{\partial x}\left[(\nu+\nu_T)\frac{\partial u}{\partial x}\right] + \frac{\partial}{\partial y}\left[(\nu+\nu_T)\frac{\partial v}{\partial x}\right] \qquad (33)$$

$$\frac{\partial v}{\partial t} + \frac{\partial(uv)}{\partial x} + \frac{\partial(vv)}{\partial y} = -\frac{1}{\rho}\frac{\partial p}{\partial y} + \frac{\partial}{\partial x}\left[(\nu+\nu_T)\frac{\partial v}{\partial x}\right] + \frac{\partial}{\partial y}\left[(\nu+\nu_T)\frac{\partial v}{\partial y}\right] + \frac{\partial}{\partial x}\left[(\nu+|\,\nu_T)\frac{\partial u}{\partial y}\right] + \frac{\partial}{\partial y}\left[(\nu+\nu_T)\frac{\partial v}{\partial y}\right] \qquad (34)$$

$$\frac{\partial T}{\partial t} + \frac{\partial(uT)}{\partial x} + \frac{\partial(vT)}{\partial y} = \frac{\partial}{\partial x}\left[\left(\frac{\nu}{Pr} + \frac{\nu_T}{Pr_T}\right)\frac{\partial T}{\partial x}\right] + \frac{\partial}{\partial y}\left[\left(\frac{\nu}{Pr} + \frac{\nu_T}{Pr_T}\right)\frac{\partial T}{\partial y}\right] \qquad (35)$$

The term ν/Pr appearing in the temperature equation (35) is obtained from the definition of the laminar Prandtl number that is already defined as $Pr = \nu/\alpha$ where $\alpha = k/\rho C_p$.

Interestingly, the time-averaged equations above have the same form as those developed for the laminar equations except for the additional turbulent viscosity found in the diffusion and non-pressure gradient terms for the momentum equations and also found in the diffusion term for the energy equation. Hence, the solution to turbulent flow in engineering problems entails greater diffusion that is imposed by the turbulent nature of the fluid flow. Additional

differential transport equations that are required for the standard k-ε model, for the case of a variable fluid property in conservative form, are given by

$$\frac{\partial(\rho k)}{\partial t}+\frac{\partial(\rho u k)}{\partial x}+\frac{\partial(\rho v k)}{\partial y}=\frac{\partial}{\partial x}\left(\frac{\mu_T}{\sigma_k}\frac{\partial k}{\partial x}\right)+\frac{\partial}{\partial y}\left(\frac{\mu_T}{\sigma_k}\frac{\partial k}{\partial y}\right)+P-D \quad (36)$$

$$\frac{\partial(\rho \varepsilon)}{\partial t}+\frac{\partial(\rho u \varepsilon)}{\partial x}+\frac{\partial(\rho v \varepsilon)}{\partial y}=\frac{\partial}{\partial x}\left(\frac{\mu_T}{\sigma_\varepsilon}\frac{\partial \varepsilon}{\partial x}\right)+\frac{\partial}{\partial y}\left(\frac{\mu_T}{\sigma_\varepsilon}\frac{\partial \varepsilon}{\partial y}\right)+\frac{\varepsilon}{k}(C_{\varepsilon 1}P-C_{\varepsilon 2}D) \quad (37)$$

with the destruction term D is given by $\rho\varepsilon$ and the production term P formulated as

$$P = 2\mu_T\left[\left(\frac{\partial u}{\partial x}\right)^2+\left(\frac{\partial v}{\partial y}\right)^2\right]+\mu_T\left(\frac{\partial u}{\partial y}+\frac{\partial v}{\partial x}\right)^2-\frac{2}{3}\mu_T\left(\frac{\partial u}{\partial x}+\frac{\partial v}{\partial y}\right)^2 -\frac{2}{3}\rho\mu_T k\left(\frac{\partial u}{\partial x}+\frac{\partial v}{\partial y}\right)$$

For the case of a constant fluid property, the differential transport equations in nonconservative form are expressed as

$$\frac{\partial k}{\partial t}+u\frac{\partial k}{\partial x}+v\frac{\partial k}{\partial y}=\frac{\partial}{\partial x}\left(\frac{\nu_T}{\sigma_k}\frac{\partial k}{\partial x}\right)+\frac{\partial}{\partial y}\left(\frac{\nu_T}{\sigma_k}\frac{\partial k}{\partial y}\right)+P-D \quad (38)$$

$$\frac{\partial \varepsilon}{\partial t}+u\frac{\partial \varepsilon}{\partial x}+v\frac{\partial \varepsilon}{\partial y}=\frac{\partial}{\partial x}\left(\frac{\nu_T}{\sigma_\varepsilon}\frac{\partial \varepsilon}{\partial x}\right)+\frac{\partial}{\partial y}\left(\frac{\nu_T}{\sigma_\varepsilon}\frac{\partial \varepsilon}{\partial y}\right)+\frac{\varepsilon}{k}(C_{\varepsilon 1}P-C_{\varepsilon 2}D) \quad (39)$$

where the destruction term D is given by ε and the production term P is formulated as

$$P = 2\nu_T\left[\left(\frac{\partial u}{\partial x}\right)^2+\left(\frac{\partial v}{\partial y}\right)^2\right]+\nu_T\left(\frac{\partial u}{\partial y}+\frac{\partial v}{\partial x}\right)^2$$

The physical significance of the above equations is the rate of change and the advection transport of k or ε equals the diffusion transport combined with the rate of production and destruction of k or ε. The equations contain five adjustable constants$C_\mu, \sigma_k, \sigma_e, C_{e1}$, and C_{e2}. These constants have been arrived at by comprehensive data fitting for a wide range of turbulent flows (Launder and Spalding, 1974):

$$C_\mu = 0.09,\ \sigma_k = 1.0,\ \sigma_e = 1.3,\ C_{\varepsilon 1} = 1.44,\ C_{\ell 2} = 1.92$$

The production and destruction of turbulent kinetic energy are always closely linked in the k-equations (36) and (38). The dissipation rate ε is large where the production of k is large. The model equations (36) and (38) assume that the production and destruction terms are proportional to the production and destruction terms of the k-equation. Adoption of such terms ensures that ε increases rapidly if k increases rapidly and that it decreases sufficiently fast to avoid nonphysical (negative) values of turbulent kinetic energy if k decreases[14]

3.3. Numerical Modelling

3.3.1. Finite Volume method.

The finite-volume method discretizes the integral form of the conservation equations directly in the physical space. The computational domain is subdivided into a finite number of contiguous control volumes, where the resulting statements express the exact conservation of relevant properties for each of the control volumes. For the finite-volume method, we now have the flexibility of representing the grid by either structured or unstructured mesh. For illustration purposes of the finite-volume method, we consider a typical representation of structured (quadrilateral) and unstructured (triangle) finite-volume elements in two dimensions shown in Fig.3.1 for the discretization of the partial differential equations.

The cornerstone of the finite volume method is the control volume integration. In a control volume, the bounding surface areas of the element are directly linked to the discretization of the first- and second-order derivatives for ϕ (the generic flow-field variable). Here, the surface areas in the normal direction ($\bar{n}$) to the volume surfaces as indicated in Fig. 3.1 are resolved with respect to the Cartesian coordinate directions to yield the projected areas A_i^x and A_i^y in the x and y directions, respectively. The projected areas are positive if their outward normal vectors from the volume surfaces are directed in the same directions of the Cartesian coordinate system; otherwise, they are negative.

By applying Gauss's divergence theorem to the volume integral, the first order derivative of ϕ in two dimensions, can be approximated by

$$\left(\frac{\partial \phi}{\partial x}\right) = \frac{1}{\Delta V}\int_V \frac{\partial \phi}{\partial x} dV = \frac{1}{\Delta V}\int_A \phi dA^x \approx \frac{1}{\Delta V}\sum_{i=1}^{N} \phi_i A_i^x \quad (3.31)$$

Where ϕ_i variables are values at the elemental surfaces and N denotes the number of bounding surfaces on the elemental volume. This equation (3.31) applies for any type of finite-volume element that can be represented within the numerical grid. For a quadrilateral element in two dimensions for the structured mesh as seen in Fig. 3.1, N has the value of four since there are four bounding surfaces of the element. In three dimensions, for a hexagonal element, N becomes six. Similarly, the first-order derivative for ϕ in the y direction is obtained in exactly the same fashion, which can be written as

$$\left(\frac{\partial \phi}{\partial y}\right) = \frac{1}{\Delta V}\int_{\Delta V} \frac{\partial \phi}{\partial y} dV = \frac{1}{\Delta V}\int_A \phi dA^y \approx \frac{1}{\Delta V}\sum_{i=1}^{N} \phi_i A_i^y \quad (3.32)$$

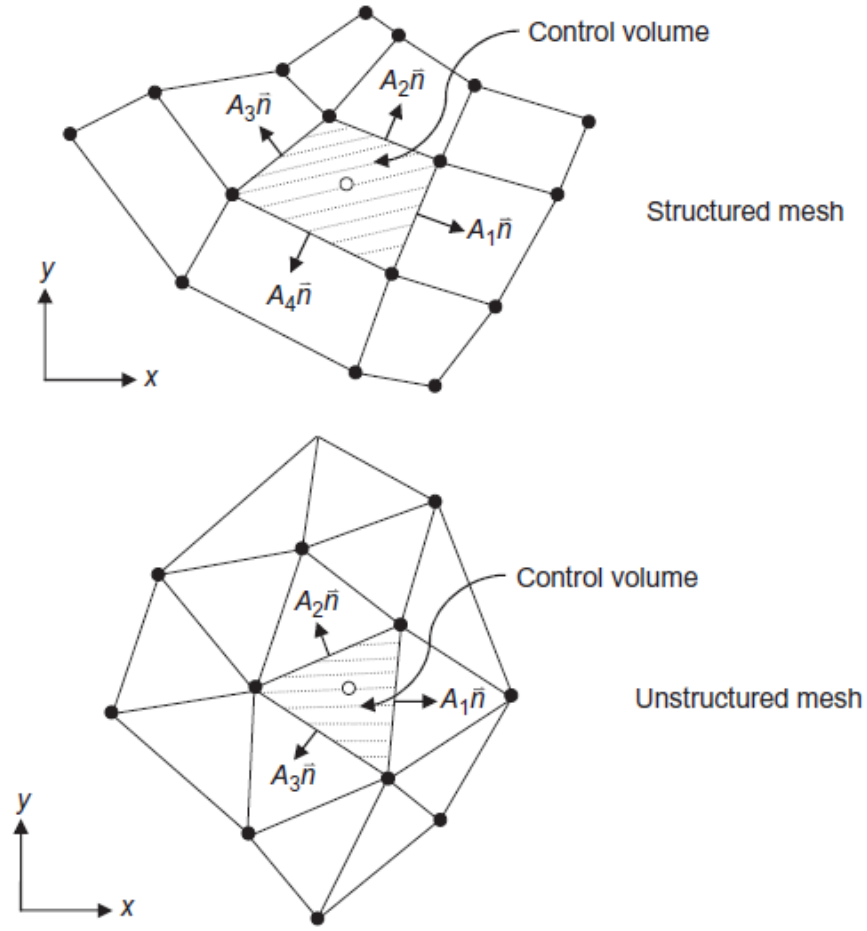

FIG. 3.1 *A representation of structured and unstructured mesh for the finite-volume method (full symbols denote element vertices, and open symbols at the centre of the control volumes denote computational nodes*).

3.3.2. CONVERTING GOVERNING EQUATIONS TO ALGEBRAIC EQUATION SYSTEM

3.3.3. Finite Volume Method

When the finite-volume method is applied, we have to consider the physical domain as being divided into finite control volumes surrounding the nodal points W,P, and E. Fig. 3.2 shows a control volume surrounding the nodal point P. The distances between the nodes W and P and between nodes P and E are identified by the respective notations δx_W and δx_E. For this one-dimensional case, the control volume width surrounding the nodal point P is Δx since Δy and Δz have dimensions of unit length.

To apply the finite-volume discretization, the gradient term can be approximated by the use of Eq. (3.31).

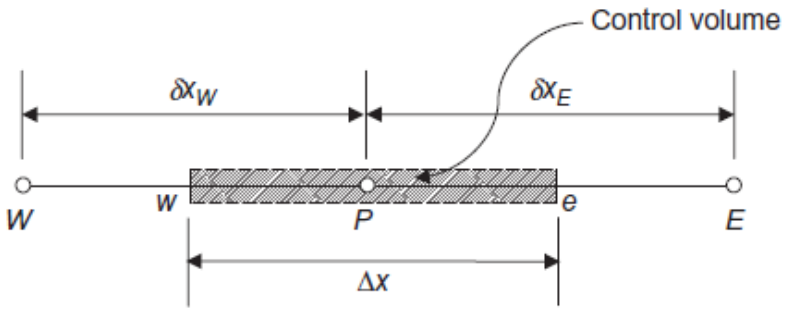

FIG. 3.2 A schematic representation of a control volume around a node P in a one-dimensional domain using the finite-volume method.

This gives

$$\frac{\partial}{\partial x}\left(\Gamma\frac{\partial\phi}{\partial x}\right)=\frac{1}{\Delta V}\int_{\Delta V}\frac{\partial}{\partial x}\left(\Gamma\frac{\partial\phi}{\partial x}\right)dV=\frac{1}{\Delta V}\int_{A}\left(\Gamma\frac{\partial\phi}{\partial x}\right)dA^{x}\approx\frac{1}{\Delta V}\sum_{i=1}^{2}\left(\Gamma\frac{\partial\phi}{\partial x}\right)A_{i}^{x} \qquad (3.33)$$

(5.24)

Here, the projected areas A_i^x for the one-dimensional case are given by $A_1^x = -A_W$ and $A_2^x = A_E$. Eq. (3.33) can thus be written as

$$\left(\Gamma\frac{\partial\phi}{\partial x}\right)_e A_E - \left(\Gamma\frac{\partial\phi}{\partial x}\right)_w A_w \qquad (3.34)$$

For the remaining term in the equation, the source term is approximated as

$$\frac{1}{\Delta V}\int_{\Delta V} S_\phi dV = S_\phi \qquad (3.35)$$

where S_ϕ is assumed to be constant within ΔV, which is the finite control volume. The final fom of the discretized equation becomes

$$\frac{1}{\Delta V}\left(\Gamma\frac{\partial\phi}{\partial x}\right)_k A_E - \frac{1}{\Delta V}\left(\Gamma\frac{\partial\phi}{\partial x}\right)_w A_w + S_\phi = 0 \qquad (3.36)$$

To express an algebraic form for Eq. (3.36) with the nodal points $W, E,$ and P, approximations to the gradients $\partial\phi/\partial x$ at the west ($^4w'$) and east ($'e'$) faces of the control volume are required. We will assume the piecewise linear gradient profiles spanning the nodal points between W and P and between P and E to sufficiently approximate the first-order derivatives at $'w'$ and $'e'$; the diffusive fluxes are evaluated as

$$\left(\Gamma\frac{\partial\phi}{\partial x}\right)_e A_E = \Gamma_e A_E\left(\frac{\phi_E-\phi_P}{\delta x_E}\right) \qquad (3.37)$$

$$\left(\Gamma\frac{\partial\phi}{\partial x}\right)_w A_W = \Gamma_w A_W\left(\frac{\phi_P-\phi_W}{\delta x_W}\right) \qquad (3.38)$$

Substitution of Eqs (3.37) and 3.38) into Eq. (3.36) gives

$$\frac{\Gamma_c A_E}{\Delta V}\left(\frac{\phi_E-\phi_P}{\delta x_E}\right) - \frac{\Gamma_w A_W}{\Delta V}\left(\frac{\phi_P-\phi_W}{\delta x_W}\right) + S_\phi = 0 \qquad (3.39)$$

Eq. (3.39) presents a very attractive feature of the finite-volume method. This discretized equation possesses a clear physical interpretation. It states that the difference between the diffusive fluxes of ϕ at the east and west faces of the control volume equals to the generation of ϕ and constitutes a balance equation for ϕ over the control volume. Eq. (3.39) can be rearranged as

$$\frac{1}{\Delta V}\left(\frac{\Gamma_e A_E}{\delta x_E}+\frac{\Gamma_w A_W}{\delta x_W}\right)\phi_P=\frac{1}{\Delta V}\left(\frac{\Gamma_t A_E}{\delta x_E}\right)\phi_E+\frac{1}{\Delta V}\left(\frac{\Gamma_w A_W}{\delta x_W}\right)\phi_W+S_\phi \quad (3.40)$$

As above, by identifying the coefficients of ϕ_E and ϕ_W in Eq. (5.31) as a_E and a_W and the coefficient of ϕ_P as a_P, the algebraic form can be written as

$$a_P\varphi_P=a_E\phi_E+a_W\phi_W+b \qquad (3.40)$$

where

$$a_E=\frac{\Gamma_e A_E}{\Delta V\delta x_E};\ a_W=\frac{\Gamma_w A_W}{\Delta V\delta x_W};\ a_P=a_E+a_W;\ b=S_\phi$$

3.3.4. CFD Solution Procedure

There are two fundamental approaches to design and analysis of engineering systems that involve fluid flow: experimentation and calculation. The former typically involves construction of models that are tested in wind tunnels or other facilities while the latter involves solution of differential equations, either analytically or computationally.

In the present section we provide a brief introduction to computational fluid dynamics (CFD), the field of study devoted to solution of the equations of fluid flow through use of a computer (or, more recently, several computers working inparallel). Modern engineers apply both experimental and CFD analyses, and the two complement each other. For example, engineers may obtain global properties, such as lift, drag, pressure drop, or power, experimentally, but use CFD to obtain details about the flow field, such as shear stresses, velocity and pressure profiles , and flow streamlines. In addition, experimental data are often used to validate CFD solutions by matching the computationally and experimentally determined global quantities. CFD is then employed to shorten the design cycle through carefully controlled parametric studies, thereby reducing the required amount of experimental testing.

The current state of computational fluid dynamics is that CFD can handle laminar flows with ease, but turbulent flows of practical engineering interest are impossible to solve without invoking turbulence models. Unfortunately, no turbulence model is universal, and a turbulent CFD solution is only as good as the appropriateness of the turbulence model. In spite of this limitation, the standard turbulence models yield reasonable results for many practical engineering problems.

Almost all current commercial and possibly in some shareware CFD packages include user-friendly graphical user interface (GUI) applications and environments to input problem parameters and to examine the computed results. Hence, these codes provide a complete CFD analysis consisting of three main elements:

- Preprocessor
- Solver
- Postprocessor

Fig. 3.3 presents a framework that illustrates the interconnectivity of the three aforementioned elements within the CFD analysis

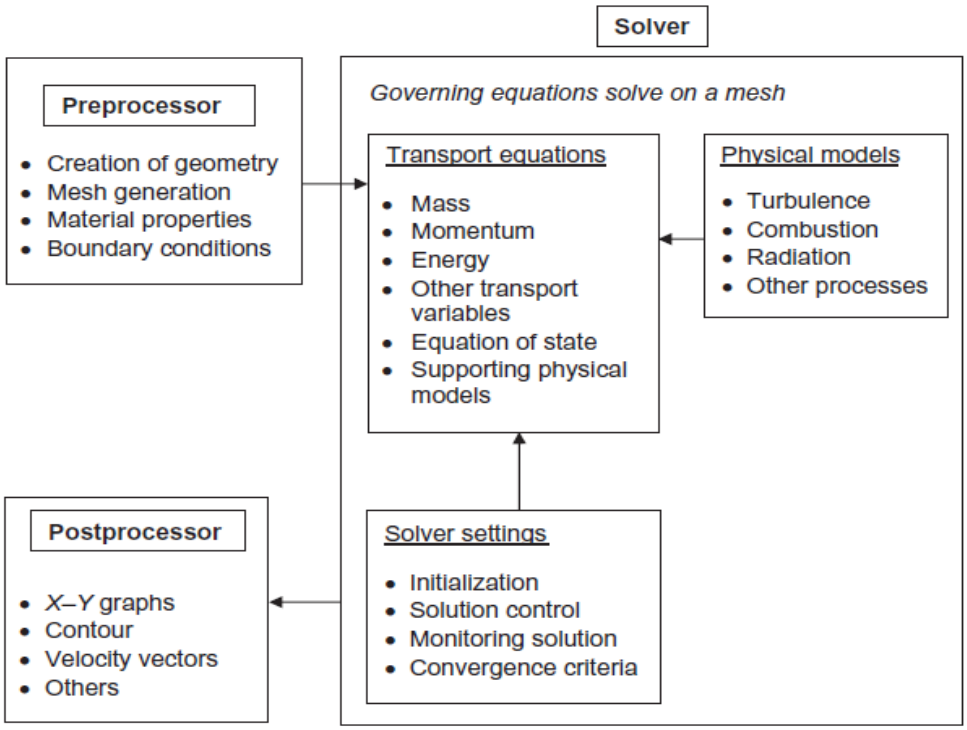

Figure 3.3 The interconnectivity functions of the three main elements within a CFD analysis framework.

3.3.4.1. PROBLEM SETUP—PREPROCESS

Creation of Geometry—Step 1

The first step in any CFD analyses is the definition and creation of geometry of the flow region, that is the computational domain for the CFD calculations. For two-dimensional (2-D) domains, the cells are areas, while for three dimensional (3-D) domains the cells are volumes

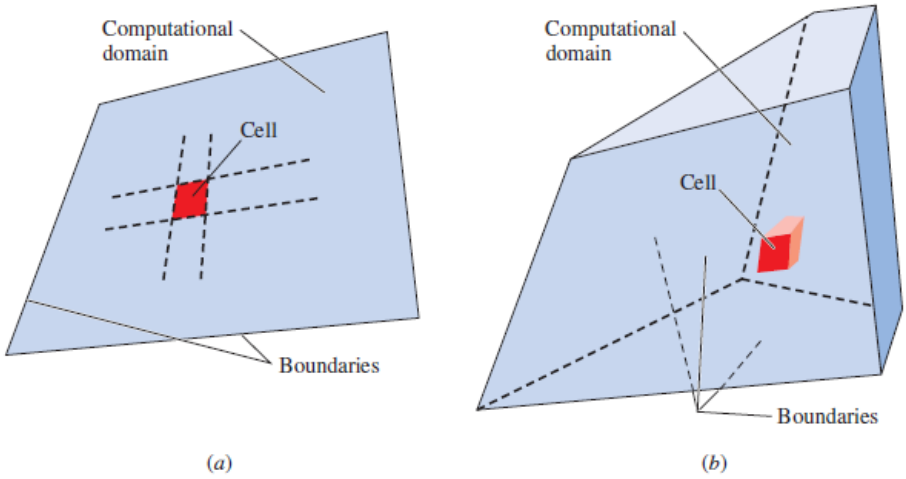

Figure 3.4 *A computational domain is the region in space in which the equations of motion are solved by CFD. A cell is a small subset of the computational domain. Shown are (a) a two dimensional domain and quadrilateral cell, and (b) a three-dimensional domain and hexahedral cell. Theboundaries of a 2-D domain are called edges, while those of a 3-D domainare called faces.*

Mesh Generation—Step 2

The second step that is mesh generation constitutes one of the most important steps during the pre-process stage after the definition of the domain geometry. CFD requires the subdivision of the domain into a number of smaller, nonoverlapping subdomains in order to solve the flow physics within the domain geometry that has been created; this results in the generation of a mesh (or grid) of cells (elements or control volumes) overlaying the whole domain geometry. The essential fluid flows that are described in each of these cells are usually solved numerically so that the discrete values of the flow properties such as the velocity, pressure, temperature, and other transport parameters of interest are determined. This yields the CFD solution to the flow problem that is being solved.

The accuracy of a CFD solution is strongly influenced by the number of cells in the mesh within the computational domain. Whilst, in general, increasing the number of cells will improve the accuracy of the solutions, it is also influenced by many other factors, such as the type of mesh, the order of accuracy of the numerical method, and the adequacy of the techniques chosen to the physics of the problem.

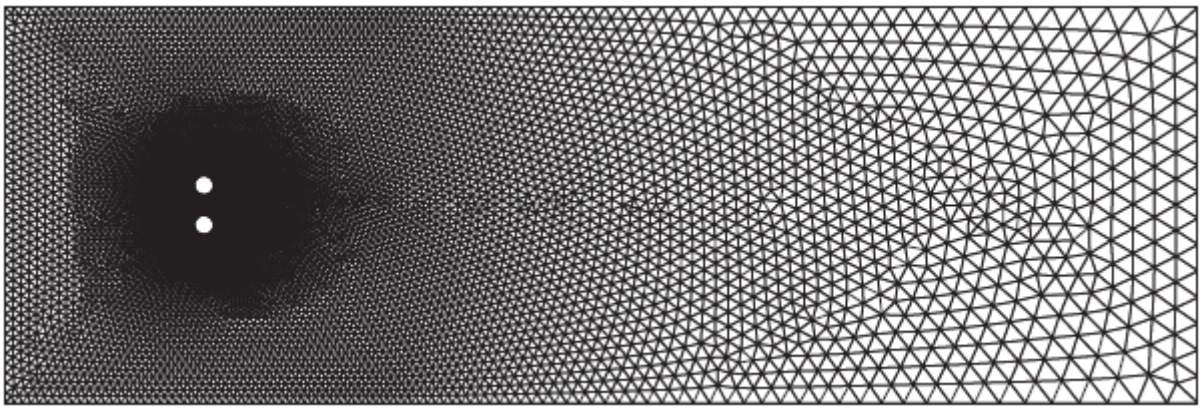

Figure 3.4 Unstructured meshing for fluid passing over two cylinders in an open surrounding.

Selection of Physics and Fluid Properties—Step 3
Many industrial CFD flow problems may require solutions to very complex physical flow processes such as the accommodation of complicated chemical reactions in combusting fluid flows The inclusion of combustion and possibly,radiation models in the CFD calculations are generally prerequisites to the successful modelling of these types of flows. Combustion and radiation processes have the tendency to strongly influence the local and global heat transport, which consequently affect the overall fluid dynamics within the flow domain. It is therefore imperative that a CFD user carefully identifies the underlyingflow physics that is unique to the particular fluid flow system

For clarity and ease of reference, a flowchart highlighting the various flow physics that may be encountered within the framework of CFD and heat transfer processes is presented in Fig 3.5

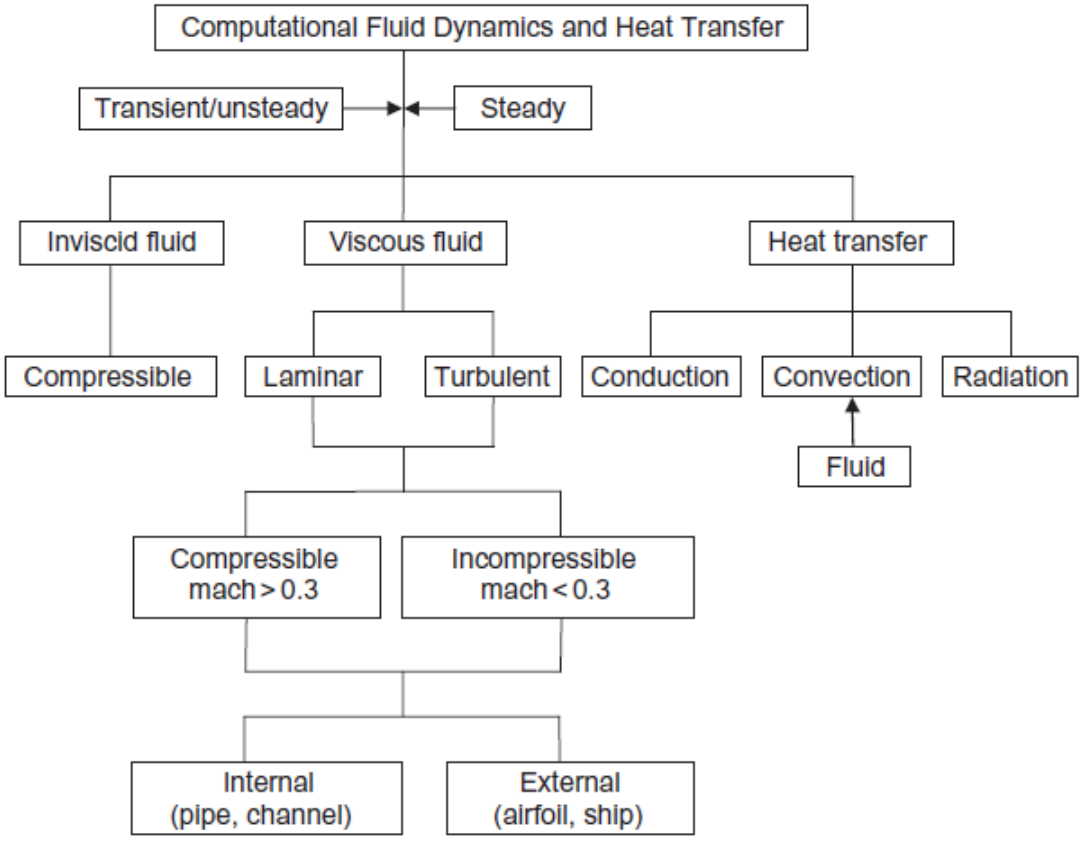

Figure 3.5 *A flowchart encapsulating the various flow physics in CFD.*

Under the main banner of *Computational Fluid Dynamics and Heat Transfer*, a CFD user declares initially whether simulations to the fluid flow system are to be attained for *transient/unsteady* or *steady* solutions. He/she subsequently defines which class of fluids that the flows may belong: *inviscid or viscous. Inviscid* fluid flows are generally compressible, and the consideration of fluid compressibility in the flow physics can usually be handled through the *panel method. Viscous* fluid flows can, however, exist in their *laminar or turbulent state.* Under these two flow conditions, prior knowledge of whether the fluids are *compressible or incompressible is required*.
The classification of *internal and external flows* for viscous fluids allows the user to appropriately treat these types of flow problems in a manner that has been discussed in

Section 3.1 and 3.2. Also, the transport of heat may contribute significantly to the fluid flow process, which comprises of three heat transfer modes: *conduction, convection, and radiation*. For convection, the dominant mode of *heat transfer* will more likely to be driven by the *convective* fluid flow rather than by other modes of *conduction* and *radiation.* Nevertheless, there are circumstances where radiation and convection can coexist and dominate the *heat transfer* especially in the expansion of fires.

Specification of Boundary Conditions—Step 4

The complex nature of many fluid flow behaviours has important implications in which boundary conditions are prescribed for the flow problem A CFD user needs to define appropriate conditions that mimic the real physical representation of the fluid flow into a solvable CFD problem.

The fourth step in the preprocess stage deals with the specification of permissible boundary conditions that are available for impending simulations. Evidently, where there exist inflow and outflow boundaries within the flow domain, suitable fluid flow boundary conditions are required to accommodate the fluid behaviour entering and leaving the flow domain. The flow domain may also be bounded by open boundaries. Although the intricacies of open boundary conditions are still subject to much theoretical debate, this boundary condition
remains the simplest and cheapest form to prescribe when compared with other theoretically more satisfying selections in CFD. Appropriate boundary conditions are also required to be assigned for external stationary solid wall boundaries that bound the flow geometry and the surrounding walls of possible internal obstacles within the flow domain.

3.3.4.2. NUMERICAL SOLUTION—CFD SOLVER

The appropriate usage of either an in-house or a commercial CFD code commands the core understanding of the underlying numerical aspects inside the CFD solver. This section focuses on the treatment of the solver element.A *CFD solver* can usually be described and envisaged by the solution procedure presented in Fig. 3.6. The prerequisite processes in the solution procedure that have implications on the computational solution are *initialization, solution control, monitoring solution, CFD calculation, and checking for convergence*. A CFD user whether applying in-house or commercial codes needs to gain the necessary insights and knowledge pertaining to the workings of these prerequisite processes in order to skillfully utilize the many solver features and better navigate the underlying ‘black box’ operations that reside in many of these codes.

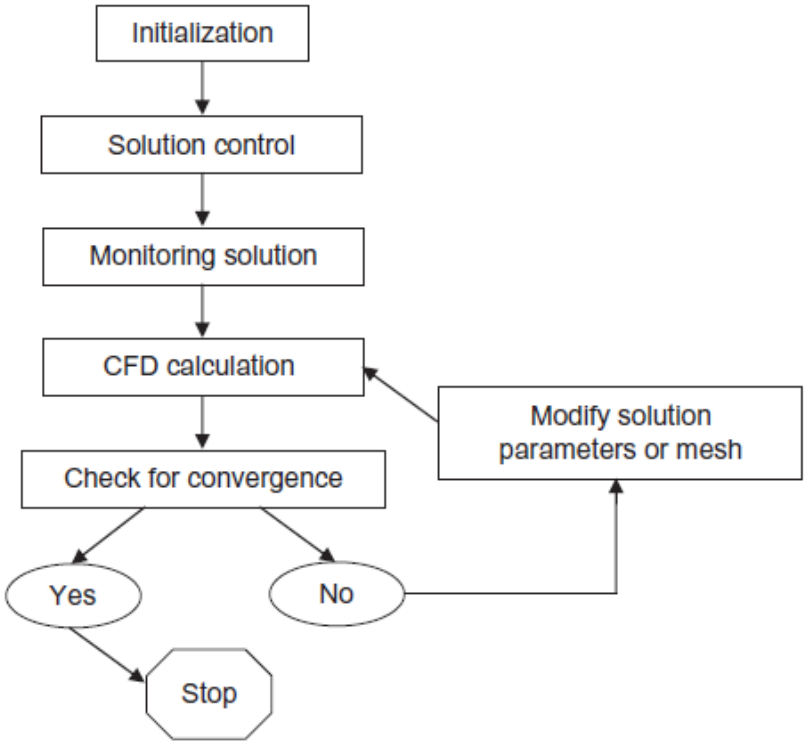

Figure 3.6 An overview of the solution procedure.

Initialization and Solution Control—Step 5

The fifth step of the CFD analysis encompasses two prerequisite processes within the CFD solver that are initialization and solution control.
Firstly, the underlying physical phenomena in real fluid flows that are generally complex and non-linear within such flows usually require the treatment of the key phenomena to be resolved through an iterative solution approach. Iterative procedure generally involves all the discrete values of the flow properties such as the velocity, pressure, temperature, and other transport parameters of interest to be initialized before calculating a solution. In theory, initial conditions
can be purely arbitrary. However, in practice, there are certain advantages to impose initial conditions intelligently. Good initial conditions are crucial to the iterative procedure; two reasons on why the reader as a CFD user should undertake the appropriate selection of initial conditions are the following:

- If the initial conditions are closed to the final steady-state solution, the quicker the iterative procedure will converge and results in shorter computational time.
- If the initial conditions are far away from reality, the computations willresult in longer computational efforts to reach the desired convergence. Also, improper initial conditions may lead to the iterative procedure misbehavingand possibly ‘blowing up’ or diverging

Secondly, the setting up of appropriate parameters in the solution control usually entails the specification of appropriate discretization (interpolation) schemes and selection of suitable iterative solvers.

Monitoring Convergence—Step 6

The sixth step of the CFD solver involves the interlinking operations of three prerequisite processes: monitoring solution, CFD calculation, and checking for convergence. Two aspects that characterize a successful CFD computational solution are convergence of the iterative process and grid independence.

Convergence can usually be assessed by progressively tracking the *imbalances* that are accentuated by the advancement of the numerical calculations of the algebraic equations through each iteration step. These *imbalances* measure the overall conservation of the flow properties; they are also commonly known as the so-called *residuals* that are generally viewed through commercial code GUIs. Example of this GUIs by ANSYS FLUENT that represent the downward trends of the residuals for Case 1 are illustrated in Figs 3.7.

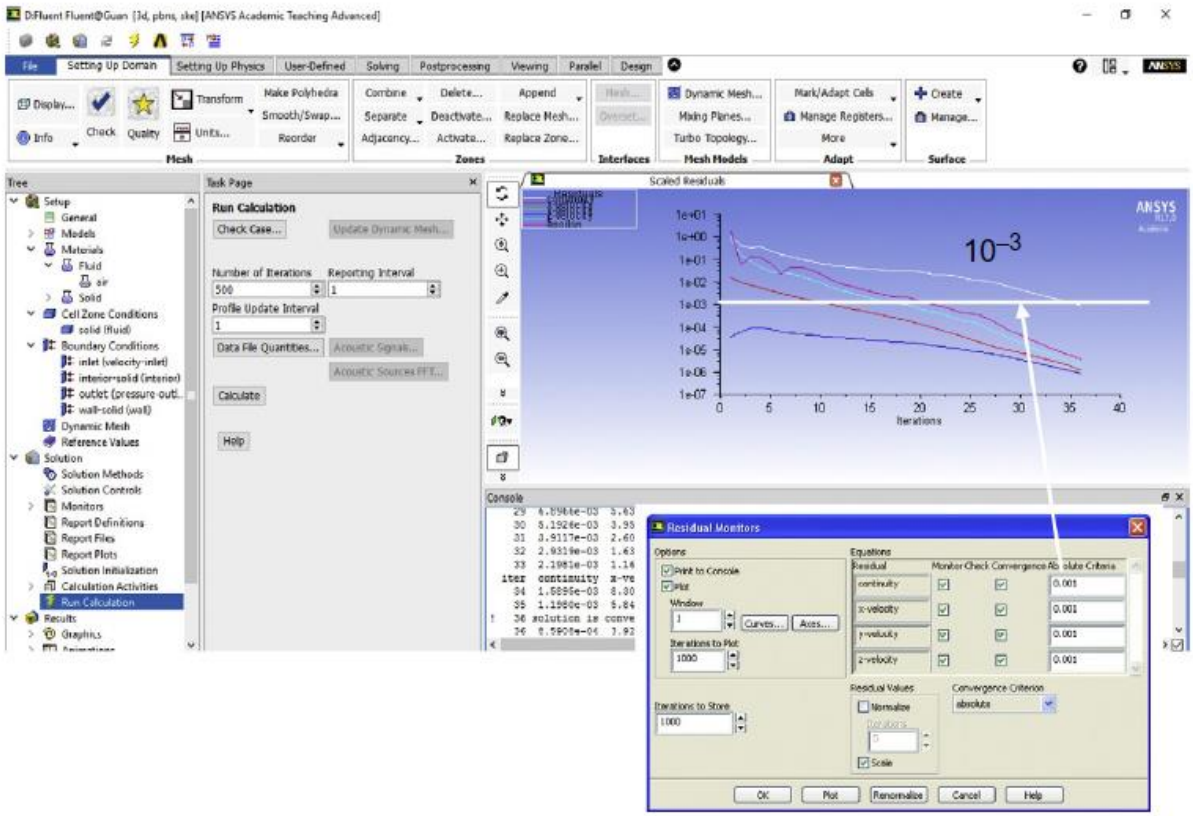

Figure.3.7 Typical FLUENT GUIs for monitoring convergence corresponding to the prescribed convergence criteria.

3.3.4.3. RESULT REPORT AND VISUALIZATION—POSTPROCESS

CFD has a reputation of generating vivid graphical images and, whilst some of them are promotional that are usually displayed in stunning and superb colourful outputs, the ability to present the computational results effectively is an invaluable design tool. Commercial CFD codes such as ANSYS CFX, ANSYS FLUENT, and STAR-CD often incorporate impressive visualization tools within their user-friendly GUIs to allow users to graphically view the results of a CFD calculation at the end of a computational simulation. Each of these codes, to assists the CFD user to better analyze and visualize the many relevant physical characteristics within the fluid flow problem **[18].**

3.4. Simulation in Ansys- Fluent

3.4.1. Geometry

Our geometry is built in ANSYS-Workbench in 3D, It is a plastic Chapel greenhouse with whose geometric characteristics are: 5m wide, 8m long and an entrance height of 3.5m. and an outlet height of 5.5 m.

Our greenhouse is located in the area of Adrar south of Algeria at longitude (0.28) and at attitude (27.86). ANSYS-Workbench made our job easier and allowed us without manual efforts in reducing time and with precision the design and preparation of the geometry of the greenhouse.

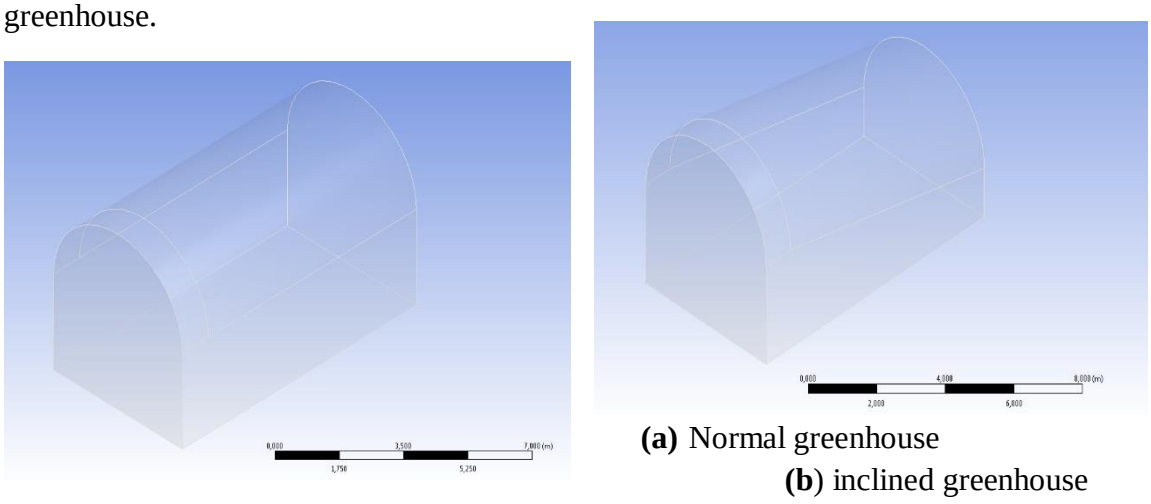

(a) Normal greenhouse

(b) inclined greenhouse

Figure 3.8 *Geometry diagram*

3.4.2. The Mesh

The generation of the mesh is was done using the ANSYS-Workbench, By relying on the previous geometry, we first defined the named selections of all the borders, we fix the dimensions of the mesh as well as the nature of the surface body , the module allows to generate a quadrilateral and triangular mesh in 2D (surface), and hexahedral or tetrahedral in 3D.

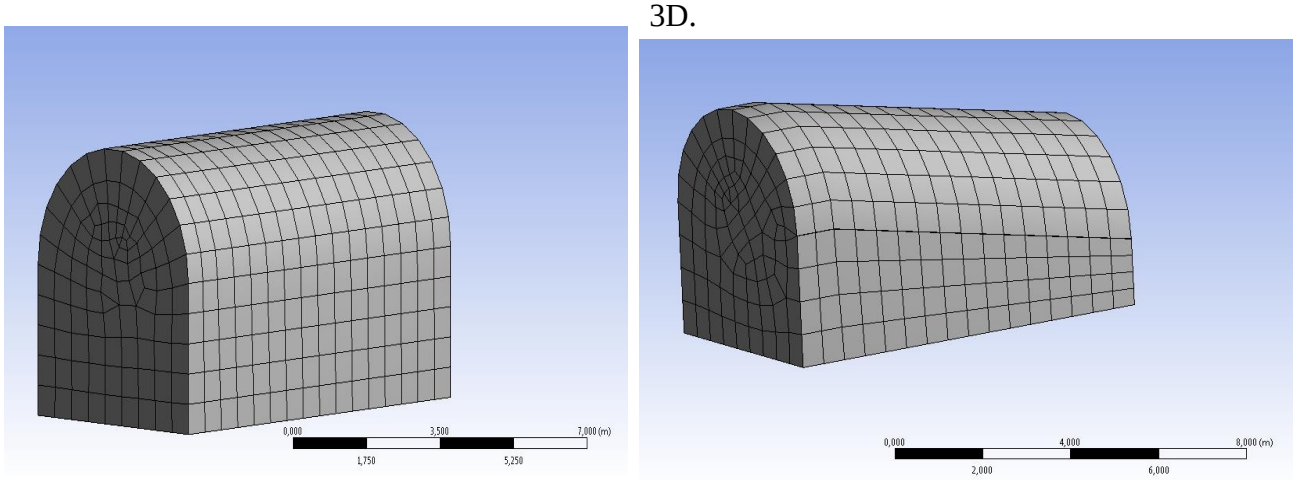

Figure 3.9 *Mesh*

3.4.3. Material Properties

The ANSYS-FLUENT software offers a library of fluids and solids, the most commonly used in fluid mechanics problems, with constant values or variables for each of its properties. In addition, it allows the user to enter and save their own fluid or solid model for other applications.

Fluid

We have chosen air as the fluid, its properties are shown in Table-III .1.

Table 3. Air Properties

Properties	Value
Dynamic Viscosity	$1.7894.10^{-5}$ kg/m-s
Specific Heat	1006.43 j/Kg-k
Thermal Conductivity	0.0242 W/m-k
Density	1.225 kg/m3

Solid

Polyethylene cover:

We use the polyethylene which is the most used. This material is transparent in the visible range, its properties are shown in Table-

Properties	Value
Emissivity	0.55
Specific Heat	1046 j/Kg-k
Thermal Conductivity	0.17 W/m-k
Density	1400 kg/m3

3.4.4. The model of the species

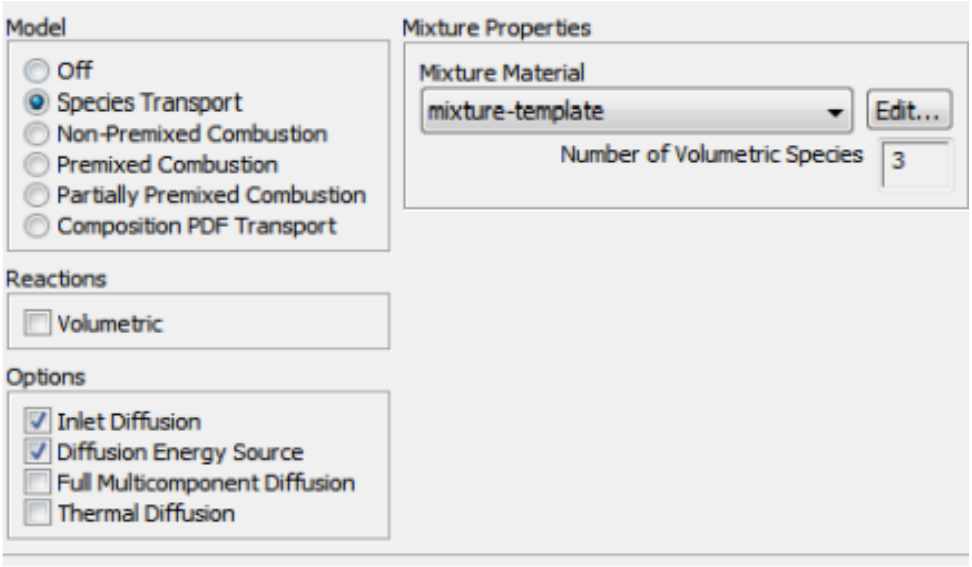

Figure 3.10 Model of Species

3.4.5. Boundary Conditions

The entrance exit and the top wall of the greenhouse is considered to be semitransparent solids that participates in solar radiation and the convection condition. Heat transfer coeffient h = 5 w/m^2

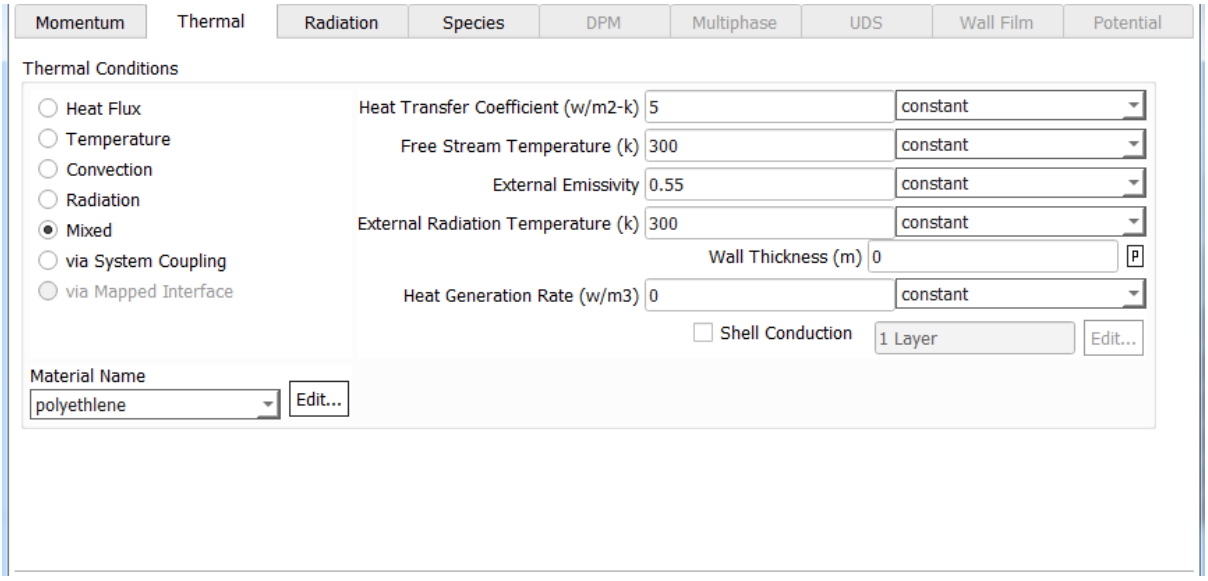

Figure 3.11 Faces and Top Walls Thermal conditions for All Greenhouses

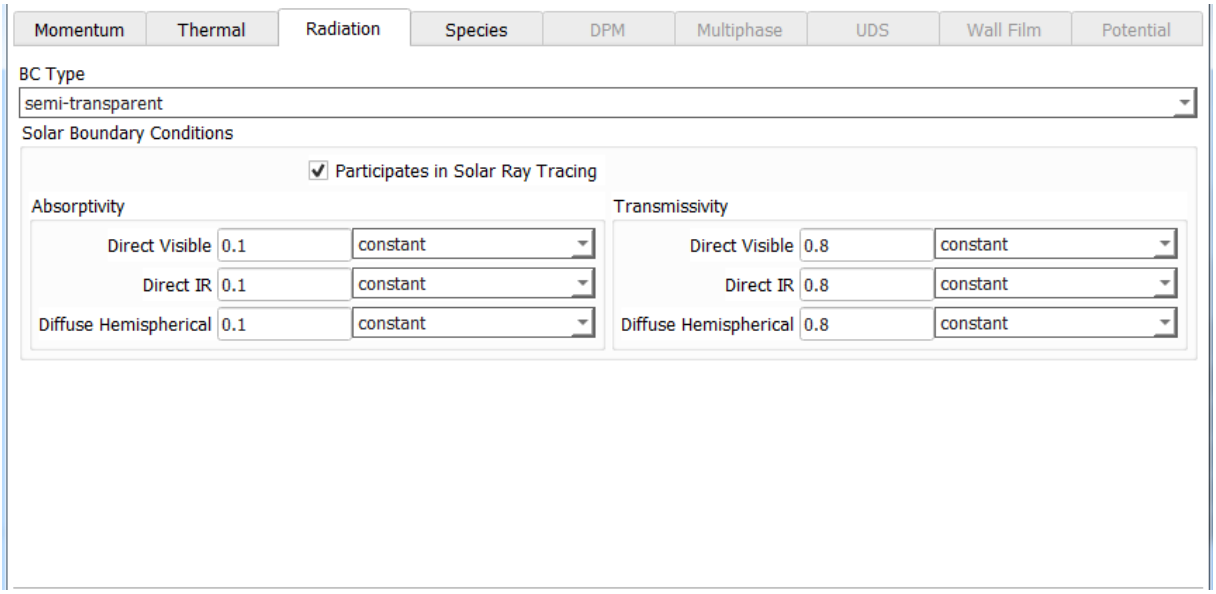

Fig 3.12: Faces and Top Walls Radiation conditions for All Greenhouses

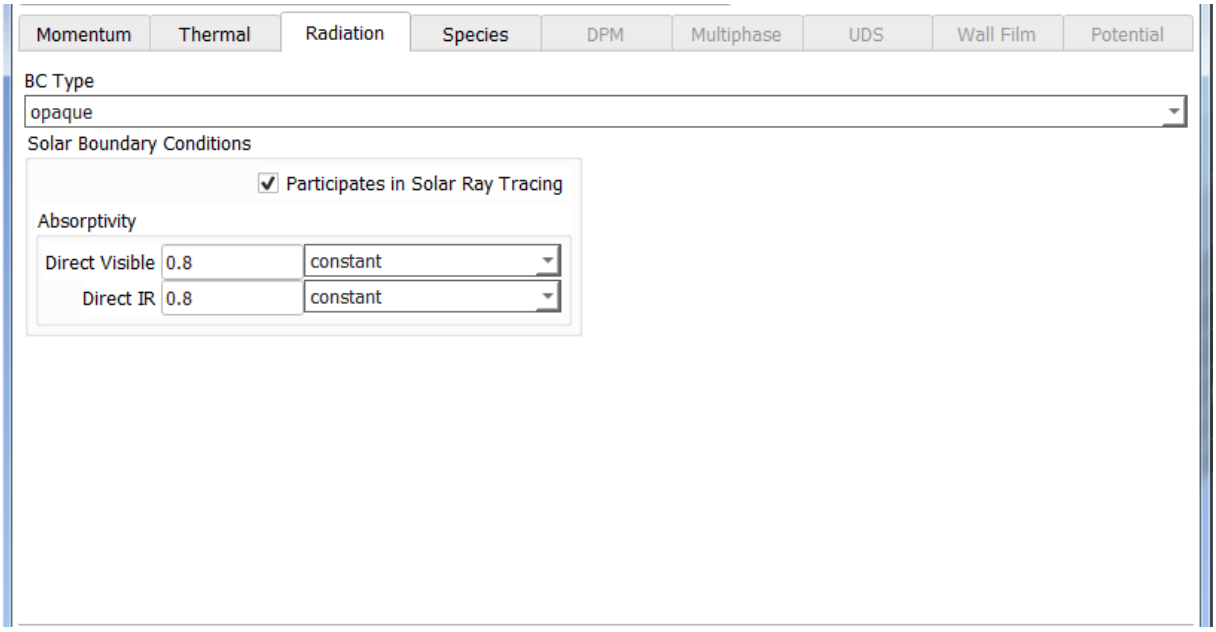

Figure 3.13: Soil Radiation Conditions for All Greenhouses

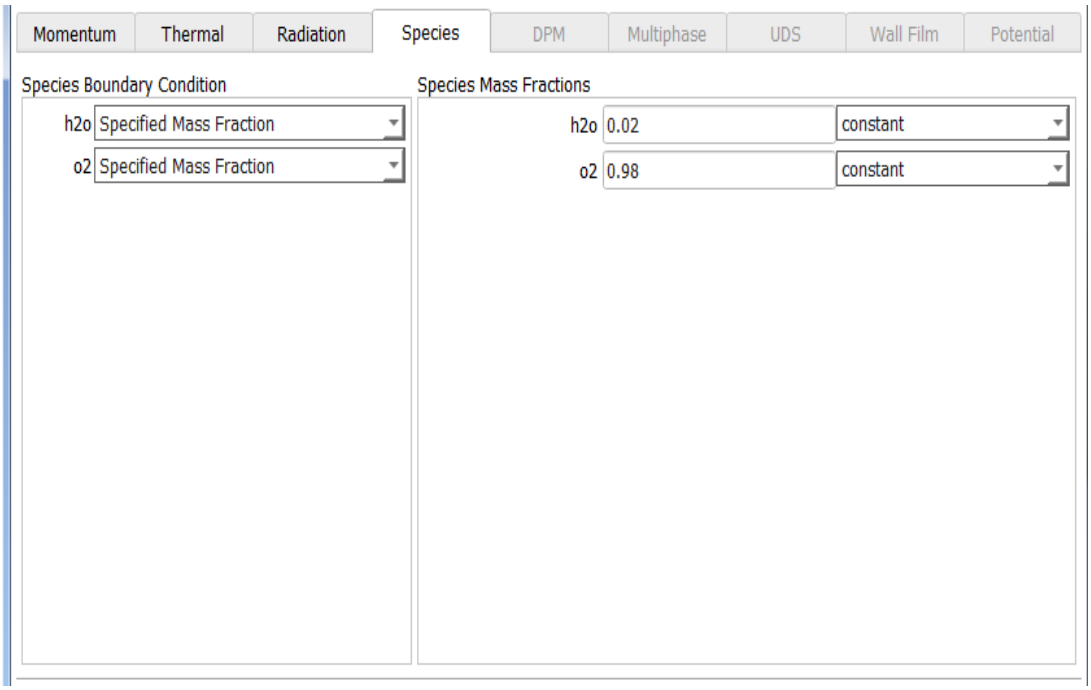

Figure 3.14: Species conditions for all Greenhouse for the floor

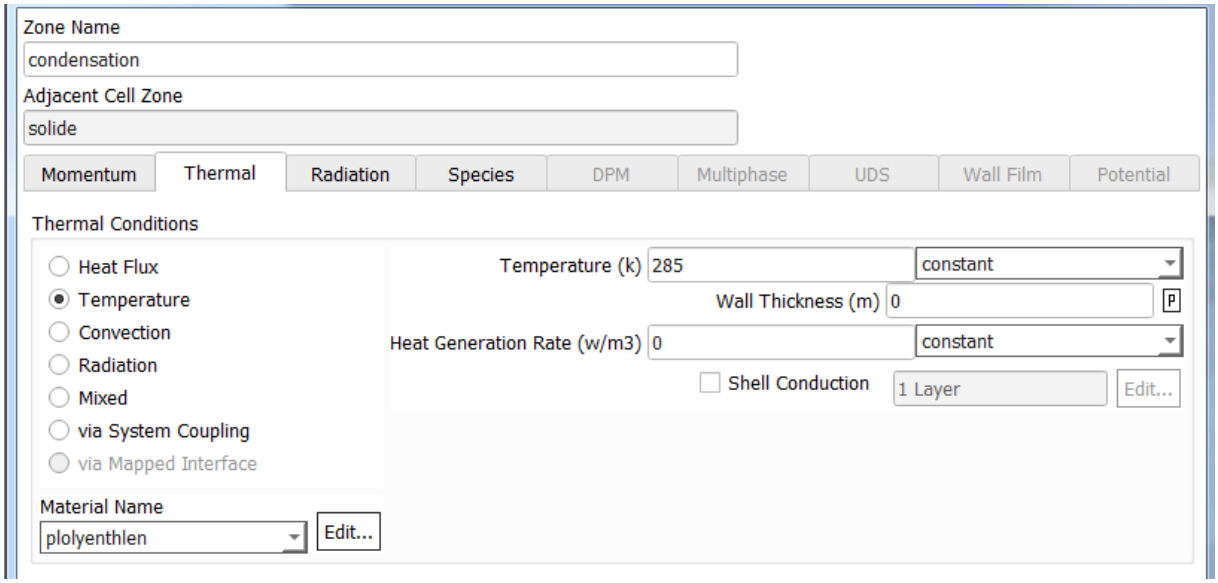

Figure 3.15: Condensation Conditions.

3.4.6. Turbulence Model

Model (**k-ε)**

The turbulence model used is a K-***ε*** model with a so-called standard coefficient

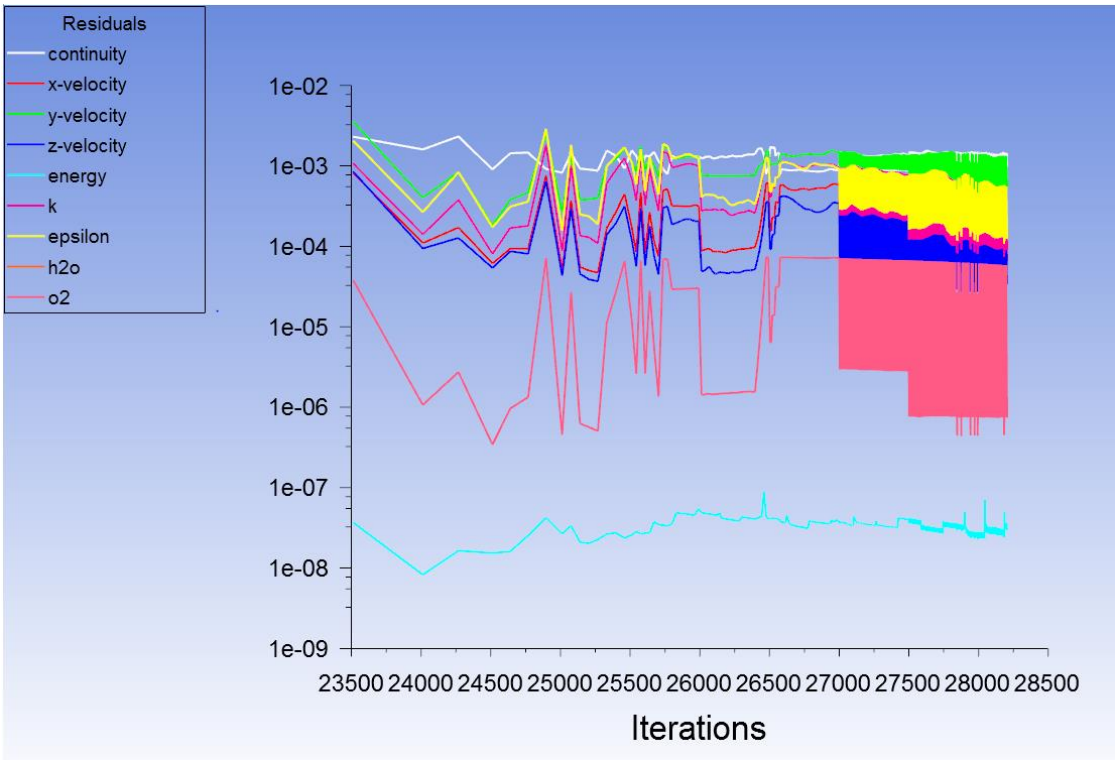

Figure 3.16: k-ε Residual

Chapter 4:

Results and Discussion

4.1Introduction

In this section we undertake a study of different physical phenomena intervening in the evolution behavior of the agricultural greenhouse taking in consideration geometric parameters particularly the inclination of the greenhouse on the distribution of temperature and water vapor in the greenhouse. This analysis is undertaken in order to take advantage of the water coming from the evapo- transpiration.

4 Geometries of the agricultural greenhouse studied are:

A. standard geometry Greenhouse .
B. Standard geometry Greenhouse with condensation,
C. Greenhouse with inclined Roof ..
D. Greenhouse with inclined roof and condensation

Evolution of the temperature, relative humidity and the velocity in the greenhouse is studied for a particular time of the day. That means only 3 times of the day are presented in this Thesis which are 14:30h 17:30h and 20: 30h for all the 4 geometries mentioned above.

We will present, discuss and compare the evolution of these 3 variables for these 3 different times of the day. The simulation was done on the 6th of June 2021 and the cooling system was kept at a condensing temperature of 285K.The time step used in this transient simulation of each calculation is t= 3s.

Greenhouse Index

A- Standard Greenhouse
B- Standard Greenhouse with Condensation
C- Inclined Greenhouse without Condensation
D- Inclined Greenhouse with Condensation**.**

4.2 Validation

My work is validated by the study carried out by **Bakhti Issam Eddine and Touileb Soheib in 2020** at the University of Tlemcen **[19].** The calculations of the results and the simulation conditions of our greenhouse are based on this study which was carried out on the 21th of June 2020 at 14:00h. It can be noted that the results are reliable.

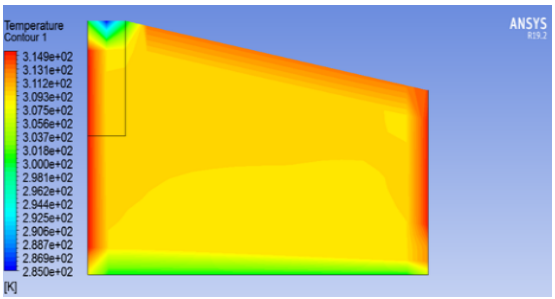

Temperature Simulation Carried Out

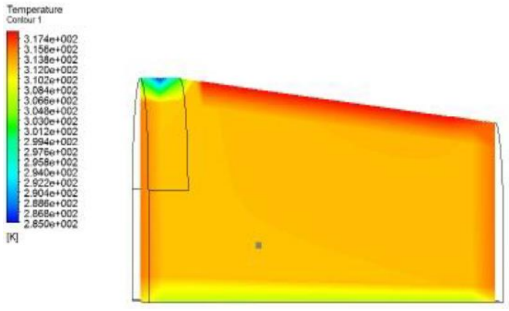

Reference Temperature Simulation

Figure 4.1 . Temperature Validation

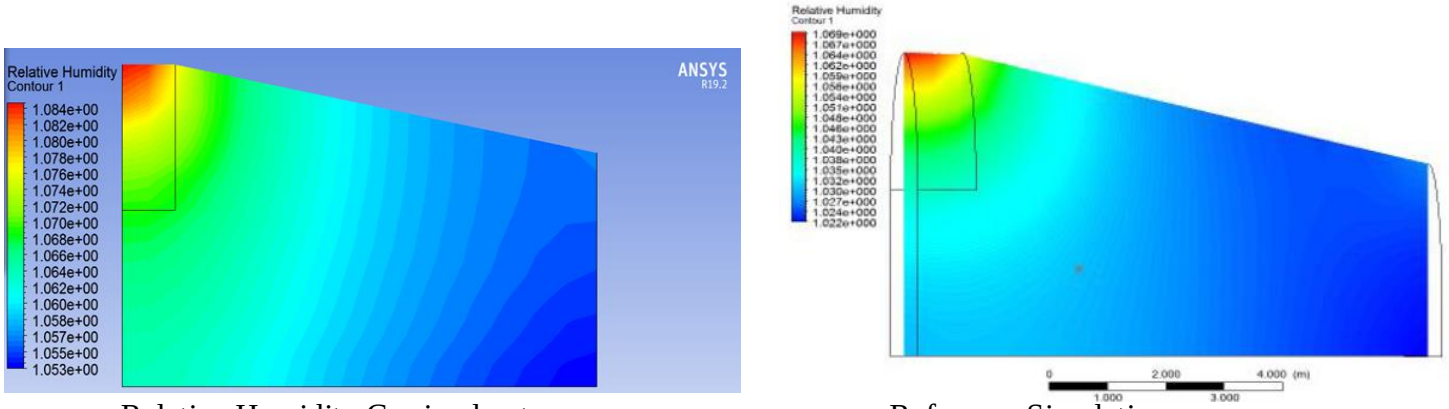

Relative Humidity Carrioud out Reference Simulation

Figure 4. 2 *Relative Humidity Validation.*

4.3. Results and Discussion

4.3.1. Temperature

Temperature at 14: 30

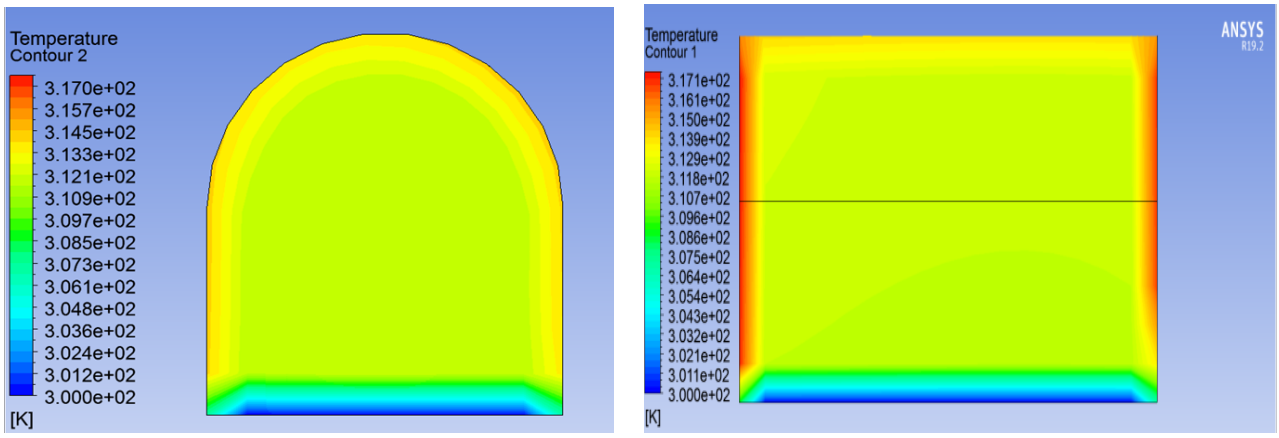

A. Standard Greenhouse

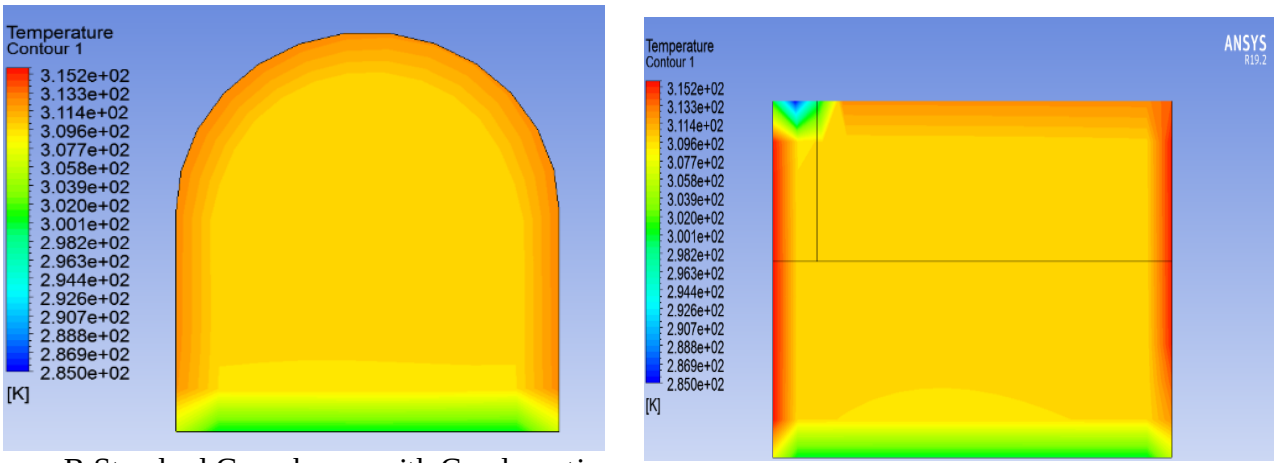

B.Standard Greenhouse with Condensation

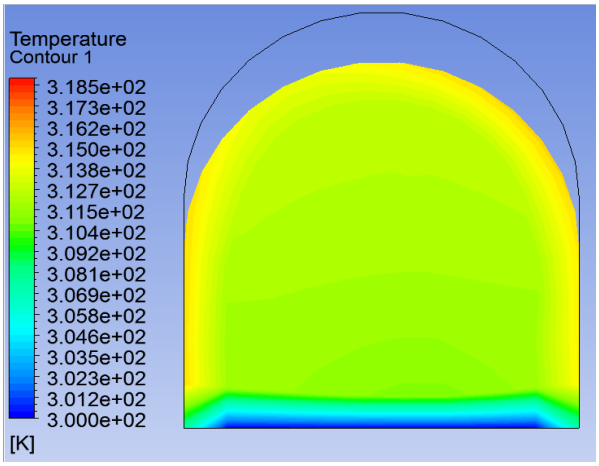

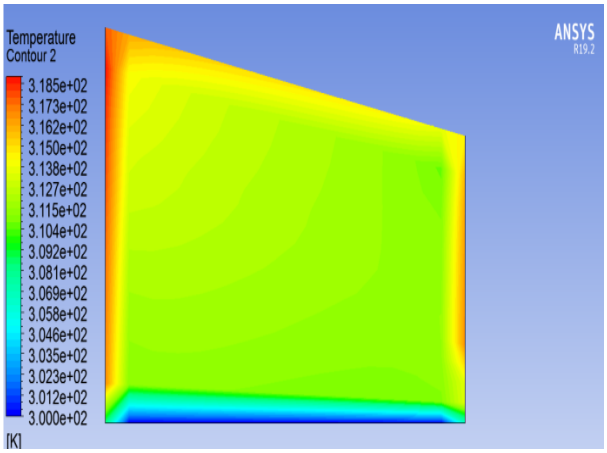

C.Inclined Greenhouse without Condensation

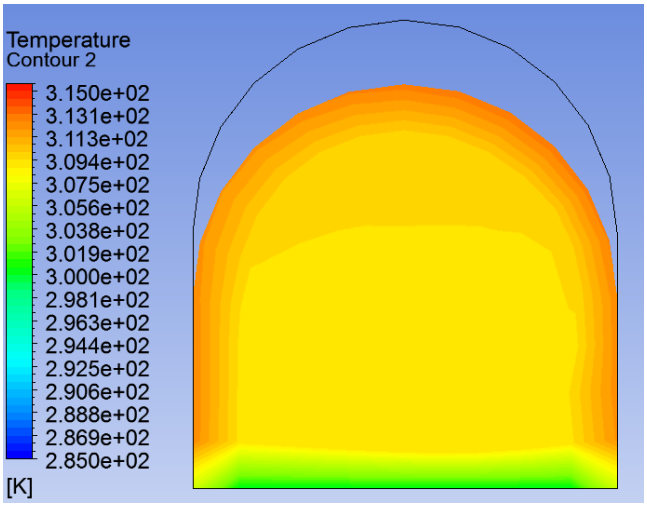

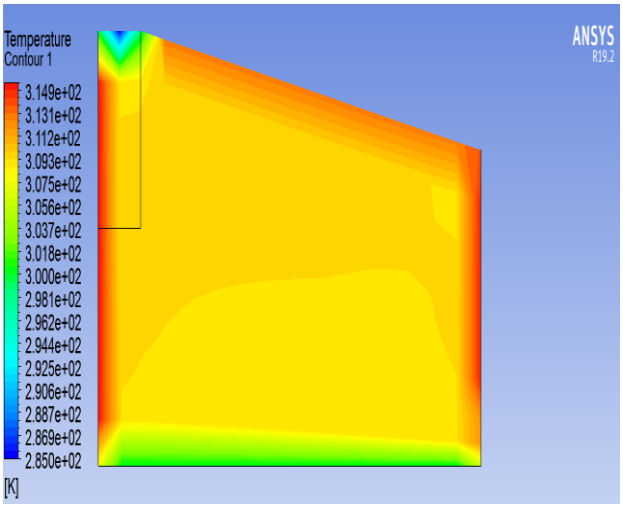

D. Inclined Greenhouse with Condensation.

Figure 4.3 . *Temperature for all greenhouses at 14: 30h*

Interpretation

The figures show the distribution of the temperature inside the 4 greenhouses at 14:30. We can note that the solar flux is well directed towards the roof of the greenhouse, this indicates to us that the sun is almost in the middle of the sky, the temperature distribution in the greenhouse spreads towards all sides especially towards moist soil. The temperature variance is between 285 K and 318 K with the lowest temperature located on the condensing side. The inclined greenhouse has a small increase in temperature compared to the normal structure without an inclination of the roof.

Temperature at 17: 30

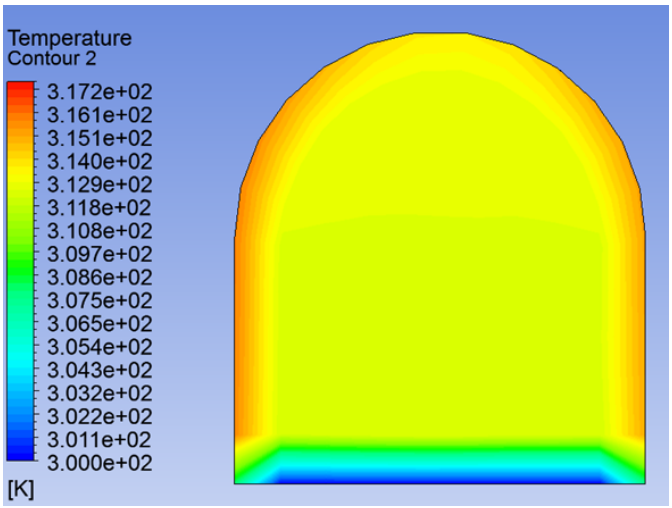

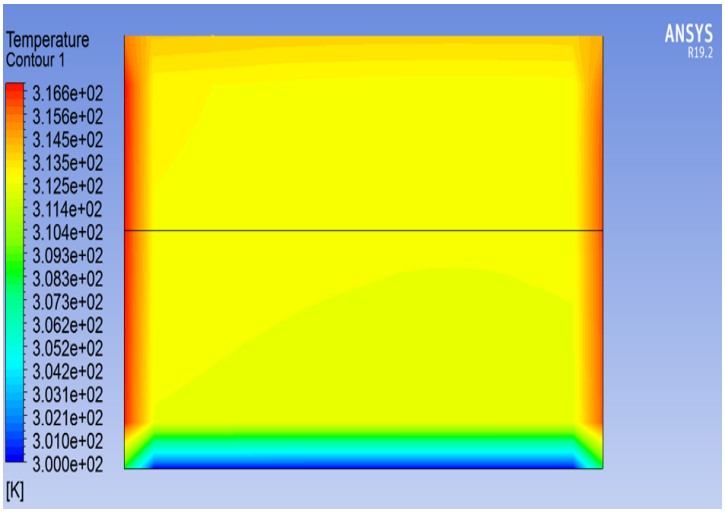

A.Standard Greenhouse

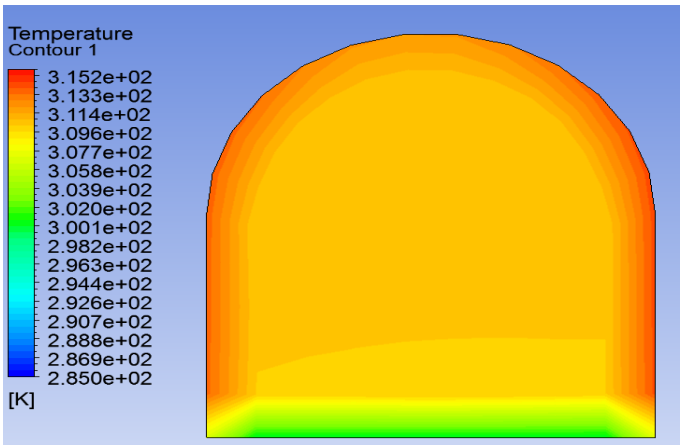

B.

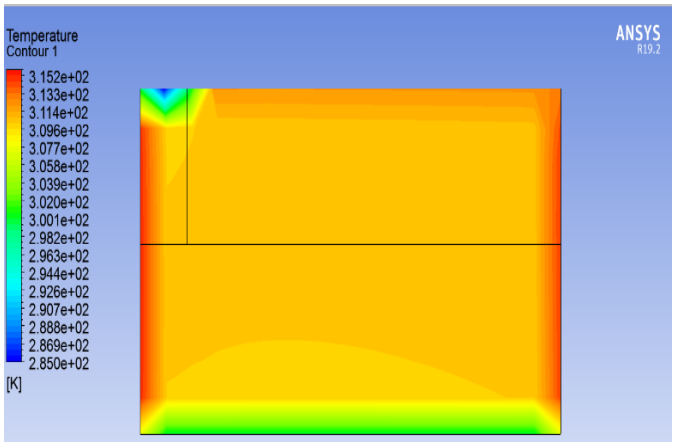

Standard Greenhouse with condensation

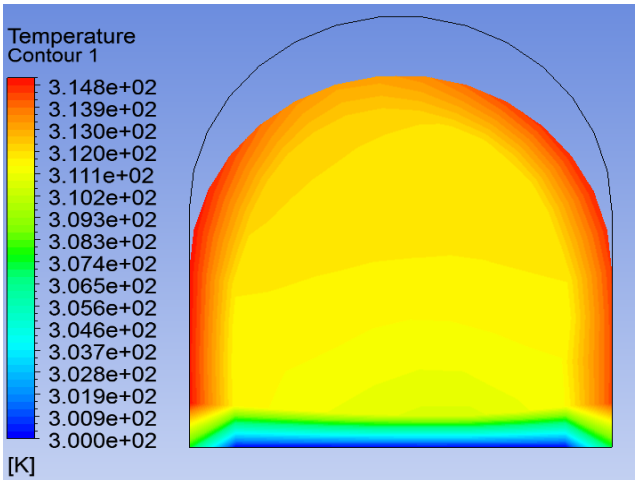

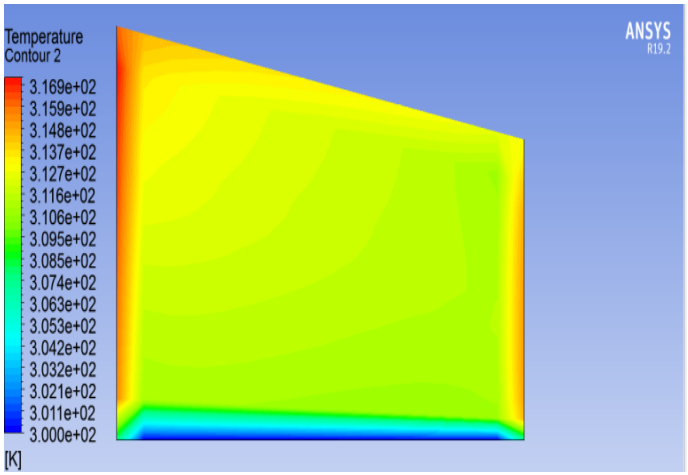

C. Inclined Greenhouse without Condensation

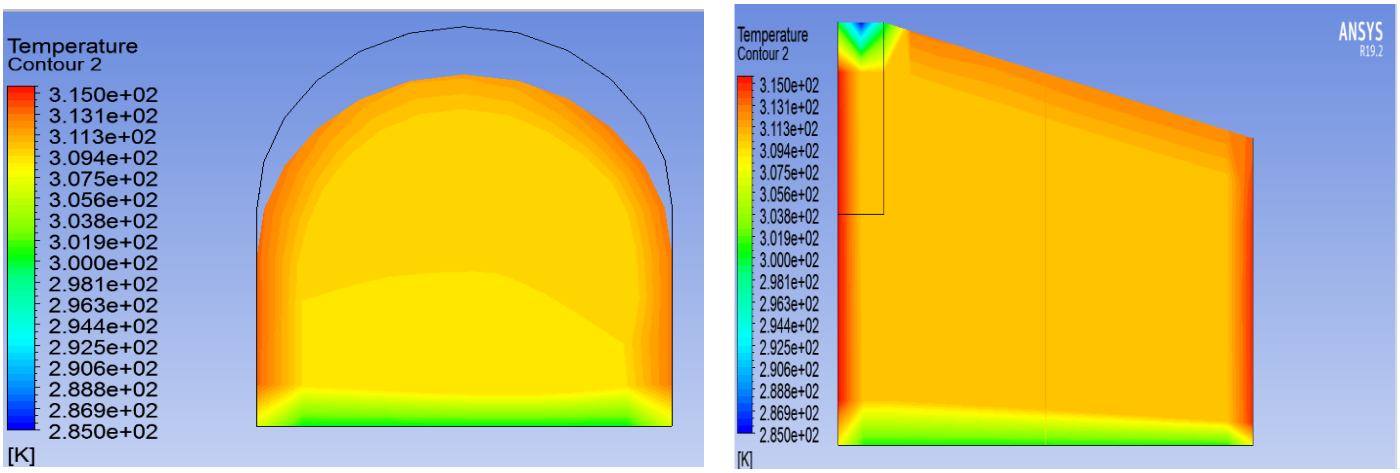

D. Inclined Greenhouse with condensation

Figure 4.4 . *Temperature for all greenhouse at 17: 30*

Interpretation

The figures show the temperature distribution of the 4 greenhouses at 17:30. We notice that over time the sun is moving towards sunset so the solar flux varies and decrease with time. Due to the decrease in solar heat flux, the temperature is slight higher at the edges because of convection and the temperature imposed by the flow decreases compared to the start time of the experiment (13h) and is distributed to the whole greenhouse. The temperature variance is between 285 K and 317 K. we also notice that the temperature is low on the condensation side and the wet soil.

Temperature at 20:30h

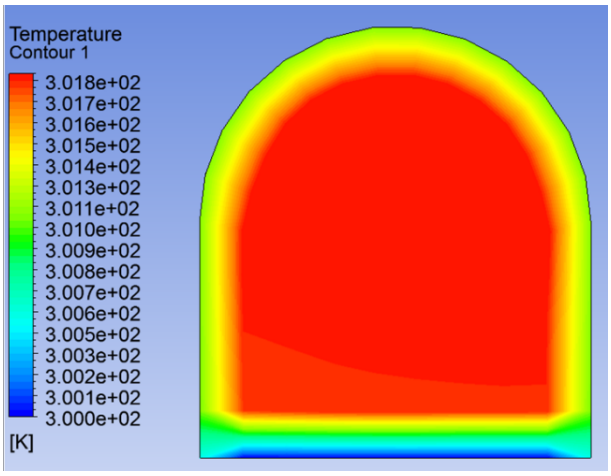

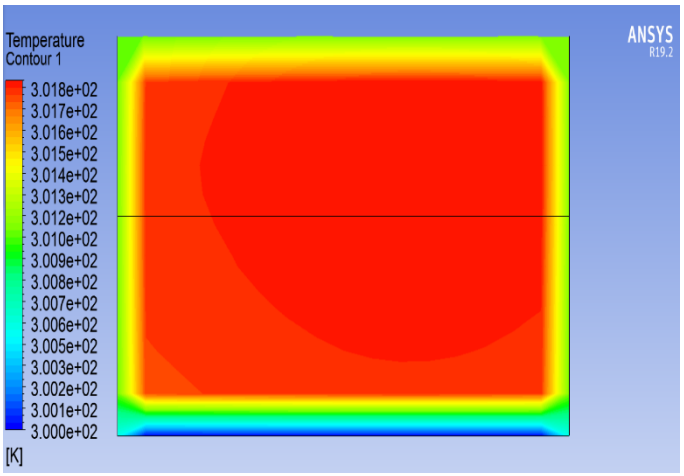

A. Standard Greenhouse

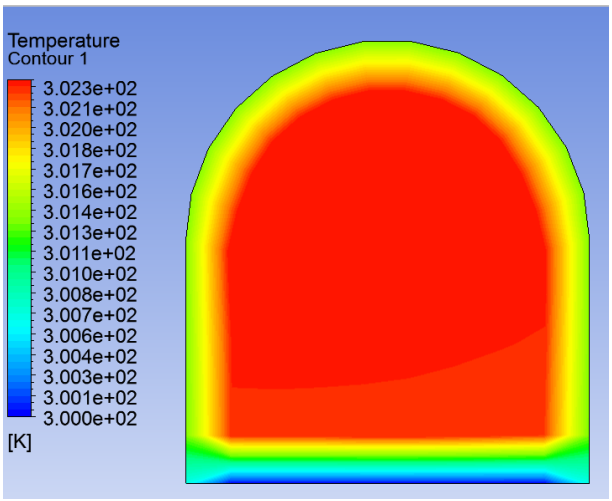

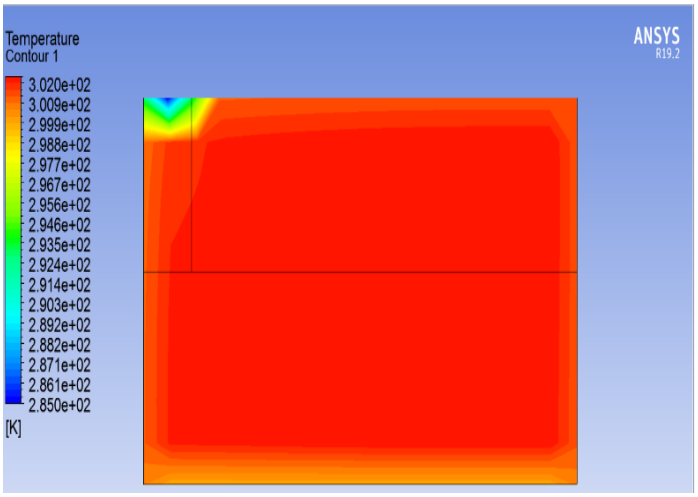

B. Standard Greenhouse with condensation

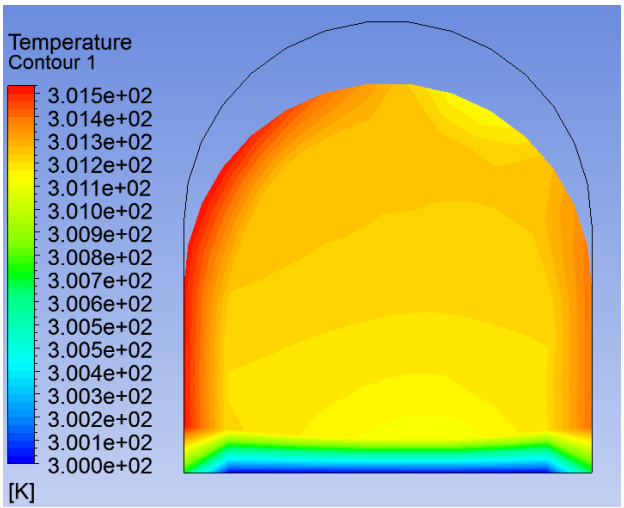

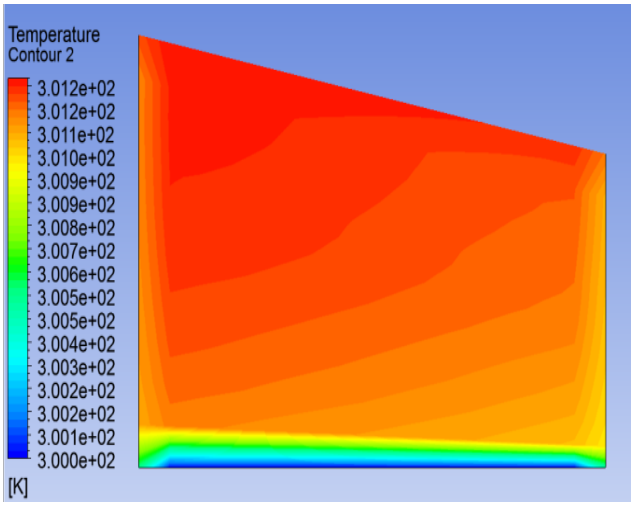

C..Inclined Greenhouse without Condensation

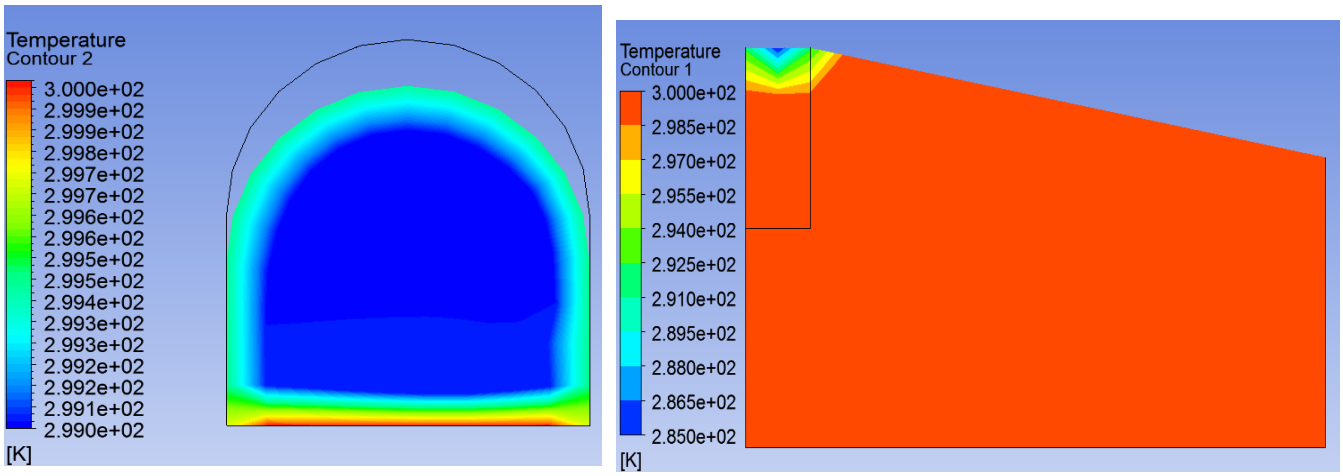

D.Inclined Greenhouse with Condensation

Figure 4.5 *Temperature for all Greenhouse at 20:30 pm*

Interpretation

The figures show the temperature distribution of the 4 greenhouses at 20: 30. We notice that the temperature in the 4 greenhouses is low compared to the day around 300 K because of the the absence of solar radiation regardless of change of geometry or condensation. The condensation temperature remains the lowest, the moist soil and the ends are warmer than the interior of the greenhouses (fluid domain).

4.3.2. Humidity

Humidity at 14:30

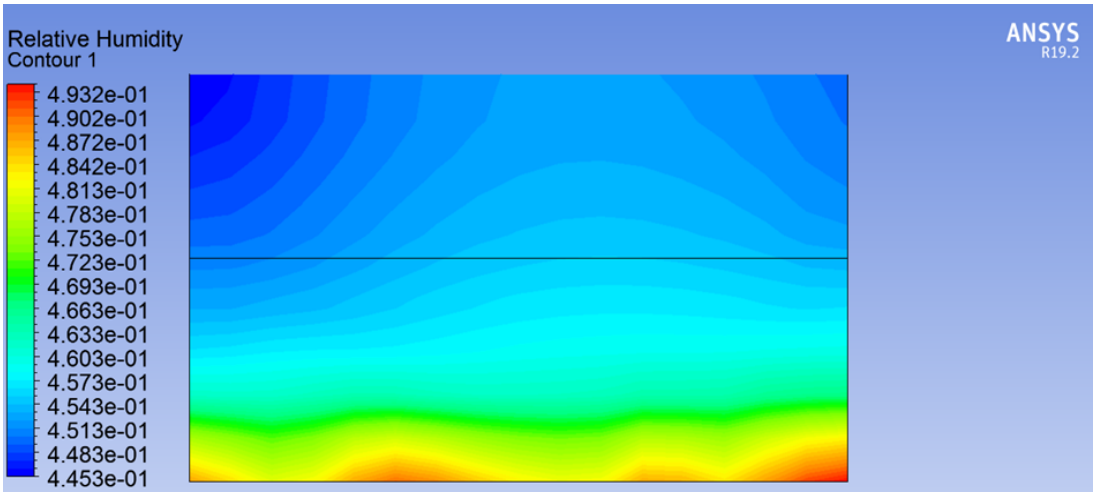

A. Standard Greenhouse

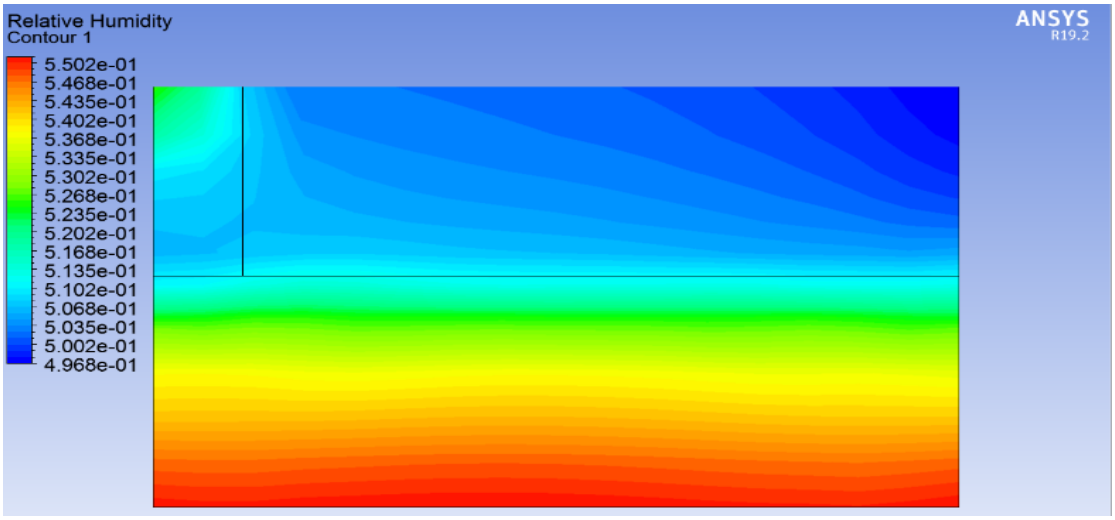

B. Standard with Condensation

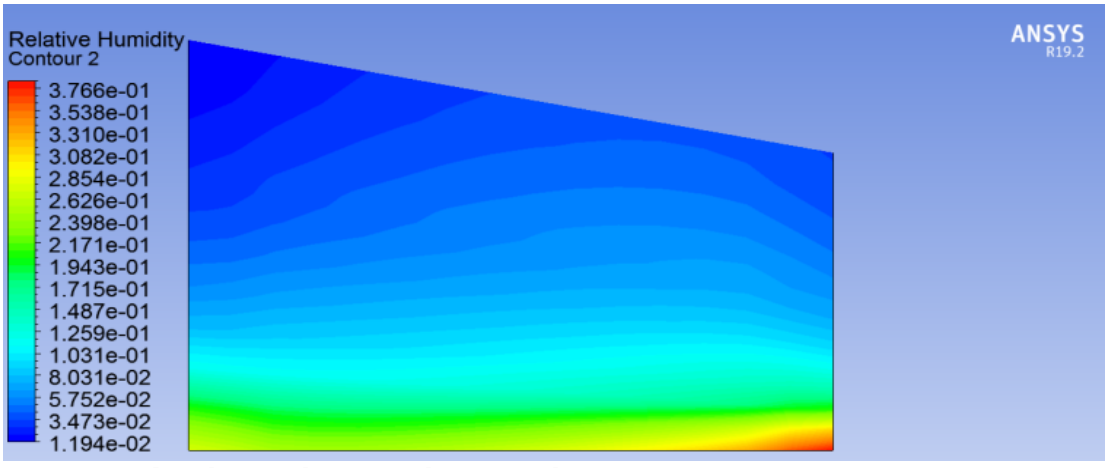

C. Inclined Greenhouse without Condensation

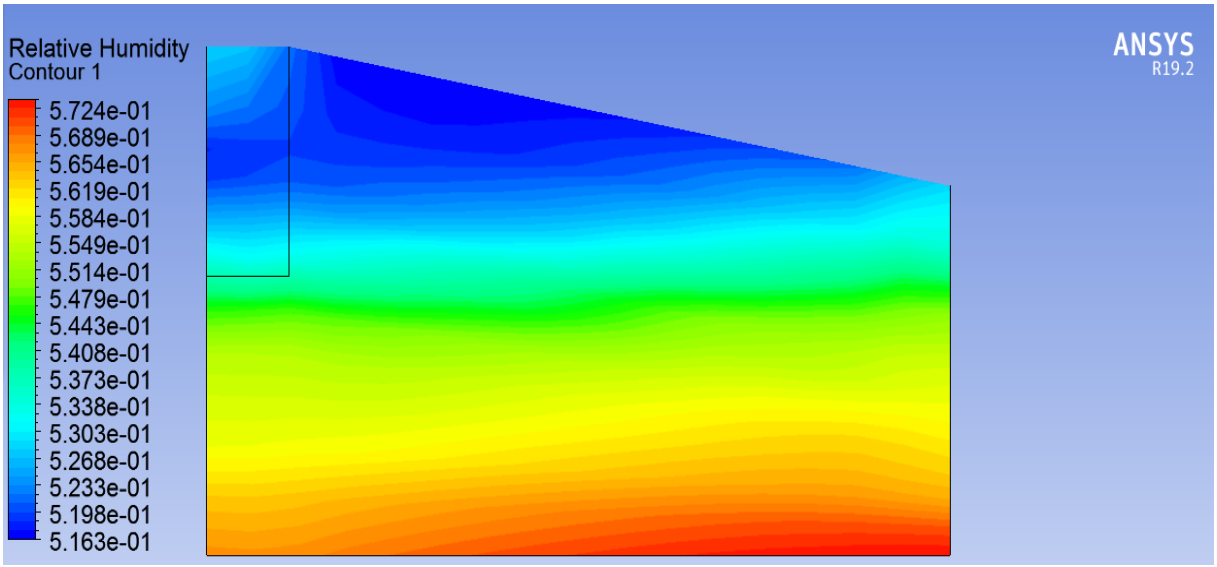

D. Inclined Greenhouse with Condensation

Figure 4.6 *Humidity for all Greenhouse at 14:30 pm*

Interpretation

The figures show the relative humidity distribution of the four greenhouses at 14:30. we notice that the distribution is almost the same for the 4 greenhouses. However it is high in the wet soil. Humidity is well distributed in the inclined greenhouse and decreases towards the roof between 0.02 and 0.57.

Humidity at 17:30

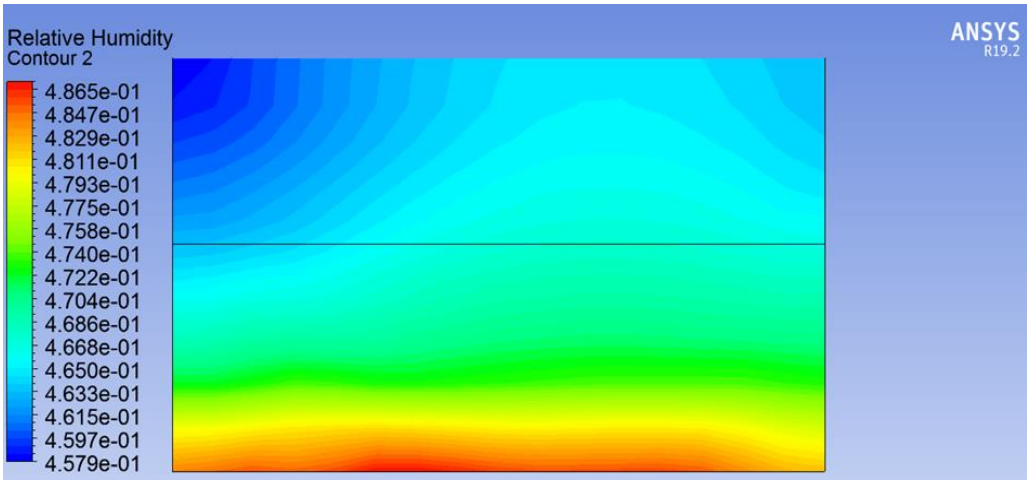

A. Standard Greenhouse

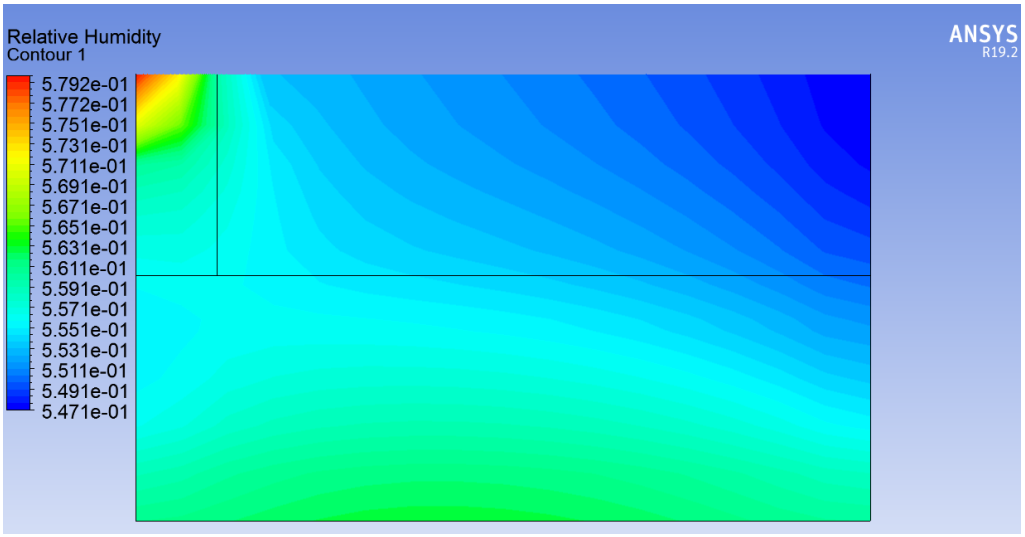

B. Standard Greenhouse with Condensation

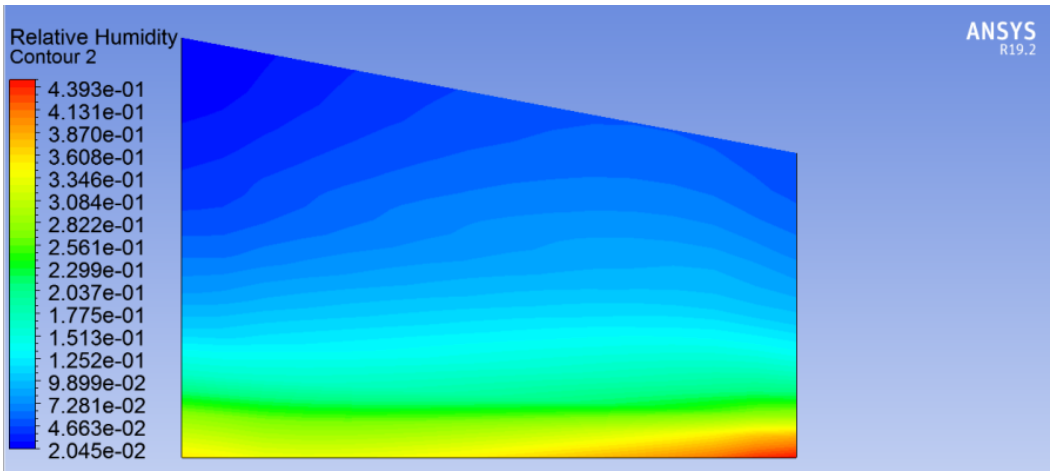

C. Inclined Greenhouse Without Condensation

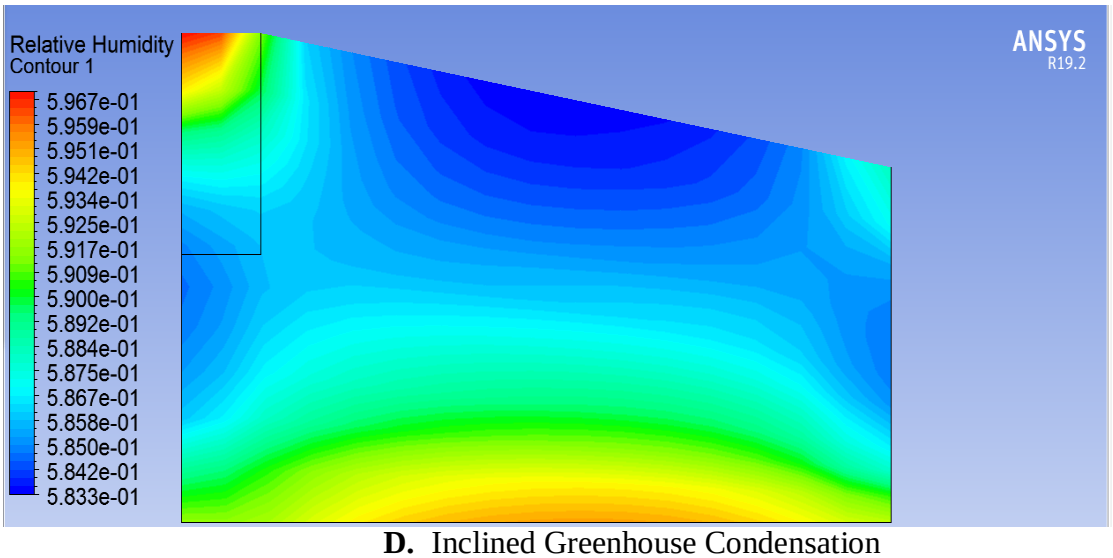

D. Inclined Greenhouse Condensation

Figure 4.7 Humidity for all Greenhose at 17:30

Interpretation

The figures show the relative humidity distribution of the 4 greenhouses at 5:30 p.m., we notice that for inclined greenhouses the humidity is moving towards the end of the greenhouse on the condensation side, the greenhouse with condensation has a faster displacement, the humidity variance increased from 14:30 and varies between 0.2 and 0.59.

Humidity at 20:30

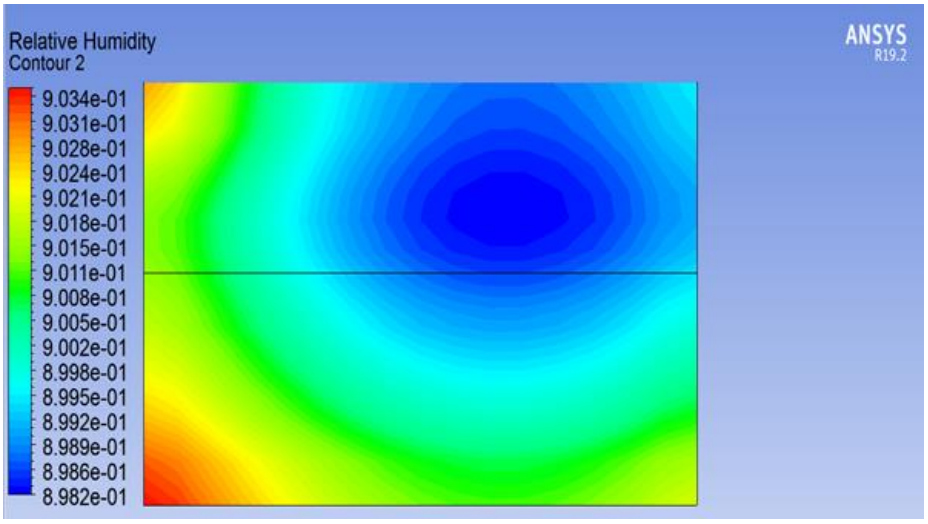

A. Standard Greenhouse without condensation.

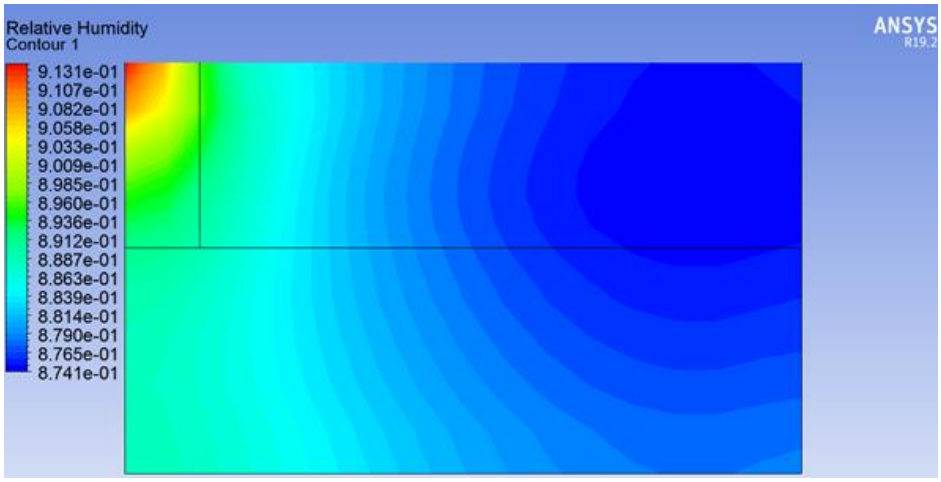

B. Standard Greenhouse with condensation.

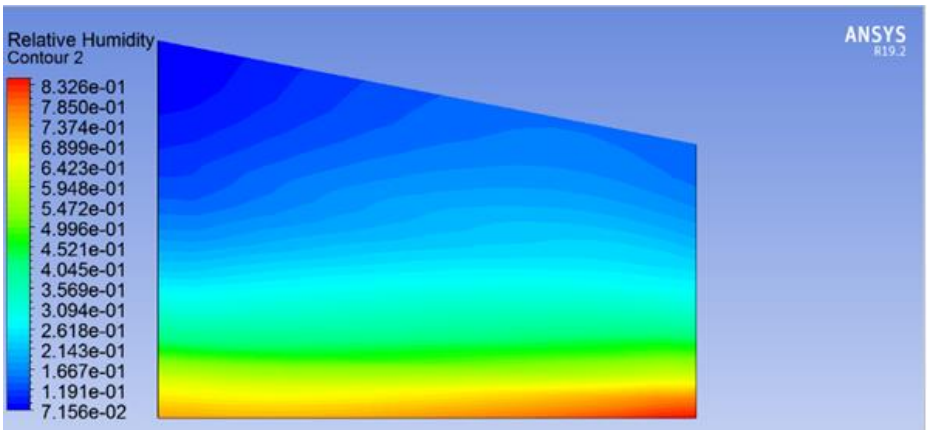

C. Inclined Greenhouse Without condensation.

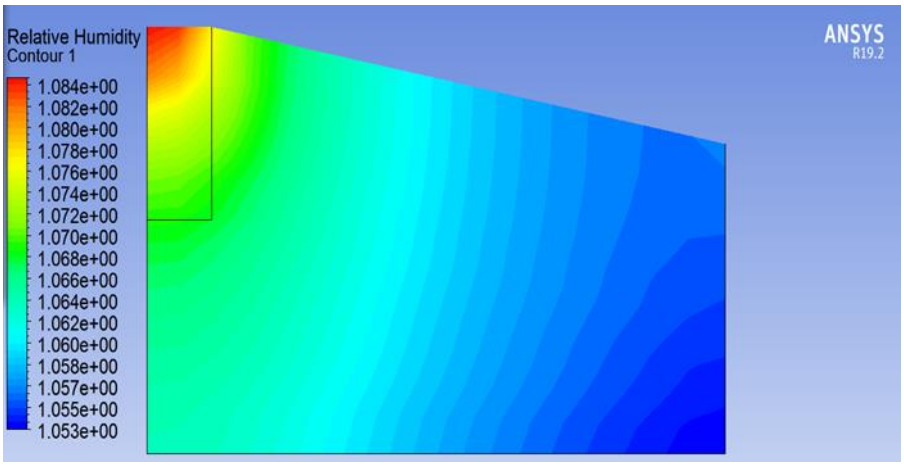

D. Inclined Greenhouse with condensation.

Figure 4.8 Humidity for all greenhouse at 20:30

Interpretation

The figures show the relative humidity distribution of the 4 greenhouses at 8 p.m., we notice that the humidity is almost shifted towards the condensation side. The inclined greenhouse at remains the fastest to accumulate water vapor we also notice that the humidity is between 0.07 and 1 this means that the water vapor is transformed into liquid which accumulates well in the condensation side for greenhouses.

4.3.3. Velocity

Velocity at 14:30

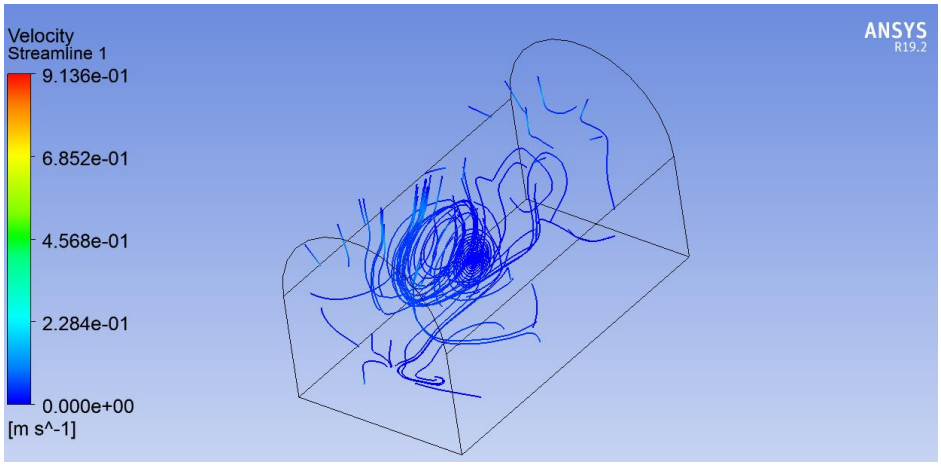

A. Standard Greenhouse

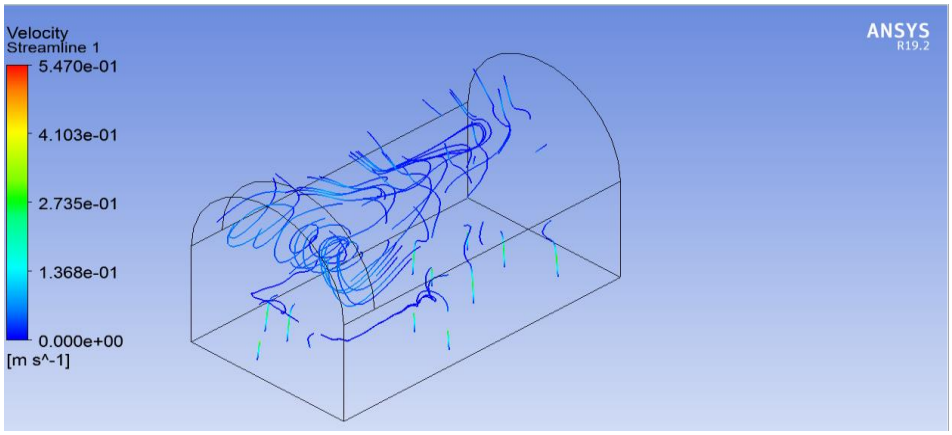

B. Standard Greenhouse with Condensation

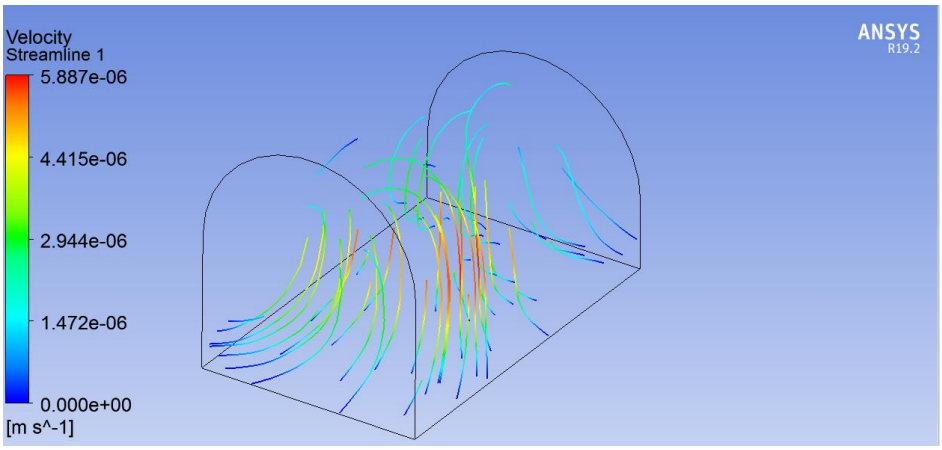

C. Inclined Greenhouse

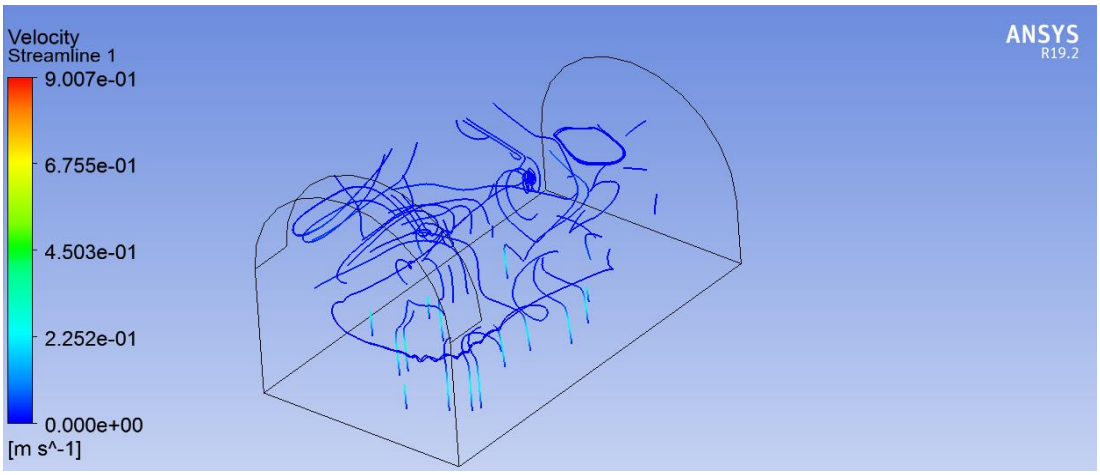

D. Inclined Greenhouse with Condensation**.**

Figure 4.9 Velocity Stream for all Greenhouse at 14: 30

Interpretation

The figures show the velocity distribution for 4 greenhouses. The movement is essentially in the region near condensation, velocity increases from the soil towards roof. The Inclined greenhouse with condensation has significant movement relative to the other greenhouses.

Velocity at 17:30

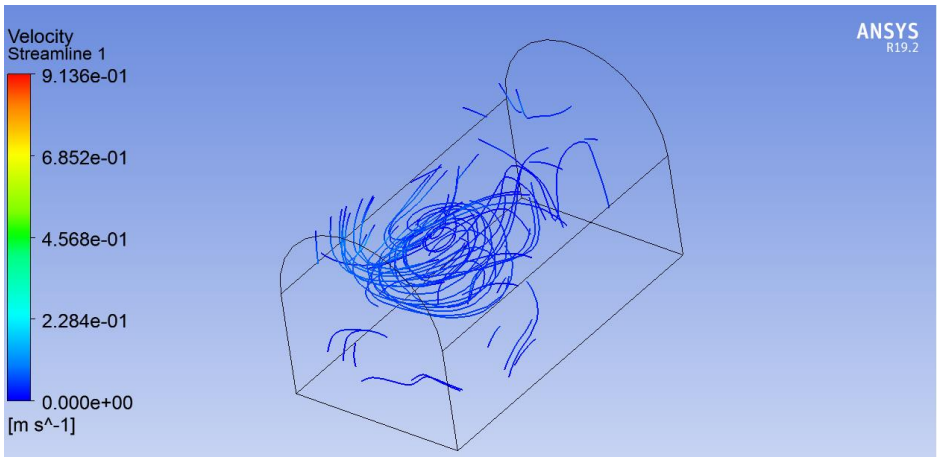

A. Standard Greenhouse

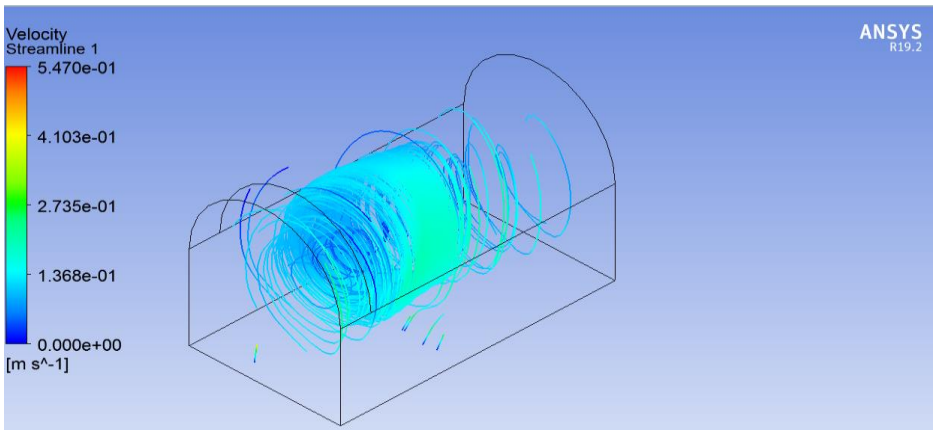

B. Standard Greenhouse with condensation

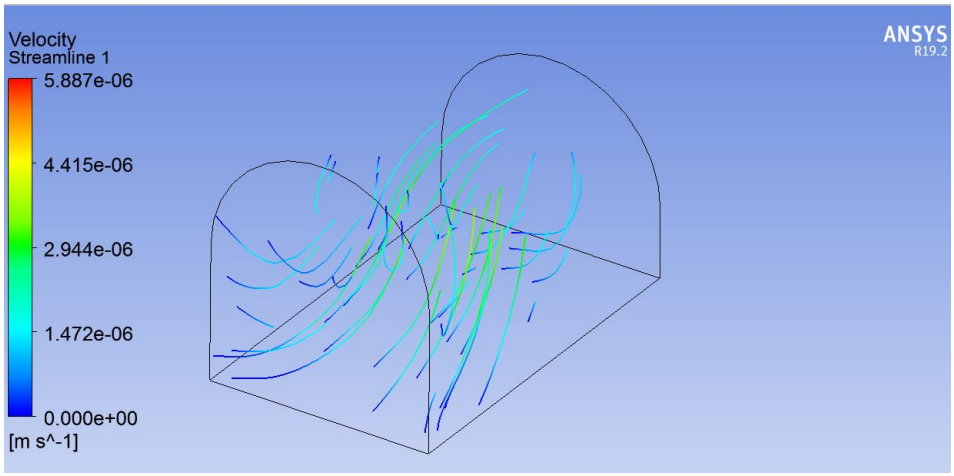

C. Inclined Greenhouse without Condensation

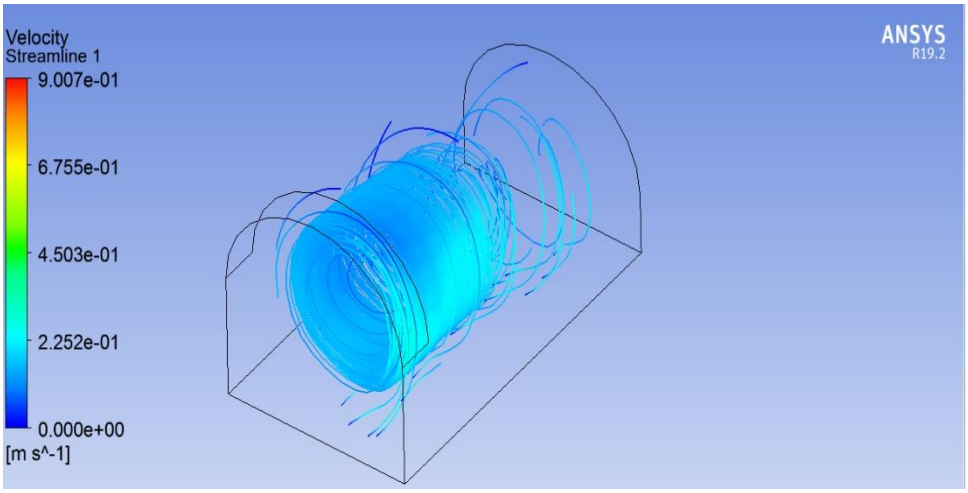

D. Inclined Greenhouse With Condensation

Figure 4. 10 Velocity Streamlines for all Greenhouses at 17:30

Interpretation

The figures show the Velocity distribution for 4 greenhouse at 17:30.

We notice that the Inclined greenhouse with condensation temperature of 285 K causes a significant air circulation compared to the other greenhouse. The velocity of the inclined greenhouse with condensation is around 0.20 m/s.

Velocity at 20:30

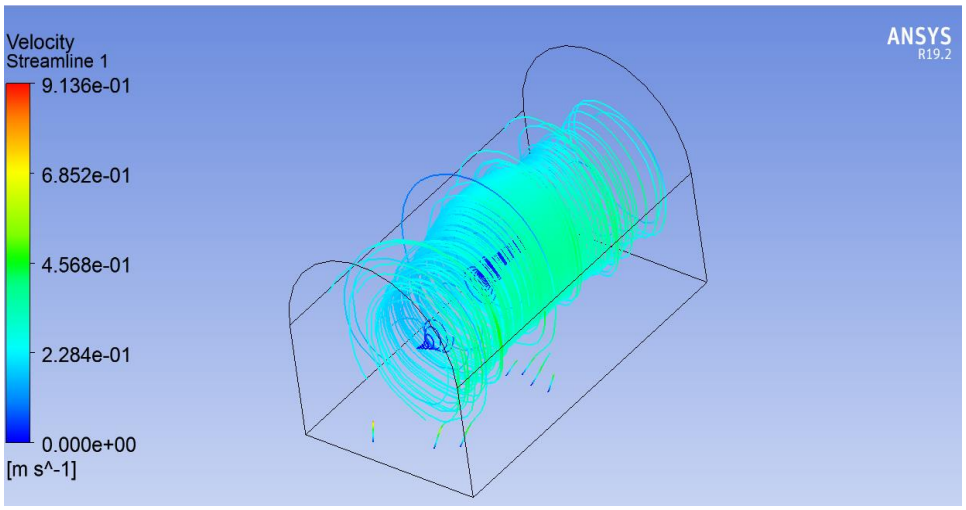

A. Standard Greenhouse

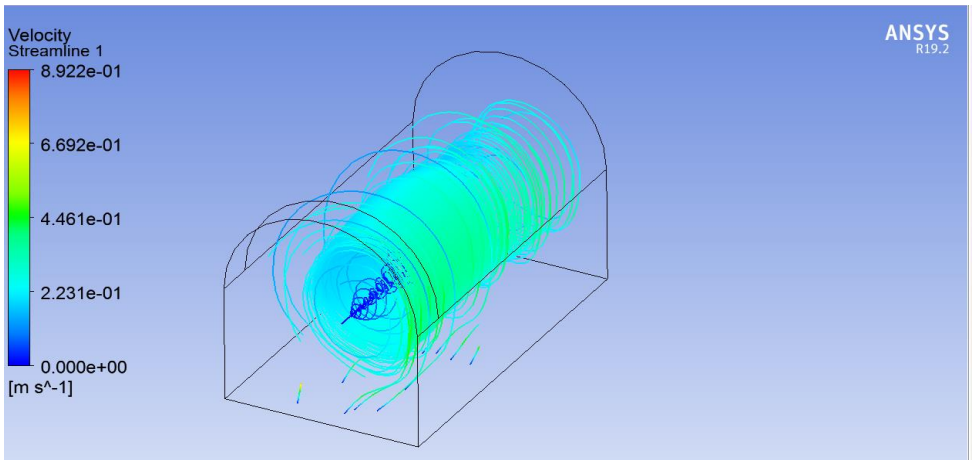

B. Standard greenhouse with condensation

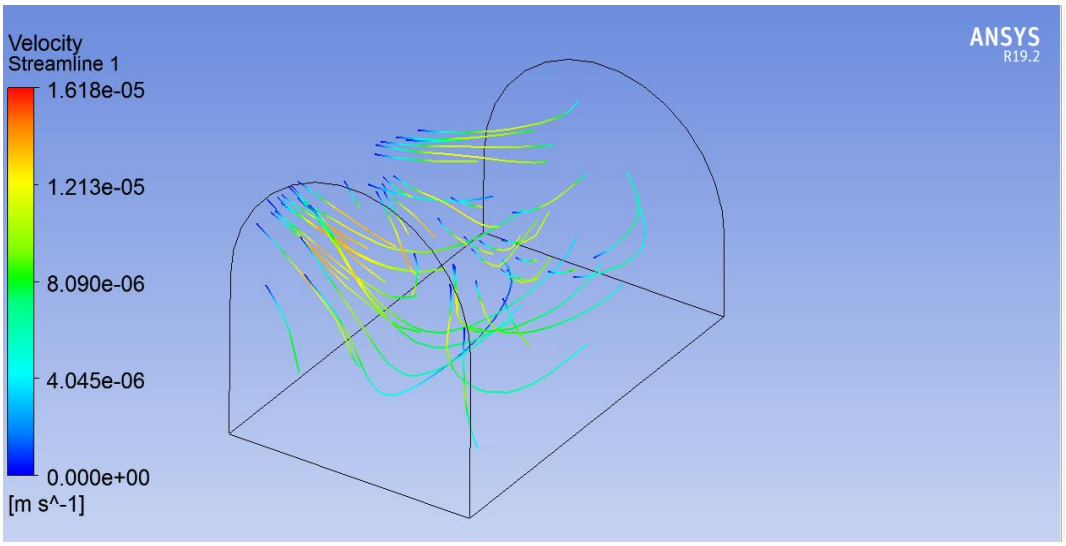

C. Inclined Greenhouse without Condensation

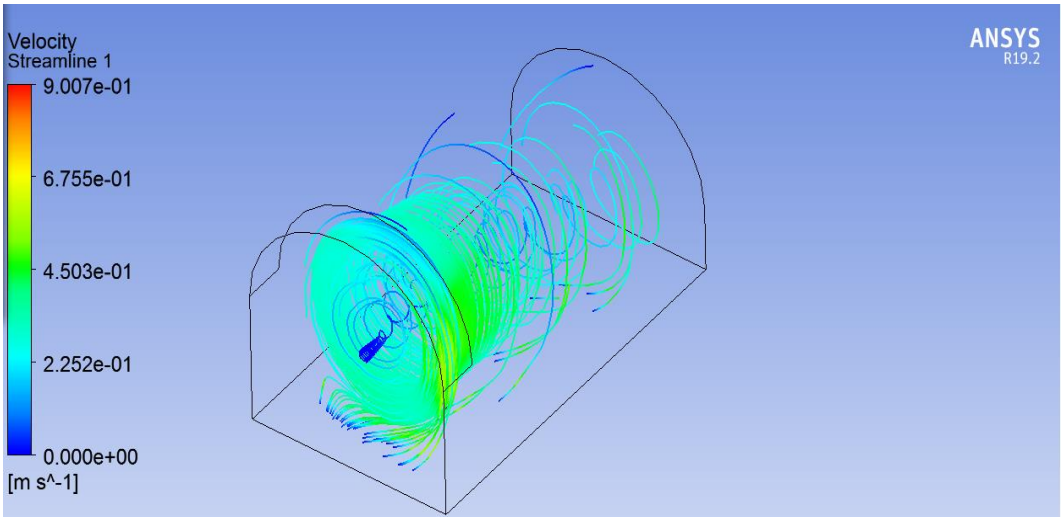

D.I Inclined greenhouse with condensation

Figure 4. 11. Velocity Streamlines for all Greenhouse at 20:30

Interpretation

The figures show the distribution of the speed for 4 greenhouses 8:30pm. We notice that the distribution is almost the same for the 4 greenhouses with a velocity ranging from 0 to 0.2 m/s. it is well distributed in the inclined greenhouse compared to other geometries.

4.4. Conclusion

Several results were presented showing the influence of the flat roof and inclined roof of the greenhouse on the temperature distribution and especially the distribution of water vapor in the greenhouse. As such, our work was based on a comparative study of the energy behaviour of a set of greenhouses under the same climatic conditions. According to the results found by our study, the influence of the design of the greenhouse and its configuration and sizing on its energy balance is quite remarkable. The results indicate that the temperature fields vary over time because of the variance of the solar flux during the day. In addition, the velocity field shows us a circular movement of air within the greenhouse. This configuration is justified by the effect of antagonistic forces opposing the volume and viscous forces on one side and the forces due to thermal effects

It should be noted that the inclination of the greenhouse promotes a greater concentration of moisture at the upper end of the greenhouse. This effect could be combined with the pathed effect in order to extract a maximum of moisture to extract water by cooling and condensation

General Conclusion

General Conclusion

The study conducted as part of this Master's work is dedicated to the analysis of the influence of the geometric parameters of the greenhouse. This contribute to the understanding and analysis of the different phenomena including the temperature and humidity involved inside a greenhouse in a dry and hot climate. It should be noted that the goal of this analysis is the recovery of water vapour produced by evapo-transpiration in order to recycle irrigation in the greenhouse thus reducing water and energy cost. Through a detailed bibliographic analysis, a mathematical model based on a heat and mass balance was adopted in order to describe the physical problem. Boundary conditions took into account solar radiation in a Saharan region as well as convective phenomena taking place around the greenhouse. In addition, it was considered that the soil is saturated with moisture throughout the process, ensured by permanent watering.

We have systematically carried out numerical calculations and the results of the simulation were obtained by exploiting the commercial software Ansys Fluent 19.2. Ansys-Fluent allowed to simulate fluid and thermal flows based on a discretization scheme finite volume which allows the resolution of the transport equations.

Turbulence was modelled using the k-e model - based on standard coefficients. This theoretical approach has yielded appreciable results and interesting details on the distribution of temperatures and humidity as a function of an angle of inclination of the roof of the greenhouses. We noticed that temperatures, velocity and humidity depends on the angle of inclination and as a comparison between the 2 types of greenhouses. WE Noticed that the mass fraction of water vapor is well distributed in a greenhouse with inclined roof that the one with the flat roof

This simple approach that we have used may contribute to the development of sheltered crops in our country and to the choices of the type and geometry of the greenhouse with a water recovery system which is energy-efficient in our region (semi-arid climate of the southern Mediterranean).

Our work focuses on the interaction of the different phenomena that exist inside the greenhouse in the presence of the vegetation cover during two periods: the day mode and the night mode. In order to conclude this work, it is wise to address some perspectives and recommendations for future work. Indeed, in order to be able to exploit water vapor in a process of recycling and optimization of water consumption, it is appropriate to introduce a condensation system taking advantage of the freshness of the night. This system can be designed by combining the path effect and a geothermal cooling system.

Bibliographic Reference

(1).**Sabeh, N. 2007**. Evaluating and minimizing water use by greenhouse evaporative cooling systems in a semi-arid climate. Ph.D. Dissertation, The University of Arizona.

(2) **Mistriotis A; Bot G P A; Picuno P; Scarascia-Mugnozza G (1997b),** Analysis of the efficiency of greenhouse ventilation using computational fluid dynamics. Journal of Agricultural Engineering Research, 85, 217-228.

(3).**Kumar Jaypuria 2008,** Heat treatment of low carbon steel.

(4).**Castilla and Hernandez 2007,** Greenhouse technological packages for high-quality crop production.

(5).**Gasso-Busquets & Solomando-Valderrabano 2011** ,Estructura e instalaciones de un invernadero.

(6). **A.Arbel M.BarakA.Shklyar,**Combination of forced ventilation and fogging systems for cooling greenhouses.

(7)**. Critten and Bailey, 2002** , A review of greenhouse engineering developments during the 1990s.

(8). **Boulard Willits, 2003a,** Dynamic modeling and simulation of greenhouse environments under several scenarios: A web-based application.

(9). **Al-Helal and Short, 1999,**A CFD study of naturally and and ventilated greenhouses in extreme arid climates.

(10)**. Arbel, A., Barak, M. & Shklyar, A. 2003.** Combination of forced ventilation and fogging systems for cooling greenhouses. J. Agric. Eng. Res., 84(1): 45–55.

(11**). Abdel-Ghany, A.M. & Kozai, T. 2006**. Cooling efficiency of fogging systems for greenhouses. Biosyst. Eng., 94(1): 97–109.

(12). **Sapounas et al. (2007)** Analysis of microclimate uniformity in a naturally vented greenhouse with a high-pressure fogging system.

(13). Greenhouse Water Recovery System for Crop Production in Semi-Arid Climate

(14) **Jiyuan Tu, Guan-Heng Yeoh, Chaoqun Liu**, Computational Fluid Dynamics A Practical Approach.

(15). **Bird, B.R., Steward, W.E., LightfoodE.N.:** Transport Phenomena, , (2002)

(16). **N. C. Markatos** The mathematical modelling of turbulent flows.

(17). **Bückle, U., & Peri´c, M. (1992).** Numerical simulation of buoyant and thermocapillary convection in a square cavity. Numerical Heat Transfer, Part A (Applications), 21, 101–121.

(18). **Jiyuan Tu, Guan-Heng Yeoh, Chaoqun Liu**, Computational Fluid Dynamics A Practical Approach.

(19). **BAKHTI Issam eddine, TOUILEB Soheib** ,Modélisation et modification d'une serre agricole avec recyclage d'eau et production d'énergie adapté à la zone saharienne Projet de fin d'étude 2020 à Tlemcen.